

**OPTIMIZING OCULAR GENE THERAPY FOR LONG TERM INTRAOCULAR
PRESSURE CONTROL IN *ADAMTS10*-OPEN ANGLE GLAUCOMA**

By

Kristin Leigh Koehl

A THESIS

Submitted to
Michigan State University
in partial fulfillment of the requirement
for the degree of

Comparative Medicine and Integrative Biology – Master of Science

2018

ABSTRACT

OPTIMIZING OCULAR GENE THERAPY FOR LONG TERM INTRAOCULAR PRESSURE CONTROL IN *ADAMTS10*-OPEN ANGLE GLAUCOMA

By

Kristin Leigh Koehl

Glaucoma is an optic neuropathy that causes irreversible damage to retinal ganglion cell axons. Most forms of open angle glaucoma (OAG) are associated with an increased intraocular pressure (IOP) due to obstruction of the aqueous humor outflow pathways (AHOP). For years our team has worked to preserve vision by targeting these outflow pathways by delivering a novel capsid mutated adeno-associated virus (AAV) mediated gene replacement therapy in a clinically relevant and well-established OAG dog model caused by a mutation in *ADAMTS10*. Past studies with *ssAAV2-(Y444F)-hGFP* (targeting) and *ssAAV2-(Y444F)-hADAMTS10* (therapy) at vector genome (vg) dose of $1-3 \times 10^{11}$ vg administered intracamerally (IC) in a 50 μ L volume delivered safe and long-term transgene expression to the AHOPs; however, an IOP reducing therapeutic effect was not achieved. Our goal was to increase transduction efficiency to the AHOPs by delivering the same vector constructs at a higher dose. In Aim 1, we showed in 5 dogs that $2.78-5.56 \times 10^{12}$ vg provided increased and clinically observable transgene expression within the iridocorneal angle (ICA). In Aim 2, 2 of 3 dogs IC injected with *ssAAV2-(Y444F)-hADAMTS10* at $1.25-1.43 \times 10^{12}$ vg experienced a significant reduction in IOP by 19-20 days post-injection with a steady and well-maintained reduction for at least 105 weeks. *ssAAV2-(Y444F)-hADAMTS10* was well-tolerated and resulted in an increased outflow facility by 3-75%. These studies provide proof-of-concept that modification of gene expression within the AHOP is possible and can result in long-term IOP control.

ACKNOWLEDGEMENTS

The amazing work that encompasses this thesis is due to a great team of people and all require acknowledgement and thanks for their hard work and dedication for great science.

My mentor deserves great acknowledgment and more thanks than I could ever return. Dr. András Komáromy is by far the kindest and most genuine human I have ever met and truly, one to model yourself after. Thank you for teaching me science and grace, the opportunities to advance my career, and your patience for my learning and questions. Thank you for the mentorship and the ability to always call you a friend.

To Dr. Vilma Yuzbasiyan-Gurkan, thank you for the opportunity to advance my education. Your kindness, enthusiasm, and pride in all your students within the program is unparalleled. To my committee, Drs. Simon Petersen-Jones, Shannon Boye, Sayoko Moroi and Arthur Weber, your guidance over the years to completion of the thesis is appreciated; and, thank you for your collaborations, expertise and enlightenment during my Master's academic career.

To the Boye Laboratory at the University of Florida, thank you for your vast and exceptional knowledge of vector technology. To Dr. Juan Pedro Steibel at Michigan State University, thank you for meeting with me and sharing your knowledge in biostatistics. To Dr. Chris Pirie at Michigan State University, thank you for your tremendous contribution to our kinetics study and for being a witty and fun person to chat up science. To Dr. Dodd Sledge at

Michigan State University's Veterinary Diagnostic Laboratory, for your wealth and expertise in ocular pathology.

To Christine Harman of the Komáromy Laboratory, thank you for everything! You are a dear friend that has imparted much wisdom in science and in friendship. To all the undergraduate students of the Komáromy Laboratory, past and present, thank you for all your hard work and impressive drive. You all are truly inspirational at your young ages.

To all the people that care for the dogs. The animals deserve great lives and each of you make that happen. Thank you, Kim Williamson, Ramona Stambaugh, and Danae Walters for all your care and affection for our great animals.

The financial support that make all things possible: NIH grants, R01EY025752, R01-EY024280, P30EY021721; The Glaucoma Research Foundation; Research to Prevent Blindness; Foundation Fighting Blindness; and Michigan State University Discretionary Funding Initiative.

Thank you to the Edward Sheppard family for the wonderful unrestricted gift.

For my friends and family outside of science. To my good friend Katie Meyer, you are an amazing woman who always inspires me with your generosity. To my parents, Terry and Margaret and my soon to be husband, David, thank you for your amazing patience and support through my life endeavors. Thank you for living all the smiles and tears with me.

Of all the acknowledgements, most importantly, ALL the dogs. Thank you to each and every one of you! Your time and lives will never be forgotten. May God always be good to you. Until we meet again.

TABLE OF CONTENTS

LIST OF TABLES	vii
LIST OF FIGURES.....	viii
KEY TO ABBREVIATIONS AND SYMBOLS	x
CHAPTER 1 - Introduction	1
1.1 Glaucoma Classification	1
1.2 Aqueous Humor Dynamics	5
1.2.1 Aqueous Humor Production	6
1.2.2 Aqueous Humor Drainage	7
1.3 Trabecular Meshwork	9
1.3.1 Uveal and Corneal Scleral Meshwork	9
1.3.2 Juxtacanalicular Tissue	9
1.4 Trabecular Meshwork Extracellular Matrix (TM-ECM)	10
1.4.1 Mechanisms that Can Change the ECM Profile	11
1.5 Schlemm’s Canal/Angular Aqueous Plexus	12
1.6 Genetics of OAG	12
1.7 Animal Models of OAG	16
1.7.1 A Disintegrin and Metalloproteinase with Thrombospondin Motifs (<i>ADAMTS</i>) – Canine OAG Models	18
1.8 Preservation of Vision by Therapeutic Lowering of IOP	21
1.8.1 Current Therapies	22
1.9 Adeno-Associated Virus (AAV) for Targeted Gene Therapy	25
1.10 Purpose	29
CHAPTER 2 – Materials and Methods	31
2.1 Study Design	31
2.1.1 Aim 1 – Targeting the AH outflow pathway – <i>hGFP</i>	31
2.1.2 Aim 2 – Therapeutic delivery - <i>ssAAV2-(Y444F)-hADAMTS10</i>	31
2.2 Animals	32
2.3 Anesthesia Protocols	33
2.4 Clinical Examination	35
2.4.1 Diurnal IOP – primary outcome measure	35
2.4.2 Pachymetry	36
2.4.3 Gonioscopy	36
2.4.4 Ultrasound biomicroscopy (UBM)	37
2.5 AAV Production	37
2.6 Intraocular injections – IC and IVit	38
2.6.1 <i>ssAAV2-(Y444F)-hGFP</i> and <i>ssAAV2-(Y444F)-hADAMTS10</i>	38
2.6.2 Optimizing Injection Technique	44
2.7 Aqueous Humor Outflow Facility - Pneumotonography	48
2.8 Aqueous Humor Flow - Fluorophotometry	49

2.9 Optical Coherence Tomography (OCT) and A-scan Biometry	49
2.10 Electroretinography (ERG).....	50
2.11 Aqueous Paracentesis and Aqueous Humor Analyses	51
2.12 Tissue Collection for Histopathology and Immunohistochemistry	52
CHAPTER 3 - Results	55
3.1 Aim 1 - Effect of Dosing and Injection Route on TM Transgene Expression	55
3.1.1 Increasing the AAV Dose	55
3.1.2 Comparing IC vs IVit injections	57
3.1.3 Effect on Pupillary Aperture	58
3.1.4 Other Observations following IC and IVit ssAAV2-(Y444F)-hGFP	60
3.1.5 Comparison of hGFP Expression Between Quadrants	63
3.1.6 Fluorescein Kinetics of the AC	64
3.1.7 Summary of Aim 1 – Targeting the AH outflow pathway – ssAAV2-(Y444F)-hGFP	67
3.2 Aim 2 – Treatment of Canine ADAMTS10-OAG – ssAAV2-(Y444F)-hADAMTS10	68
3.2.1 Long-term IOP control following IC injection of ssAAV2-(Y444F)-hADAMTS10	68
3.2.2 Increased Outflow Facility in Successfully Treated Eyes	71
3.2.3 Aqueous Humor Flow Remained Unaffected by Gene Therapy.....	73
3.2.4 ICA Morphology	74
3.2.5 Optic Nerve Head (ONH) Morphology and Retinal Function	76
3.2.6 ssAAV2-(Y444F)-hADAMTS10 Safety Measures – Clinical Examination, Pachymetry and A-scan Biometry.....	84
3.3 Adverse Events – Ocular Inflammation	86
3.3.1 Aim 1 - Severe Inflammation	86
3.3.2 Neutralizing Antibody (NAb) Assays	88
3.3.3 Aim 2 – Protein Concentration and Cell Count of AH	89
Chapter 4 – Discussion	91
REFERENCES	100

LIST OF TABLES

Table 1.1. Glaucoma Phenotypes	3
Table 1.2. Genes and Susceptible Loci.....	13
Table 1.3. Animal Models of OAG.....	17
Table 1.4. <i>ADAMTS10</i> Mutation Comparisons	20
Table 1.5. Traditional Topical Medication Synopsis	23
Table 1.6. Capsid Mutations Investigated by Bogner et al	30
Table 2.1. Aim 1 and 2 Study Participants	33
Table 2.2. <i>hGFP</i> and <i>hADAMTS10</i> Dosing Assignments.....	40
Table 2.3. Fluorescein Kinetics of the Anterior Chamber Assignments	47
Table 2.4. Photopic ERG Protocol	51
Table 3.1. Summary of Target Tissues Identified in Aim 1	68
Table 3.2. Dog 1: ERG a-, b-, and PhNR Wave Amplitudes and Peak Time Comparisons	78
Table 3.3. Dog 2: ERG a-, b-, and PhNR Wave Amplitudes and Peak Time Comparisons	80
Table 3.4. Dog 3: ERG a-, b-, and PhNR Wave Amplitudes and Peak Time Comparisons	82
Table 3.5. Percent Variation of Pachymetry in <i>ssAAV2-(Y444F)-hADAMTS10</i> Treated and Control Eyes	84
Table 3.6. A-scan Biometry Comparing <i>ssAAV2-(Y444F)-hADAMTS10</i> Treated and Control Eyes	85
Table 3.7. Aim 2 – NAb Titers for T Cell Response to <i>scAAV2-(Y444F)-smCBA-mCherry</i>	89
Table 3.8. Protein Concentration and Cell Count of AH of Aim 2 Dogs.....	90

LIST OF FIGURES

Figure 1.1. Schematic drawing of aqueous humor drainage pathways.....	8
Figure 2.1. Anterior segment embedding and sectioning map.....	54
Figure 3.1. Effective TM targeting with <i>ssAAV2-(Y444F)-hGFP</i> in dogs.....	56
Figure 3.2. Relative % area of IHC hGFP labeling within the ICA when comparing doses and routes of administration.....	58
Figure 3.3. Effect on relative % area of IHC hGFP labeling within the ICA when comparing pupil size when utilizing the 2.78E12vg dose.....	60
Figure 3.4. <i>hGFP</i> expression in the TM and other intraocular tissues when comparing IC injections with variable pupil sizes and IVit injection.....	62
Figure 3.5. Comparison of % IHC <i>hGFP</i> expression between four quadrants following IC delivery of <i>ssAAV2-(Y444F)-hGFP</i>	64
Figure 3.6. AC fluorescein kinetics as a function of temperature and vehicle.....	66
Figure 3.7. Lens capsule fluorescence shown with blue slit beam.....	66
Figure 3.8. Anterior diffusion of AH through the pupillary aperture followed by convection-like movement within the AC.....	67
Figure 3.9. Diurnal IOP for <i>ssAAV2-(Y444F)-hADAMTS10</i> treated and untreated control eyes.....	69
Figure 3.10. Linear regression fitted trendline with CI for treated and untreated eyes.....	70
Figure 3.11. Linear regression fitted trendline with CI for difference between treated and untreated eyes.....	71
Figure 3.12. Outflow facility measured by pneumotonography.....	72
Figure 3.13. Aqueous humor flow measured by fluorophotometry.....	73
Figure 3.14. ICA morphology of treated and untreated fellow eyes compared by gonioscopic examination and UBM.....	75

Figure 3.15. Morphologic comparison of ONH and comparison of retinal function..... 77

Figure 3.16. Photomicrographs depicting inflammation induced by injection of ssAAV2-(Y444F)-hGFP. 88

KEY TO ABBREVIATIONS AND SYMBOLS

AAALAC	Association for the Assessment and Accreditation of Laboratory Animal Care International
AAP	Angular Aqueous Plexus
AAV	Adeno Associated Virus
AC	Anterior Chamber
ACAID	Anterior Chamber-associated Immune Deviation
ACD	Anterior Chamber Depth
ACG	Angle Closure Glaucoma
ADAMTS10	A Disintegrin and Metalloproteinase with Thrombospondin Motifs 10
AH	Aqueous Humor
AHOP	Aqueous Humor Outflow Pathway
ARVO	Association for Research in Vision and Ophthalmology
AVMA	American Veterinary Medical Association
AXL	Axial Length
CCT	Central Corneal Thickness
cd	Candela
CI	Confidence Interval
CLANs	Cross-linked Actin Networks
CSTM	Corneoscleral Trabecular Meshwork
CYP1B1	Cytochrome P450 1B1

ECM	Extracellular Matrix
ERG	Electroretinography
F	Phenylalanine
FBN1	Fibrilin 1
FDA	Food and Drug Administration
GC	Glucocorticoid
GFP	Green Fluorescent Protein
hADAMTS10	Human ADAMTS10
HCl	Hydrochloride
hGFP	Humanized Green Fluorescent Protein
HSPGs	Heparin Sulfate Proteoglycans
HSS	High Salt Solution
Hz	Hertz
H&E	Hematoxylin and Eosin Stain
IACUC	Institutional Animal Care and Use Committee
IC	Intracameral
ICA	Iridocorneal Angle
IHC	Immunohistochemistry
IM	Intramuscular
IOP	Intra-ocular Pressure
IV	Intravenous
IVit	Intravitreal

JCT	Juxtacanalicular Tissue
LA	Light Adapted
LCA	Leber Congenital Amaurosis
LT	Lens Thickness
LOX	Lysyl Oxidase
m	Meter
mg/dL	Milligrams per Deciliter
MIGS	Micro-invasive Glaucoma Surgery
mm	Millimeters
MMP	Matrix Metalloproteinase
ms	Milliseconds
MSU	Michigan State University
MTP	Micro Total Protein
MYOC	Myocilin
N/A	Not Available
n/a	Not Applicable
NAb	Neutralizing AAV Antibody
NC	Not Collected
NE	Not Examined
nm	Nanometer
NO	Nitric Oxide
NTF4	Neurotrophin 4

OAG	Open Angle Glaucoma
OCT	Optical Coherence Tomography
ONH	Optic Nerve Head
OPTN	Optineurin
PI	Post Injection
RBC	Red Blood Cells
RGC	Retinal Ganglion Cells
RNFL	Retinal Nerve Fiber Layer
ROCK	Rho Kinase
s	Second
SC	Schlemm's Canal
scAAV	Self-complimentary AAV
smCBA	Small Chicken β-actin
ss	Single-stranded
TBK1	Tank-binding Kinase 1
TM	Trabecular Meshwork
TM-ECM	Trabecular Meshwork Extracellular Matrix
tx	Treated
UBM	Ultrasound Biomicroscopy
un-tx	Untreated
UTM	Uveoscleral Trabecular Meshwork
vg	Vector Genomes

WDR36	WD Repeat Domain 36
WMS	Weill-Marchesani Syndrome
Y	Tyrosine
μV	Microvolts
μL	Microliters
™	Trademark
®	Registered

CHAPTER 1 - Introduction

1.1 Glaucoma Classification

Glaucoma is a leading cause of irreversible vision loss. This collective of optic neuropathies, globally, affects more than 70 million people. By 2020, it is estimated to surpass 76 million people. And, between 2013 and 2040, our global populous afflicted by glaucoma is expected to increase by 74%(1, 2).

These optic neuropathies result in vision loss by the progressive death of retinal ganglion cells (RGCs)(2). RGCs are located in the inner retina, and their axons relay visual information in the form of action potentials via optic nerve head and optic nerve to the brain(3). Their death is multifactorial, encompassing heterogenous genetic and environmental variables(4) which include excitotoxicity caused by amino acid release of glutamate and aspartate(5, 6); neurotrophin deprivation from inhibition of retrograde axonal transport(7-10); excessive intracellular calcium(11); blood flow impedance to the ONH and retina(12-18); oxidative stress(19, 20); inflammation and autoimmunity against retinal and optic nerve antigens(21-23); and reactive gliosis(24-27).

IOP is a major risk factor of glaucoma and the main focus of this thesis. It is regulated by the careful balance of aqueous humor (AH) production and drainage in the anterior segment of the eye. This normal regulation not only maintains the necessary constant IOP needed for functional shape and vision but is also responsible for exchange of crucial metabolites for the avascular tissues of the globe, such as cornea and lens(2, 28, 29). In hypertensive forms of

glaucoma an increased AH outflow resistance through the ICA results in accumulation of AH and increased IOP.

Depending on the presence or absence of an identifiable underlying etiology, glaucomas are categorized as primary or secondary, the latter being caused by a detectable disease process that results in impairment of AH drainage. Characterization of the phenotypes is what categorizes the various types of primary and secondary glaucomas (Table 1.1). The two main forms of primary glaucoma are OAG, the topic of this thesis, and angle-closure glaucoma (ACG). Clinically, ACG is characterized by the obstruction of the AHOP by the iris against the ICA(2).

Table 1.1. Glaucoma Phenotypes

Type	IOP; Drainage Angle	Significant Clinical Presentation	Risk Factors
Open angle glaucoma	Elevated; open	ONH cupping	Age, family history, African heritage, use of corticosteroids, elevated IOPs(2)
Angle closure glaucoma	Elevated; closed or partially closed	Regional or full obstruction of ICA; ONH cupping	Age, female gender, first degree relatives with disease, Asian heritage, eyes with short axial length(2)
Normal-tension glaucoma	Normal; open	ONH cupping	Age, female gender, Asian descent(30)
Congenital glaucoma	Typically, elevated; delayed/failed development	ONH cupping; various corneal changes; buphthalmia	Sporadic but mostly inherited and varies by ethnicity(31)
Pigmentary glaucoma	Elevated; pigmented deposits	ONH cupping; illuminated iris defects; Krukenberg's spindle; uniformly heavy pigmentation of trabecular meshwork (TM)	Pigment dispersion syndrome(32)
Pseudoexfoliative glaucoma	Elevated; deposits	ONH cupping; classic pattern deposits of exfoliation on anterior lens	Exfoliation syndrome(33)
Traumatic glaucoma	Elevated; varying degrees of recession or exacerbating damage	Closed: decreased baseline vision, hyphema, angle reduction, traumatic lens incidences, iris afflictions Open: damage to globe and globe anatomy, peripheral anterior iris synechia, vitreous hemorrhage ONH cupping	Inducing ocular injury and any secondary complications in the closed globe or inducing ocular injury and any complications from the open-globe and its subsequent repair which may include use of corticosteroids(34, 35)
Neovascular glaucoma	Elevated; development of vasculature	ONH cupping; neovascularization of ICA and iris; vascular retinal changes	Various retinal vessel occlusions, diabetic retinopathy, various ocular tumors, various systemic diseases and retinopathies(36)

Table 1.1. (cont'd)

Type	IOP; Drainage Angle	Significant Clinical Presentation	Risk Factors
Iridocorneal endothelial syndrome	Elevated; appearance of open but obstructed by clear endothelium	ONH cupping; changes in corneal endothelium and cornea; iris atrophy; peripheral anterior iris synechia	Chandler syndrome, progressive iris atrophy, Cogan-Reese syndrome(37)
Uveitic glaucoma	Very elevated; initial appearance is open however chronic inflammation can create collapse or obstruction	ONH cupping; proteinaceous and cellular particulates present in anterior chamber; anterior and posterior iris synechia	No known propensities; however, some systemic conditions can result in chronic uveitis which can produce glaucomatous damage(38, 39)

Abbreviations: ONH, optic nerve head; ICA, iridocorneal angle; TM, trabecular meshwork

Unlike ACG, OAG is clinically identified with an open and fully accessible ICA(2, 40). The iris remains stationed in its respective location and does not contribute to the primary impedance of AH outflow. OAG-affected individuals may live long lengths of their lives unaware of their disease until there are noticeable changes in their visual fields. The pathogenesis of increased AH outflow resistance in OAG is not fully understood but appears to be associated with plaque formation(41) within the extracellular matrix (ECM) within the ICA. The following risk factors have been identified for OAG: older age, family history in first degree relatives, African descent, Hispanic descent, elevated IOP, thin cornea, low perfusion pressure, and use of corticosteroids(2, 28, 29).

1.2 Aqueous Humor Dynamics

Aqueous humor is a clear fluid medium that fills the anterior and posterior chambers of the eye. It is produced by the ciliary body and released into the posterior chamber. It then moves through the pupillary aperture into the anterior chamber, and then exits the eye through two pathways: either the ICA/TM (conventional pathway) or uveoscleral pathway (unconventional pathway)(28, 29). Due to temperature gradients, the AH circulates in a convection current within the anterior chamber, washing all interfacing structures before exiting through the ICA(42, 43).

In order to remain optically clear, the protein concentration is lower in the AH compared to the blood plasma. It also contains electrolytes/ions, ascorbic acid, and a multitude of other components that include growth factors, enzymes, prostaglandins, cyclic adenosine monophosphate, catecholamines, steroid hormones and hyaluronic acid(43, 44). As AH moves in its normal capacity, its composition will change as it passes interfacing structures: vitreous,

lens, iris and cornea. The AH is responsible for the maintenance of the avascular cornea and lens and their transparency by providing them with nutrition and oxygen, removal of waste from all interfacing surfaces, and aiding in the ocular immune response (28, 43, 44).

1.2.1 Aqueous Humor Production

AH is produced by the ciliary body at the site of its species specific, uniquely shaped processes(45). Each of the processes has stroma that is double layered by epithelium, containing a rich supply of fenestrated capillary beds that are necessary for the generation of oncotic pressure. The tight junctions that affix the inner, non-pigmented epithelium to the outer, pigmented epithelium create part of the blood-aqueous barrier of the eye. AH is formed by (1) active secretion, (2) ultrafiltration and (3) simple diffusion(43, 44, 46).

Active Secretion: The majority, about 80-90%, of AH is secreted by active transport. This energy demanding movement of fluid across the bilayer requires changes in the electrochemical gradient of electrolytes and the use of two valuable ion transporters: $\text{Na}^+:\text{K}^+:\text{2Cl}^-$ cotransporter and the Na^+/K^+ pump. Movement of anions and cations with these transporters creates an osmotic pressure gap across the epithelial bilayer that is then supportive of hydrostatic and oncotic movement of fluid from the ciliary body stroma to posterior chamber via aquaporins (cell membrane water channels). Additionally, fluid is also influenced to move due to changes in the sodium gradient that are determined by bicarbonate formation that is subsequently regulated by the reverse hydration of carbon dioxide by carbonic anhydrase(43, 46, 47).

Ultrafiltration: Hydrostatic pressure or osmotic gradients created by the differences between the capillary beds, the current IOP of the eye, and difference in solute will allow for natural and passive movement of fluid and solutes down their gradient(44, 48).

Simple Diffusion: Some ions and pooled fluid move passively, or leak, across the ciliary epithelial membrane in the direction of their electrical or concentration gradients(44, 48).

1.2.2 Aqueous Humor Drainage

Trabecular Meshwork/Conventional Pathway: AH predominantly exits the anterior chamber via the conventional pathway (Figure 1.1). Varying by species, between 50% and 75% of AH will filter through the three layers of the TM prior to valvular-like entry into a species-specific structure such as Schlemm's Canal (SC), in mice and primates, or the angular aqueous plexus (AAP) in canines and other mammals. Distal drainage from these trabecular vessels occurs through the adjacent aqueous veins and episcleral vessels(28, 45, 49). As the site that regulates volume changes within the eye, a measure of its resistance (or compliance) can help to characterize the change between a healthy or diseased state. Compliance can be estimated by calculating outflow facility which is the inverse of the resistance of the conventional outflow pathway(50, 51).

Uveoscleral/Unconventional Pathway: The alternative flow of AH can include the corneal, iridial and retinal route but is more commonly considered as egress through the posterior uveal meshwork (Figure 1.1). The uveal meshwork will move a bulk of this fraction of the AH while the alternative routes move negligible volumes. The estimated fraction of AH that departs the anterior chamber via the uveoscleral pathway varies greatly among species; e.g. 3-

82% in humans (52) and 15% in canines(53). The AH reaches the orbital vasculature through the interstitial spaces of the ciliary muscle, suprachoroidal space, sclera and episclera(52).

Comparatively between humans and canines, structural differences of the ICA correlate to the accommodation of the species and not to the physiology of movement and drainage of AH(54). In carnivores, the ciliary body musculature is more developed and in canines the wide and deep ciliary cleft requires additional support for appropriate anchorage of the iris(55). Unlike humans, this additional support of the iris is compensated for by a circumferential series of fibrous strands called the pectinate ligament(55).

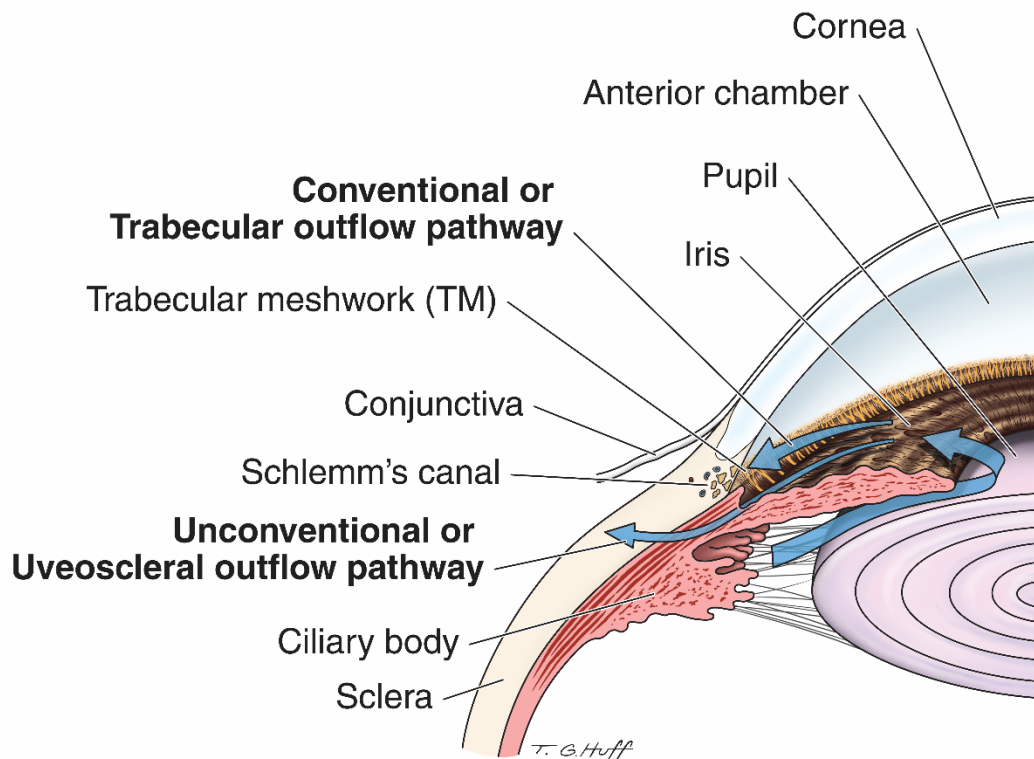


Figure 1.1. Schematic drawing of aqueous humor drainage pathways.

1.3 Trabecular Meshwork

The TM is a multifunctional, complex network of connective tissue that bridges the full 360° circumference of the ICA to its' distal drainage anatomy; it is the main focus of this thesis. Functionally, the TM is a filtration network for the AH and works intimately with SC or the AAP to regulate the resistance of AH outflow for healthy maintenance of IOP. The TM consists of three regions: (1) uveal meshwork, (2) corneal scleral meshwork and (3) juxtacanalicular tissue (JCT).

1.3.1 Uveal and Corneal Scleral Meshwork

The uveal meshwork is the most proximal layer of the TM and is structured as a cobweb of collagen and elastin lamellae beams sheathed in a thin continuous monolayer of TM cells and oriented radially with large open spaces, also known as Fontana's spaces(48). The middle layer, or corneal scleral meshwork, is comprised of similar components, collagen and elastin, but arranged more tightly in a plate-like fashion with holes(48), and sheathed in TM cells of same continuous fashion. Both proximal layers of the meshwork act as the filtration unit of the eye, removing biological components such as large cellular debris and reactive oxygen species that have been washed away as waste components in the AH. The phagocytic activity of these two layers is critical to the final and most distal layer's, known as the JCT, regulating function. Additionally, these first two layers of the TM also function as a site of antigen presentation and production of histocompatible proteins(29).

1.3.2 Juxtacanalicular Tissue

The most distal and perhaps most OAG influencing layer of the TM is a loose layer of connective tissue that bridges the tighter plate-like network of the corneal scleral layer to the

bordering inner wall of SC or AAP. This loose layer contains TM cells that are sheathed in ECM. This loose bridging tissue and the inner wall of SC/AAP are what regulate the resistance of AH outflow. Like the corneal scleral meshwork, the JCT also has contractility features of smooth muscle actin and myosin. These elastic extensions of smooth muscle reach and terminate at the inner wall of SC/AAP. This feature gives the JCT and SC/AAP the ability to regulate AH outflow resistance by countering tension of the ciliary muscle. As ciliary muscle contracts, it will open up the TM's network thus increasing outflow; when the TM contracts this will counter regulate the outflow by increasing resistance with smaller openings(29).

1.4 Trabecular Meshwork Extracellular Matrix (TM-ECM)

The TM-ECM consists of a multi-protein, loose collagen and elastin fiber filled ground material that embeds the collagen and elastin beams of the TM offering structural support and attachment of TM cells to each other and to SC/AAP endothelial cells. The ECM is responsible for a complex and diverse array of functions and cellular communications(56, 57); and, its molecules have a signature profile that changes to meet the needs of the embedded cells based on their external challenges. These external challenges on the TM-ECM include mechanical forces (e.g., eye rubbing, ocular movements, changes in body position) as well as metabolic, phagocytic and UV radiation stress(29, 57).

The ECM of the JCT and its intimate association to the channel forming inner wall of SC/AAP, is where most of the resistance to AH outflow occurs, and it is thought to be where dysregulation and stiffening develop with age and OAG(48, 58). This interface between the JCT and inner wall of SC/AAP is thought to be the site of increased AH outflow resistance in OAG,

and it is caused by increased deposition, stiffening, or thickening of sheath-derived plaques of the ECM, resulting in an increase in IOP(2, 43, 58, 59).

1.4.1 Mechanisms that Can Change the ECM Profile

The dynamically evolving maintenance profile of the TM-ECM is necessary for preservation of normal outflow facility(57) of AH; however, some biological factors can alter the rate at which ECM regulates deposition and remodeling of itself.

Hormones and cytokines: Transforming growth factor beta-2 (TGF β -2) belongs to the superfamily of transforming growth factors. It is a profibrotic cytokine that can arise from the depletion of TM cells and may contribute to OAG pathogenesis by upregulating expression of elastin, collagen and fibronectin of the TM-ECM(29, 59, 60). TGF β -2 and one of its isoforms, TGF β -1, can also signal connective tissue growth factor (CTGF), which in turn will activate production of ECM proteins - fibronectin and various collagens – modifying the profile to become less elastic and permeable. Additionally, TGF β -2 can change signaling of ECM crosslinking enzymes and genes associated to them such as all five lysyl oxidase (*LOX*) genes(29, 57).

Non-endogenous glucocorticoids (GC), typically received by an individual in the form of a topical steroid therapy, are known to alter the metabolism and cytoskeletal ultrastructure of the ECM as well as gene expression of the cell. Most notably, Myocilin (*MYOC*) is modified by GC, resulting in formation of cross-linked actin networks (CLANs) within the TM cells, thereby decreasing their elasticity and increasing their rigidity(29, 58, 61, 62).

1.5 Schlemm's Canal/Angular Aqueous Plexus

Conventional outflow of AH will cycle fluid back to the primary blood supply by species specific drainage vessels, SC or AAP. Dynamic movement from JCT to either of these trabecular veins can be either paracellular or more commonly transcellular(43) through vacuole-like structures, pores or pinocytotic vesicles, of the inner endothelium. From the SC/AAP, the AH flows via radial collector channels on to the intrascleral venous plexus back to systemic blood supply (45, 48).

1.6 Genetics of OAG

In humans, genome wide association studies have found numerous susceptible loci that contribute to the development of OAG (Table 1.2).

Table 1.2. Genes and Susceptible Loci (40, 63, 64)

Gene/Susceptible Loci	Associated Biological Process	Associated Human Population	Systemic Therapy that Suggestively Benefits Glaucoma	Expressed Outside of the TM
8q22	Non-coding enhancer of both the ciliary body and choroid plexus	United States - European		Yes
<i>ABCA1</i>	Lipid membrane and cholesterol metabolism	Chinese and Australian	Statin Therapy	Yes
<i>AFAP1</i>	ECM modulator	Australian		Not specified
<i>ARHGEF12</i>	Lipid membrane and cholesterol metabolism	European	Statin Therapy	Yes
<i>ATXN2</i>	Neurodegenerative functions	United States - European		Yes
<i>CAV1/CAV2</i>	Development of caveolae invaginations	Iceland		Yes
<i>CDKN2B-AS1</i>	Cell division regulation	Australian and Japanese		Yes
<i>CYP1B1</i>	Monooxygenase involved in phase 1 metabolism	Multiple populations		Yes
<i>FNDC3B</i>	Cytokine signaling for function of ECM	Multiple populations		Yes
<i>FOXC1</i>	Coding for ocular development	United States - European		Yes
<i>GAS7</i>	Cell division regulation	United States - European		Yes
<i>GMDS</i>	First step in the coalescence of GDP-fucose to GDP-mannose	Australian		Yes
<i>NTF4</i>	Survival and differentiation within the nervous system	Not specified		Yes

Table 1.2. (cont'd)

Gene/Susceptible Loci	Associated Biological Process	Associated Human Population	Systemic Therapy that Suggestively Benefits Glaucoma	Expressed Outside of the TM
<i>OPTN</i>	Cellular function trafficking and signaling regulation	Japanese		Yes
<i>PMM2</i>	Marshals the reaction of mannose 6-phosphate to mannose 1-phosphate	Chinese		Not specified
<i>SIX6</i>	Coding for ocular development	United States - European		Yes
<i>TBK1</i>	Phosphorylation of upstream signals for gene transcription	Not specified		Yes
<i>TGFBR3</i>	TGFβ-3 cytokine signaling ECM remodeling	Multiple populations		Yes
<i>TMCO1</i>	Transmembrane calcium channel of the endoplasmic reticulum	Australian		Yes
<i>TXNRD2</i>	Thioredoxin reductase 2 which is responsible for the breakdown of the mitochondrial by product reactive oxygen species	United States - European		Yes
<i>WDR36</i>	T-cell activation	Not specified		Yes

Abbreviations: ECM, extracellular matrix

The genes that have a causative role in OAG in humans are *MYOC*, *optineurin (OPTN)*, *cytochrome P450 1B1 (CYP1B1)*, *neurotrophin 4 (NTF4)*, *Tank-binding kinase 1 (TBK1)* and *WD repeat domain 36 (WDR36)*(2, 63, 65, 66).

MYOC mutations were discovered in 1997 and account for 4% of adult onset OAG(67, 68). The gene's normal function is elusive but the thought on how the mutations initiate and advance OAG is by accumulation of myocilin within the cell. Myocilin should naturally be secreted; however, the mutations related to the gene seem to keep the protein sequestered in the peroxisomes allowing for accrument of myocilin deposits that are thought to be cytotoxic. Cytotoxicity will lead to a depletion of TM cells and as they become less, outflow facility of AH(68) decreases. Additional studies with transgenic mice expressing the same *MYOC* mutations will facilitate the evaluation of the sequestered protein and the effects on healthy TM cells and ECM(68).

OPTN is a gene that is thought to interact with other pathways that arbitrate several cellular functions such as apoptosis, inflammation and morphogenesis(69). It is still unknown what functional role *OPTN* plays in the initiation and development of OAG but it has been associated normal tension glaucoma(2, 69). A possible change in *OPTN* expression leading to OAG could be attributed to the aging eye.

People with *CYP1B1* mutations typically present with congenital or juvenile OAG. Like *OPTN*, the role of *CYP1B1* is still ambiguous but is thought to be a functional factor during ocular development in enzyme metabolism of compounds. The polymorphisms associated with

this gene result in a loss-of-function and decrease in overall numbers of enzymes, subsequently leading to OAG(70).

NTF4 belongs to a family of neurotrophin proteins and is the upstream regulator of tyrosine kinase receptor B (TrkB) phosphorylation. Normal maintenance of this signaling pathway is thought to have neuroprotective qualities, and its disruption caused by *NTF4* mutations negatively affect neuron survival, resulting in OAG(71).

Copy number variants that span the *TBK1* gene are what generate a downstream dysregulation of intermediate kinases that activate protein complex NF- κ B (nuclear factor kappa-light-chain-enhancer of activated B cells). This complex is responsible for numerous cell functions and cytokine responses, and disruption of its expression is believed to be another possible etiology of normal-tensive OAG(72).

Multiple sources seem to concur that genetic multiple variants of *WDR36* are associated with OAG. Still elusive in its overall contribution to OAG, many believe that these variants act as modifying components that contribute to RGC death by apoptosis(66, 73).

Many susceptibility loci and genes can contribute to an OAG phenotype in humans. Animal models of OAG, offer the ability to study disease etiology and contributing pathophysiology while also facilitating the development of novel therapies that can prevent or offset the risk factors that lead to RGC death.

1.7 Animal Models of OAG

Table 1.3, summarizes a wide variety of animal models that have helped in the study of disease mechanism and therapeutic advancements in OAG.

Table 1.3. Animal Models of OAG (74-77)

Species	Mechanistic Mode	Gene or Protein or Colony Associated
Non-human primate	Natural occurring inheritance	Cayo Santiago colony, based in Puerto Rico
	TM scarring by laser photocoagulation	
	IC injection of microbeads	
	IC injection of autologous erythrocytes	
Dog	Autosomal recessive inheritance (natural/spontaneous model)	<i>ADAMTS10</i> mutations(65)
Cat	Autosomal recessive inheritance (natural/spontaneous model)	<i>LTBP2</i> mutation(78)
Mouse	Transgenic (many)	Human <i>MYOC</i> point mutation
		Mutations in collagen type I
		<i>OPTN</i> overexpression
	Corticosteroid induced	
	IC injection of microbeads	
	Limbus scarring by laser photocoagulation	
Rat	Corticosteroid induced	
	IC injection of microbeads	
	Sclerosing scleral vessels	
	TM scarring by laser photocoagulation	
	Cauterization of episcleral veins	
Zebrafish	Genetic mutation	Nonsense mutation <i>Irp2^{-/-}</i> (79)
	Transgenic (many)	<i>WDR36</i>
Rabbit	Corticosteroid induced	
	TM blockage – by rupturing zonular fibers with an intravitreal injection of α -chymotrypsin(80)	
	IC injection of microbeads	
	TM scarring by laser photocoagulation	
Sheep	Steroid induced	
Cow	Steroid induced	
Avian	Light induced	

Abbreviations: IC, intracameral; TM, trabecular meshwork

Animal models are an indispensable tool in biomedical research. While all the models listed (Table 1.3) have their own relevance, the dogs with *ADAMTS10*-OAG offers a predictive and spontaneous model, and are the focus of this thesis. These dogs develop characteristic ECM changes in the AH outflow pathways that are similar to the changes observed in human OAG (65), therefore representing a relevant large animal model.

1.7.1 A Disintegrin and Metalloproteinase with Thrombospondin Motifs (*ADAMTS*) – Canine OAG Models

ADAMTS genes represent a super family of metalloproteinases that have varied roles across the body and are heavily involved in the structure, function and integrity of ECM supramolecular networks(81, 82). These secreted proteinases' genetic framework contains a pro-domain, catalytic domain, and an ancillary domain that are involved in regulating the enzyme's activity associated with ECM composition. Notably, *ADAMTS10* and *ADAMTS17* that are homonymous to respective genes, inhibit appropriate interactions with fibrillin-1 (FBN1) and produce abnormal microfibrils when they are mutated. In humans, *ADAMTS10* mutations result in Weill-Marchesani syndrome (WMS), an autosomal recessive disease. The WMS phenotype consists of short-stature, stunted digits, stiff joints, narrowing of cardiac valves, various lens anomalies including luxation, and glaucoma(82-84). *ADAMTS17* mutations also result in a lack of proper microfibril formation and result in WMS-like syndrome. This WMS-like phenotype shares short-stature and ocular irregularities, like lens luxation and glaucoma with WMS but lacks the cardiac features, stunted digits and joint stiffness. The shared features are suggestive of mechanistic overlap(81, 85).

Several breeds of dogs also have mutations within the *ADAMTS10* and *ADAMTS17* genes, but only a partial phenotypic profile is shared with humans(65), (Table 1.4). And while it is unknown if the dogs feature other sub-clinical attributes (such as body size, joint stiffness or narrowing of cardiac valves) that are clinically expressed in their human counterparts, they typically present within normal limits of health. However, the microfibrillopathies that induce similar clinical ocular anomalies of OAG (*ADAMTS10* mutations in Beagles and Norwegian Elkhound and *ADAMTS17* mutations in some breeds, such as PBGV) and lens luxation (*ADAMTS17* in many breeds, including small terriers) across the many breeds are well documented(65, 86-88).

Table 1.4. *ADAMTS10* Mutation Comparisons(88-92)

Species	Inheritance	Mutation	Domain Location	Phenotype	Expression Outside of the Eye
Human	Autosomal Recessive	Null mutations: non-sense (R237X); splice mutation (1190+1G→A); splice mutation (810+1G→A) Loss of function: missense mutation (73G>A); nonsense mutation (952C>T)	Null mutations: metalloprotease domain Loss of function mutations: 73G>A, peptidase cleavage site; 952C>T, catalytic domain	Short stature; short digits; stiff joints; microspherophakia; ectopia lentis; myopia; glaucoma; occasional cardiac anomalies	Chondrocytes (accounting for short stature and digits); heart (attributing to cardiac defects); skin fibroblast with abnormal extrafibrillar space and increase bundle size of microfilaments (suggests ECM impairment)
Dog	Autosomal Recessive	Missense mutation: G661R (Beagle) Missense mutation: 1441G>A (Norwegian Elkhound)	Beagle mutation: cysteine -rich domain Norwegian Elkhound mutation: metalloprotease domain	Beagle mutation: primary OAG Norwegian Elkhound mutation: secondary lens luxation and primary OAG	Requires continued analysis
Mouse	Induced model	Null allele: Frame-shift mutation in exon 5	Null allele: catalytic domain	Decreased body weight compared to wild-type mice of the same litters; decrease in anterior chamber depth after 2 years of life; subtle increase in alveolarization of alveolar ducts; stiff skin	Limbs: cartilage; bone; skeletal muscle; tendons and skin Thoracic and abdominal parenchyma: lungs and vessels of the heart and liver

Abbreviations: ECM, extracellular matrix; OAG, open-angle glaucoma

ADAMTS10-OAG in Beagles is caused by a missense mutation at amino acid 661 of *ADAMTS10*, where the glycine residue has been substituted for an arginine (G661R)(88). This missense mutation results in sheath derived plaques in the JCT of the TM where it interfaces the AAP(65, 88, 93). These plaque formations create an increase in resistance to AH outflow that subsequently generates an increase in IOP, contributing to the development of glaucoma(93). In Beagles with this mutation, seemingly only OAG is a shared phenotype with humans. It is yet to be known if the other phenotypes listed for humans (Table 1.4) are shared by the dogs on a subclinical level. A well-established colony of Beagles with this deleterious mutation, rendering them a clinically relevant form of OAG is housed at Michigan State University (MSU). This *ADAMTS10*-mutant dog model is the focus species of this thesis as it shares the same molecular obstruction of AHOPs as humans. The advantageous connection of a highly expressed gene in the TM of both dogs and humans(88), poises the canine eye as a significantly relevant large animal OAG model to test the concept of TM-targeted gene therapy.

Advantages of canine ocular disease models: Dogs share many anatomical features of the eye with humans. Outside of a few evolutionary accommodations between the two species, both have eyes that are very similar in size, anatomy, and physiology. In recent years, the canine eye has been used many times as a translatable model for application of drug therapies and diagnostic tools for lateral use in humans(94-100), including AAV-mediated ocular gene therapy, thus supporting the use of this dog model in our study.

1.8 Preservation of Vision by Therapeutic Lowering of IOP

Preservation of vision and the overall comfort and quality of life are the goals in glaucoma therapeutics. Current therapies for all species are limited to lowering IOP, a major

risk factor of glaucoma, and comprise of topical medicines, surgical procedures, or a combination of the two. IOP is lowered by either increasing outflow of AH or by decreasing its production(101).

1.8.1 Current Therapies

Topical medications are a predominant method for both humans and canines in reduction of IOP (Table 1.5). The most effective IOP reducing drug class are prostaglandin analogs, and while the full mechanism of action is elusive, they are known to induce remodeling of the ECM by upregulation of matrix metalloproteinases (MMPs) resulting in an increase in uveoscleral outflow of AH (101). Second-line topical drug classes are β -blockers, alpha2-agonists, and carbonic anhydrase inhibitors. Beta blockers are thought to cause vasoconstriction in the ciliary body, reducing blood supply and therefore decreasing AH production. Alpha2-agonists work similarly in decreasing AH production; however, they additionally can modulate uveoscleral outflow by altering expression of MMPs. Carbonic anhydrase inhibitors also decrease AH production by inhibiting formation of bicarbonate and reducing active secretion. Third-line topicals are parasympathomimetic drugs and are utilized less commonly due to the frequency of needed application within a 24-hour period. These topicals induce miosis via iris sphincter muscle contraction thus allowing for increased conventional outflow(101, 102).

Table 1.5. Traditional Topical Medication Synopsis(101-103)

Drug Class	Mechanism of Action	Target	Side Effects	Drug Example
First Line	Prostaglandin analogs: MMP remodeling of ECM; relaxation of ciliary muscle	Outflow	Conjunctival hyperemia; increase in eyelash length and pigmentation; increased darkening of iris; increased pigmentation of periocular skin;	Latanoprost; travoprost; bimatoprost; tafluprost; unoprostone
Second Line	B-blockers: Adrenoceptors β_1 and β_2 are blocked; ciliary body also experiences vasoconstriction	Production	Bradycardia; exacerbation of heart block with possible cardiac rhythm effects; hypotension; increased intolerance to exercise; depression of central nervous system	Timolol; carteolol; betaxolol; levobunolol; metipranolol
	Carbonic anhydrase inhibitors: Hinders formation of bicarbonate	Production	Blurred vision; fatigue/weakness; bitter/metallic taste and possible associated nausea and vomiting; punctate keratopathy	Dorzolamide; brinzolamide; acetazolamide; methazolamide
	Alpha2-agonists: (rare in use) Alpha2 adrenergic receptors are blocked while prostaglandin expression is increased	Production and outflow	Generalized ocular irritation which can include aching, photopsia/blurring of vision, pruritis and eyelid edema; ocular ischemia and blanching of conjunctiva; vasovagal syncope and hypotension; fatigue; depression and anxiety; headache, dizziness and dry mouth	Apraclonidine; brimonidine
Third Line	Parasympathomimetics: Inducing miosis through contraction of iris sphincter muscle	Outflow	Posterior iris synechiae; cataract development; increased risk for angle closure glaucoma; increased retinal sensitivity along with increased risk for retinal tears and detachments; possible changes to color vision; pupillary stenosis and epiphora; increased gastric secretions with abdominal cramps	Pilocarpine; echothiophate iodide

Abbreviations: MMP, matrix metalloproteinases; ECM, extracellular matrix

Recently emerged topicals on the market include nitric oxide (NO) donors and rho kinase (ROCK) inhibitors. NO donors are one of the first topicals that can have vast effects on the conventional outflow pathway by relaxing and shrinking the cells of the TM(102). The moiety they offer to smooth muscle regulators can also help improve the permeability and dilation of SC(104, 105). ROCK inhibitors also target the conventional outflow pathway by decreasing the rigidity and relaxing TM contraction, thereby opening Fontana's spaces. ROCK inhibitors also reduce ECM synthesis and increase SC permeability resulting in a greater frequency of giant vacuoles as well as widening of the vessel itself(101, 102, 106). Traditional and new classes of topicals can be used in combination to achieve a more effective, multi-parameter approach to IOP reduction.

A multitude of surgical procedures and implants are being used separately or in combination with medical therapies to lower IOP. Just like topical medicine approaches, the ultimate goal of the listed procedures is to alter the production or outflow of AH(43, 107). These procedures include the placement of AH drainage devices, trabeculectomy, laser trabeculoplasty, lens extraction and cyclophotocoagulation (the partial destruction of the ciliary epithelium for reduction of AH production). Recent advances in glaucoma therapy for more effective IOP control include micro-invasive glaucoma surgery (MIGS) and continuous, sustained drug delivery by ocular implants. Despite all these advances, vision loss continues to progress in many glaucoma patients. Non-compliance or nonadherence to prescribed therapies and surgical complications can exacerbate the rate of vision loss(108). A more effective IOP control could be achieved by newer treatments that specifically target underlying disease mechanisms.

1.9 Adeno-Associated Virus (AAV) for Targeted Gene Therapy

Gene therapy is a delivery tool that offers much to the idea of preventative or potentially curative approach to ocular defects. It is a technique that utilizes genetic code to prevent and potentially treat heritable diseases. This therapeutic approach offers the ability to replace or inactivate mutated genes or even introduce a new gene that can combat disease(109). Targeting of the TM with gene therapy that can replace genetic defects causing elevated IOPs could be considered for long-term control of IOP by maintaining open and patent AHOPs.

In the early infancy of TM targeted gene therapy there were several investigations carried-out to determine the appropriate viral vector tool approach that could safely and efficaciously express transgene long-term. Early attempts in targeting the TM, with adenoviruses were successful in species such as rodents, canines and non-human primates; however, their ability to maintain expression was limited to just a few weeks or months(110) which is not sufficient for the duration of effect for a chronic disease like glaucoma. Additionally, lentiviruses (FIV and HIV-1) had been used and successfully expressed in explanted and perfused human trabecular meshwork for 16 days(111) and as long as 10 months when delivered in vivo to cats (lentivirus, FIV)(112).

While adenovirus has had some short-term success and lentivirus proving good long-term success both can come with adverse effects. Adenovirus is associated with generating a robust innate immune response(113) and lentivirus integrates into the genome which risks changes in expression of adjacent genetic code(114). AAV is a nonenveloped parvovirus with low immunogenicity and when stripped of its rep-binding genetic code, loses its ability to

integrate into the host genome. Twelve serotypes and several hybrid combinations of these serotypes have been identified over the decades of research, all allowing for unique benefits in cellular tropism and immune response(115). By the mid-90's, AAV had breakthrough discoveries in its ability to mediate long-term transgene expression(116) making it a viable option for long-term targeted TM gene therapy. This non-pathogenic, safe and efficient delivery tool targets many cell types including in the eye, and even quiescent, post-mitotic cells(117-119). AAV notably, has had a lot of success in safety and efficacy in both pre-clinical and clinical research targeting the retinal disease, *RPE65*-Leber congenital amaurosis (LCA)(94, 120-124). In October of 2017, the Food and Drug Administration's (FDA), Tissue and Gene Therapy Advisory Committee had a unanimous vote to recommend approval of the single-dose treatment of Luxturna, an AAV2 mediated gene therapy targeting *RPE65*-LCA(125). On December 19th, 2017, the FDA released to the press its groundbreaking approval of Luxturna, which is the first ever gene therapy approved to target and treat an inherited genetic mutation(126). While there has been some grand success in retinal approaches with AAV, the initial attempts of using this vector tool to target the TM showed no success in transducing the target tissue across multiple species and human tissue culture(110). Interestingly, pioneering attempts in 2010 by Buie et al., challenged the use of AAV again by approaching with a strategy to transduce living TM cells by utilizing self-complimentary AAV (scAAV). Buie et al. hypothesized that the reason for AAV's failure in past attempts to transduce the TM was because of a rate limiting step at the point of double stranded DNA synthesis. This limitation was thought to be the confounding factor for successful transgene expression. When utilizing scAAV in rats and monkeys this team was able to feature the ability to target multiple

structures in the front of the eye including the TM(127). Additionally, this team also used scAAV to deliver MMP1, a protein thought to be downregulated in steroid responsive individuals, in a steroid induced sheep model of glaucoma and successfully reduced IOP for at least 3 weeks(128).

The ability of AAV capsids to transduce cells depends on their ability to attach to glycans in the vicinity. Serotype AAV2 can bind to heparin sulfate proteoglycans (HSPGs) which are receptors that are very plentiful and integral in the ECM of the TM(129, 130). This serotype was used in both experiments aforementioned by Buie et al and Borrás et al. for successful targeting of the TM(127, 128). The limiting factor of utilizing scAAVs is the reduced cargo capacity of the cassette (131), thus decreasing the size of the transgene within the cassette by half.

Recognizing this limitation, Wang et al. compared the ability of scAAV2 to target both cornea and TM *in vitro* and *in vivo* (mice) with single-stranded (ss) AAV2, AAV8, and the synthetic, capsid mutated AAV Anc80L65. While traditional AAVs were still unsuccessful in targeting the TM the ss synthetic AAV proved capable of overcoming the rate limiting step of second stranded synthesis(92), previously hypothesized by other teams.

Point mutations of specific amino acids on the icosahedral structure of the AAV capsid can alter the affinity of AAV to a specific cell's external profile, allow for evasive maneuvering for avoidance of the proteasome while in the cytoplasm, and adjust capsid stability for appropriate breakdown once in the nucleus(132, 133). Bogner et al. used these capsid mutations in varying degrees to improve transduction efficiency of traditional AAVs to the TM(134). Given AAV2's natural affinity to HSPGs and previous success in transduction of the retina and TM, it along with AAV8 (an AAV that lacks the receptor affinity to HSPG but has

targeting capability to other anterior eye structures where HSPGs are present) were used as parent serotypes to test different mutant capsid structures. These mutations were acquired by modifying surface exposed amino acid tyrosine (Y) to phenylalanine (F). Utilizing rodent cohorts, these scAAVs and varying mutations (Table 1.6) were equipped with reporter gene, *humanized green fluorescent protein (hGFP)* and injected IC. Cohorts that utilized *scAAV2-(Y444F)-hGFP* and *scAAV2-(Y444+500+730F)-hGFP* had the most success in transducing the AHOPs(134).

These two successful vector constructs from the Bogner et al. team, were then moved forward into higher order species (canine) studies with *wild type* and mutant *ADAMTS10-OAG* Beagles(135). Given the size of the *ADAMTS10* gene, the full cargo capacity of AAV is required to deliver the entire sequence of the replacement gene. Therefore, ssAAV was utilized to deliver both reporter gene (*hGFP*) and therapeutic trials of *human ADAMTS10 (hADAMTS10)*. Of the vector constructs trialed for TM targeting capabilities, only one construct was successful. IC injections of *ssAAV2-(Y444F)-hGFP* in both *wild type* and *ADAMTS10-OAG* Beagles (at doses 10^8 - 10^{10} vector genomes (vg)) successfully targeted transgene expression to the TM (135). However, during therapeutic trials of this single mutated capsid construct, *ssAAV2-(Y444F)-hADAMTS10* with doses similar to the *ssAAV2-(Y444F)-hGFP* trials (10^{10} vg delivered IC) did not result in a therapeutic IOP lowering effect(136). It was hypothesized that a therapeutic response could potentially be achieved with a dose escalation of the single mutant capsid construct.

1.10 Purpose

The purpose of our study was to further develop the single capsid mutant gene therapy vector *ssAAV2-(Y444F)* for treatment of OAG by (Aim 1) optimizing the targeting of transgene expression to the canine AHOPs, including the TM, and (Aim 2) modifying gene expression by gene replacement therapy within the AHOPs in order to achieve a therapeutic effect in a clinically relevant and well-established canine model of *ADAMTS10*-OAG.

Table 1.6. Capsid Mutations Investigated by Bogner et al.(134)

scAAV	Number of Mutated Surface Exposed Amino Acids	Site of Amino Acid	Gene	Full Construct
2	1	444	<i>hGFP</i>	<i>scAAV2-(Y444F)-hGFP</i>
	3	444, 500, 730		<i>scAAV2-(Y444+500+730F)-hGFP</i>
	7	252, 272, 444, 500, 700, 704, 730		<i>scAAV2-(Y252+272+444+500+700+704+730F)-hGFP</i>
8	1	733		<i>scAAV8-(Y733F)-hGFP</i>

Abbreviations: *hGFP*, human green fluorescent protein

CHAPTER 2 – Materials and Methods

2.1 Study Design

2.1.1 Aim 1 – Targeting the AH outflow pathway – *hGFP*

Because of our previously failed attempts to achieve an IOP-lowering, therapeutic effect(136), the goal of Aim 1 (targeting) was to improve transgene expression within the ICA by increasing vector dose and optimizing administration techniques, most importantly intracameral (IC) vs. intravitreal (IVit) injection and variation of pupil size with IC injection. Utilizing *ssAAV2-(Y444F)-hGFP*, we injected either IC or IVit, 14 eyes across 9 normal dogs (Table 2.1). These dogs were then clinically followed for 5-20 weeks. The following techniques were used to closely monitor safety: slit lamp biomicroscopy, indirect ophthalmoscopy and gonioscopy. Immediately after the 5-20 week time-frame, eyes were collected and evaluated by immunohistochemistry (IHC) for *hGFP* reporter gene expression. Additionally, to optimize our IC injection techniques, we injected 10 eyes across 5 normal, healthy dogs with fluorescein solutions and immediately monitored distribution within the anterior chamber.

2.1.2 Aim 2 – Therapeutic delivery - *ssAAV2-(Y444F)-hADAMTS10*

Applying the optimal injection technique developed under Aim1, three *ADAMTS10*-mutant Beagles with early stages of *ADAMTS10*-OAG were treated unilaterally by IC injections of *ssAAV2-(Y444F)-hADAMTS10*, leaving the fellow eye as an untreated control. The dogs were clinically followed for 62-105 weeks. The main outcome measured was weekly diurnal IOP by rebound tonometry. The following additional techniques were used to closely monitor efficacy and safety: slit lamp biomicroscopy, indirect ophthalmoscopy, gonioscopy, pneumotonography (AH outflow facility), fluorophotometry (AH flow), high-resolution imaging of the anterior and

posterior segments by optical coherence tomography (OCT) and ultrasound biomicroscopy (UBM), A-scan ultrasonography (globe size), pachymetry (central corneal thickness, CCT), and electroretinography (ERG; retinal function). AH and serum samples were collected throughout the post-injection period to measure protein concentration, cell counts and neutralizing AAV antibody (NAb) titers.

2.2 Animals

All dogs (Table 2.1) were group-housed in the MSU College of Veterinary Medicine's Vivarium with a 12-hour light-dark cycle. This facility is accredited by the Association for the Assessment and Accreditation of Laboratory Animal Care International (AAALAC). All performed procedures were approved by the MSU Institutional Animal Care and Use Committee (IACUC) and done in accordance with the Association for Research in Vision and Ophthalmology (ARVO) statement on the use for Animals in Ophthalmic and Vision Research. Purpose-bred, normal dogs (n=14) aged 4.9-33 months (Marshall BioResources, North Rose, NY, USA) and *ADAMTS10*-mutant beagle dogs (n=3) aged 21-25.5 months old were used in this study. All MSU-bred dogs from the *ADAMTS10*-mutant line were genotyped to determine the genotype regarding the G661R *ADAMTS10*, autosomal recessive, missense mutation(137).

Table 2.1. Aim 1 and 2 Study Participants

Dog ID	Gender	Status	Age at injection (months)	Vector/Study Assignment	Eye treated
Ja55	M	Normal	5.1	<i>ssAAV2-(Y444F)-hGFP</i>	OD
Ja76	M		4.9		OD
Es12	M		4.9		OS
St80	M		5.1		OS
Na25	M		6.5		OU
Me66	F		6.5		OU
Wi43	F		6.5		OU
Cl24	F		6.5		OU
Su01	F		6.5		OU
Ba84	M		11.5		100mg/mL Fluorescein
Ma32	M		22	100mg/mL Fluorescein	OU
Tu63	F		33	0.2mg/mL Fluorescein	OU
La98	F		33	0.2mg/mL Fluorescein	OU
Ha57	M		16	0.2mg/mL Fluorescein	OU
Ep00/Dog 1	M	<i>ADAMTS10-mutant</i>	21	<i>ssAAV2-(Y444F)-hADAMTS10</i>	OS
Em40/Dog 2	M		25.5		OS
El42/Dog 3	M		25.5		OD

Abbreviations: OD, right eye. OS, left eye. OU, both eyes.

2.3 Anesthesia Protocols

Most clinical evaluation techniques, such as routine ophthalmic examination, tonometry, pachymetry, gonioscopy and UBM required no anesthesia. Pneumotonography and fluorophotometry required only light sedation with a single intravenous (IV) injection of 0.3mg/kg of butorphanol tartrate (Henry Schein Animal Health, Dublin, OH, USA) and 0.3mg/kg of midazolam HCl (Hospira, Inc., Lake Forest, IL, USA). Dogs received either an oral dose of 4mg of ondansetron (Heritage Pharmaceuticals Inc., Eatontown, NJ, USA) up to one hour prior to delivery of sedation or an IV dose of 0.25mg/kg ondansetron within 5 minutes of sedation for relief of any nausea that may have been associated with sedation. If additional sedation was

needed for either procedure, butorphanol tartrate was re-administered at a 0.1mg/kg dose and never exceeding a total amount of 0.5mg/kg. General anesthesia was utilized to immobilize the dogs for longer periods of time and the need to control eye positioning. For ERG and OCT, dogs were premedicated with acepromazine maleate IV at 0.02mg/kg (Butler Schein Animal Health, Dublin, OH, USA), followed by aseptic placement of a peripheral IV catheter (either cephalic or saphenous vein), IV induction with propofol (PropoFlo™28, Abbott Laboratories, North Chicago, IL, USA) at 4mg/kg or to effect and maintenance with inhalant isoflurane (Akorn Inc., Lake Forest, IL, USA) in O₂. A-scan measures were performed at the end of OCT under general anesthesia. For longer procedures like ERG and OCT, dogs were given IV replacement fluids (Normosol-R, Hospira Inc., Lake Forest, IL, USA) at 5-10mls/kg/hour as needed based on preliminary physical examination findings (hydration status was assessed by capillary refill time, tackiness of gums, skin turgor and other general overall appearances such as a dry nose) and intra-procedure blood pressure measurements. For intraocular injections or aqueous paracentesis, dogs were premedicated with buprenorphine hydrochloride (HCl) (Par Pharmaceutical, Chestnut Ridge, NY, USA) at 0.015mg/kg and acepromazine maleate at 0.02mg/kg either IV or intramuscularly (IM), followed by aseptic peripheral catheter placement, IV induction and maintenance with propofol. Dogs that participated in a short study to optimize IC injection technique with fluorescein were premedicated as previously noted for IC injections, followed by aseptic placement of an IV catheter and then delivered induction and maintenance anesthesia as described for ERG and OCT.

2.4 Clinical Examination

For safety assessment and measure of any adverse effect, all animals received baseline and regularly scheduled ocular examination by a boarded veterinary ophthalmologist. Immediately post IC injections, examinations were performed daily for up to one week, followed by weekly for up to one year, then followed monthly for the remaining duration of follow-up examinations. Each exam consisted of slit-lamp biomicroscopy, indirect ophthalmoscopy and rebound tonometry (TONOVET, iCare). CCT was measured monthly by pachymetry (PachPen, Accutome Inc.). Gonioscopy (RetCam II, Clarity) was performed monthly. Lastly, UBM (UBM Plus[®], 48MHz, Accutome Inc.) was performed at least once over the duration of the study for assessment of safety.

2.4.1 Diurnal IOP – primary outcome measure

All *ssAAV2-(Y444F)-hADAMTS10* treated dogs had diurnal IOPs measured by rebound tonometry once a week. Consistently on the same day each week, at the same morning (8am), noon (12pm) and early evening (4pm) times, we evaluated both treated and untreated eyes for variable ranges and up to 105 weeks. Each eye was measured for a total of 6 single values at each of the three time points. Single values were calculated by the iCare TONOVET following 6 rebound measures; the device excludes the 2 most extreme outliers and averages the remaining 4 measures. Daily averages for each eye were calculated from the 18 single values. These daily values were compared between treated and non-treated eyes in a generalized linear model and estimating equation. At completion, statistical analysis included a fitted trendline of these average daily IOPs over time. For this, values were obtained using the non-parametric LOESS curve fitting method(138) and corresponding confidence intervals (CI)

determined with Bonferroni correction of multiple comparisons, set at $1-\alpha=0.99$. Testing for significant changes in IOP was done by calculating the difference in daily average IOPs between the treated and the untreated eye. From the difference, a fitted trendline was again obtained with corresponding CIs. Calculated differences that were considered significant, when $\alpha\leq 0.01$, were for values that had CIs not containing the number zero (values would have to be less or greater than zero).

2.4.2 Pachymetry

Once monthly CCT was measured by pachymetry. Each eye was locally anesthetized with proparacaine HCl 0.5% ophthalmic solution (Akorn Inc., Lake Forest, IL, USA), and the pachymeter placed perpendicularly on the central cornea. The instrument measured 9 individual readings, discarding the most extreme outlier and averaging the remaining 8 for a single value. Percent variation of CCT was calculated for the duration of the study as $((\text{highest reading across study timeline} - \text{lowest reading across study timeline}) / \text{lowest reading across study timeline}) \times 100$ (139, 140).

2.4.3 Gonioscopy

Monthly gonioscopy was performed (141) to ensure that the ICA remained open and does not show any signs of AAV-associated adverse effects. Proparacaine HCl 0.5% ophthalmic solution was applied for ocular surface anesthesia, followed by ultrasound gel (Sonotech Clear Image, Medium Viscosity, A Division of Illinois Tool Works Inc., Bellingham, WA, USA) for optimal contact between the RetCam lens and the cornea for viewing of the ICA. Inferior, temporal, superior and nasal quadrants were assessed separately.

2.4.4 Ultrasound biomicroscopy (UBM)

Assessment of the ciliary cleft and surrounding structures was done by high-resolution, cross-sectional UBM(142). Dogs rarely needed sedation with 0.02mg/kg of acepromazine maleate IV. Ocular surface anesthesia was applied with topical proparacaine HCl 0.5% ophthalmic solution prior to application of ultrasound gel and covered probe tip emerged in sterile water.

2.5 AAV Production

The two recombinant AAV2 vectors, *ssAAV2-(Y444F)-GFP* and *ssAAV2-(Y444F)-hADAMTS10*, were designed and manufactured as previously described by Dr. Shannon Boye's laboratory at the University of Florida(143, 144). The surface-exposed capsid amino acid 444 was modified from a tyrosine (Y) to a phenylalanine (F) on the AAV helper plasmid containing AAV2 "Cap". Because no TM-specific promoter was available to drive gene expression, vectors were assembled with a ubiquitous small chicken β -actin promoter (smCBA). The small size of the promoter permitted fitting of the larger *hADAMTS10*, cDNA. Generation of vectors was done by plasmid co-transfection in HEK293T cells. Further purification and concentration of nuclear and cytoplasmic fractions was accomplished with iodixanol (Sigma-Aldrich, St. Louis, MO, USA) gradient centrifugation and ion exchange column chromatography (HiTrap Sp Hp 5 mL, GE Healthcare Bio-Sciences, Piscataway, NJ, USA). Final vector titers were established by real-time PCR and purity was met by use of silver-stained sodium dodecyl sulfate-polyacrylamide gel electrophoresis. Final aliquots of *ssAAV2-(Y444F)-hGFP* were resuspended in sterile balanced salt solution (BSS, Alcon Laboratories, Fort Worth, TX, USA) containing 0.014% Tween 20; *ssAAV2-(Y444F)-hADAMTS10* was resuspended in sterile BSS/0.014% Tween

supplemented with NaCl, we termed high salt solution (HSS), to increase the ionic strength of the suspension so to reduce self-aggregation of AAV2(145). BSS/0.014% Tween 20 suspension has a concentration established at ~300mOsm, when supplemented with NaCl the concentration will increase to ~600mOsm.

The ~3.3 kb *hADAMTS10* amino acid code for the therapeutic vector, was synthesized according to Genbank accession number NM_030957, with an addition of a consensus 'Kozak' sequence as well as a silent G to A change at nucleotide 3150. This resulted in a full mRNA of about 4.3 kb, including 5' and 3' untranslated regions. Due to the functionally efficient cargo capacity of AAV (4.1-4.5 kb) (119), untranslated regions were dropped to achieve a more efficacious fit. The substitution of G to A resulted in a loss to internal restriction enzyme Not I. Following a Not I/Sal I digest, the synthesized cDNA sequence was finally cloned into the AAV vector plasmid containing the smCBA promoter.

2.6 Intraocular injections – IC and IVit

2.6.1 ssAAV2-(Y444F)-hGFP and ssAAV2-(Y444F)-hADAMTS10

The AAV vectors varied in genetic contents (*hGFP* vs. *hADAMTS10* transgene), total virus particles and volume delivered (Table 2.2). As described under study design, treatments with AAV were staged over two aims 1) targeting and 2) therapeutics. Because of our previously failed attempts to achieve an IOP-lowering, therapeutic effect(136), the goal of Aim 1 (targeting) was to improve transgene expression within the ICA by increasing vector dose and optimizing administration techniques, most importantly IC vs. IVit injection and variation of pupil size with IC injection. Normal dogs that were used for Aim 1 had either one randomly selected eye or both eyes injected (Table 2.2) with ssAAV2-(Y444F)-hGFP. Additionally, to

optimize our IC injection techniques, we injected, *in vivo*, 10 eyes of 5 normal, healthy dogs with fluorescein solutions and immediately monitored distribution within the anterior chamber (see 2.6.2 Optimizing Injection Technique).

Applying the optimal injection technique developed under Aim1, 3, *ADAMTS10*-mutant Beagles were selected for Aim 2 (therapeutics) with 1 eye per dog randomly chosen for ssAAV2-*(Y444F)-hADAMTS10*, leaving the fellow eye as an untreated control (Table 2.2).

Table 2.2. *hGFP* and *hADAMTS10* Dosing Assignments

Dog ID	Gender	Vector/Study Assignment	Eye treated	Dose - Vector Genomes (vg)	Vehicle	Volume	Route	Pupil Size
Ja76	M	<i>ssAAV2-(Y444F)-hGFP</i>	OD	1x10 ⁹ vg	BSS/0.014% Tween	50µL	IC	
St80	M	<i>ssAAV2-(Y444F)-hGFP</i>	OS	1x10 ¹⁰ vg	BSS/0.014% Tween	50µL	IC	
Ja55	M	<i>ssAAV2-(Y444F)-hGFP</i>	OD	1x10 ¹¹ vg	BSS/0.014% Tween	50µL	IC	
Es12	M	<i>ssAAV2-(Y444F)-hGFP</i>	OS	1x10 ¹¹ vg	BSS/0.014% Tween	50µL	IC	
Na25	M	<i>ssAAV2-(Y444F)-hGFP</i>	OD	2.78x10 ¹² vg	BSS/0.014% Tween	50µL	IC	mydriatic
		<i>ssAAV2-(Y444F)-hGFP</i>	OS	2.78x10 ¹² vg	BSS/0.014% Tween	50µL	IC	
Me66	F	<i>ssAAV2-(Y444F)-hGFP</i>	OD	2.78x10 ¹² vg	BSS/0.014% Tween	50µL	IC	
		<i>ssAAV2-(Y444F)-hGFP</i>	OS	2.78x10 ¹² vg	BSS/0.014% Tween	50µL	IC	miotic
Wi43	F	<i>ssAAV2-(Y444F)-hGFP</i>	OD	2.78x10 ¹² vg	BSS/0.014% Tween	50µL	IVit	
		<i>ssAAV2-(Y444F)-hGFP</i>	OS	2.78x10 ¹² vg	BSS/0.014% Tween	50µL	IVit	
Cl24	F	<i>ssAAV2-(Y444F)-hGFP</i>	OD	2.78x10 ¹² vg	BSS/0.014% Tween	50µL	IC	mydriatic
		<i>ssAAV2-(Y444F)-hGFP</i>	OS	2.78x10 ¹² vg	BSS/0.014% Tween	50µL	IC	miotic

Table 2.2. (cont'd)

Dog ID	Gender	Vector/Study Assignment	Eye treated	Dose - Vector Genomes (vg)	Vehicle	Volume	Route	Pupil Size
Su01	F	<i>ssAAV2-(Y444F)-hGFP</i>	OD	5.56x10 ¹² vg	BSS/0.014% Tween	100µL	IC	
		<i>ssAAV2-(Y444F)-hGFP</i>	OS	5.56x10 ¹² vg	BSS/0.014% Tween	100µL	IC	
Ep00	M	<i>ssAAV2-(Y444F)-hADAMTS10</i>	OS	1.25x10 ¹² vg	HSS	75µL	IC	
Em40	M	<i>ssAAV2-(Y444F)-hADAMTS10</i>	OS	1.43x10 ¹² vg	HSS	75µL	IC	
EI42	M	<i>ssAAV2-(Y444F)-hADAMTS10</i>	OD	1.43x10 ¹² vg	HSS	75µL	IC	

Abbreviations: OD, right eye; OS, left eye; BSS, balanced salt solution; HSS, BSS high salt solution

Pre- and post-operative standard of care protocols with ophthalmic medications were given bilaterally to all dogs, so not to bias IOP readings. In order to prevent post-injection ocular hypertension following the IC or IVit injection of reagent without the need of an additional aqueous paracentesis, the eyes were pretreated with the IOP-lowering glaucoma medication dorzolamide hydrochloride-timolol maleate (Bausch & Lomb Inc., Tampa, FL, USA). Pre-injection treatment also included the topical non-steroidal anti-inflammatory drug flurbiprofen sodium 0.03% (Bausch & Lomb Inc., Tampa, FL, USA), the topical steroid prednisone acetate 1% (Pacific Pharma, Irvine, CA, USA) and the systemic steroid prednisolone administered orally and tapered over 3 weeks post-injection (Henry Schein Animal Health, LLOYD Inc., Shenandoah, IA, USA; 1 mg/kg, twice daily for 7 days, then once daily for 8 days, then once every other day for 6 days). For eyes that enrolled in Aim 1 requiring alteration of pupillary aperture, were either pre-treated with topical latanoprost 0.005% ophthalmic solution (Bausch & Lomb Inc., Tampa, FL, USA) to induce miosis or topical tropicamide 1% ophthalmic solution (Akorn, Inc., Lake Forest, IL, USA) to induce mydriasis. Treatment with the systemic antibiotic amoxicillin/clavulanic acid (Clavamox[®], GlaxoSmithKline, Zoetis Inc., Kalamazoo, MI, USA; orally, at 14-22mg/kg, twice daily) was started before the injection and continued for 7 days to minimize the risk of bacterial infections.

Anesthesia protocols were followed as previously described (see 2.3 Anesthesia Protocols). Once a surgical plane of anesthesia was achieved, dogs were placed in sternal recumbency. While procedures were very short, body temperature was thermo-regulated by a warm water circulating blanket (T/Pump[®], Gaymar Industries Inc., Orchard Park, NY, USA). Patient parameters (heart rate, oxygen saturation, end-tidal CO₂, respiratory rate and blood

pressure) were assessed by hand and a patient monitor (PM-9000Vet, Shenzhen Mindray Bio-Medical Electronics Co., Ltd., Nanshan, Shenzhen, China). Ocular surface and periocular skin of the treatment eye was prepped aseptically with 0.2% dilute povidone-iodine solution (Poviderm™ Solution, Henry Schein Animal Health, Dublin, OH, USA) then topically anesthetized with proparacaine HCl 0.5% ophthalmic solution. Conjunctival stay sutures (4-0 silk; Ethicon Inc., San Lorenzo, Puerto Rico, USA) were placed near the superior and inferior limbus at the 12 and 6 o'clock positions to assist with stability and gaze of the eye. Prepared vector was delivered via insulin syringe (30 gauge x 1/2 inch needle; BD Insulin Syringes with BD Ultra-Fine™ needle, BD, Franklin Lakes, NJ, USA) by IC injection at the superior-temporal limbus. The scleral-limbal margin was visualized with use of a binocular loupe (EyeMag Pro, Carl Zeiss Inc., Oberkochen, Germany) with illumination. The anterior chamber was entered in an oblique angle to the iris surface by tunneling the needle over several millimeters through the conjunctiva, sclera, and cornea, starting posterior to the limbus. Once the 50-75 µL vector solution was delivered, the needle remained in place for up to 10 minutes to reduce leakage of any AH containing virus particles on exit. Upon removal of the needle, the surrounding conjunctiva was held closed by 0.12mm Castroviejo forceps for 2 minutes in order to further prevent leakage. IVit injections followed a similar protocol; however, the injection entry was premeasured to 6 mm posterior of the dorsolateral limbus at the location of the pars plana of the ciliary body. Post-operatively, a 4-mg subconjunctival injection of triamcinolone acetonide suspension was administered (Kenalog®-40, Bristol-Myers Squibb Company, Italy) followed by neomycin-polymyxin B sulfates--dexamethasone 0.1% ophthalmic ointment (Bausch & Lomb Inc., Tampa, FL, USA). Post injection treatment was continued with twice daily topical

application of the latter ointment for 21 days and then tapered to once daily for 5 days. For dogs participating in Aim 2, an initial attempt to discontinue the topical steroid dexamethasone resulted in minor anterior uveitis in the AAV-injected eyes; hence, topical steroid therapy was continued in both eyes with twice-daily administration of 0.05% difluprednate ophthalmic emulsion (Durezol®; Alcon Laboratories Inc., Fort Worth, TX, USA) or neomycin-polymyxin B sulfates-dexamethasone 0.1% ophthalmic ointment (Bausch & Lomb Inc., Tampa, FL, USA) for the duration of study. In order to minimize the development of steroid keratopathy/corneal degeneration, the twice daily topical steroid treatment was combined with 0.2% topical cyclosporine ointment (Optimmune®, Intervet International B.V., Merck Animal Health, France).

2.6.2 Optimizing Injection Technique

Between Aims 1 and 2 a short fluorescein kinetics of the anterior chamber study was performed to assess the full circumferential reach of the ICA following a one-time IC injection. This short study was performed in two stages to assess the following parameters: body and globe position, temperature of reagent, and vehicle suspending reagent (Table 2.3). All normal dogs that participated followed the previously described anesthetic protocol for the short fluorescein kinetics study (see 2.3 Anesthesia Protocols) as well as the pre-operative ophthalmic drop protocols as described for dogs participating in Aims 1 and 2 (see subsection 2.6.1 *ssAAV2-(Y444F)-hGFP* and *ssAAV2-(Y444F)-hADAMTS10*). The post-operative care protocol for this study was less intense than following AAV injections since no protein or virus was administered. The dogs received a one-time subcutaneous 4.4-mg/kg injection of non-steroidal anti-inflammatory drug carprofen (Rimadyl®, Zoetis LLC., Lincoln, NE, USA) and a one-time topical application of neomycin-polymyxin B sulfates-dexamethasone 0.1% ophthalmic ointment. The

fluorescein kinetics study procedures mimicked the following parameters of Aims 1 and 2: aseptic preparation of the ocular surface and periocular skin, visualization and delivery approach, IC delivery of reagent, volume delivered and needle track closure. All chamber distributions were monitored immediately upon injection and followed every two minutes for 10 minutes. Image acquisition at each injection and consecutive time points was by use of a modified (full spectrum) dSLR camera, dSLR camera adaptor, and camera lens. The camera for digital acquisition used was a Canon 7D (Canon, Tokyo, Japan) with lens (Canon EF 85 mm f/1.4L USM lens). For conducting angiography, excitation and barrier filters were inserted within the illumination and optical pathways of the adaptor, respectively. Camera settings used included a shutter speed of 1/100 second, effective aperture of f/8, and a sensitivity (International Standards Organization) setting of 200. The excitation filter was MF479/40 nm (Thorlabs, Newton, NJ, USA) with peak transmission centered at 479 nm with a width of 40nm and barrier MF525/39 nm (Thorlabs, Newton, NJ, USA) with peak transmission centered at 525 nm and width of 39 nm.

Two dogs participated in STAGE ONE, which focused on body position and globe stability. Both eyes of these dog were IC injected with 50 μ L of 10% fluorescein (Fluorescite; Alcon Inc., Fort Worth, TX). The first dog (Ma32, Table 2.3) in our standard IC injection technique where the head is placed in an up-right position, similar to Aim 1 and 2. The second dog (Ba84, Table 2.3) was first placed in dorsal recumbency with head positioning so that the iris surface was in a horizontal plane; this is consistent with the positioning for cataract surgery/phacoemulsification. The first eye was maintained in forward gaze position by conjunctival stay sutures (5-0 Ethilon, Ethicon Inc., San Lorenzo, Puerto Rico, USA). Once the

injection and imaging of the first eye was completed, the dog was positioned in lateral recumbency and the second eye was stabilized by a retrobulbar saline injection (0.9% Sodium Chloride, Hospira Inc., Lake Forest, IL, USA). Immediately after injection of the second eye, the dog was rotated from left to right lateral positions every 1-2 minutes for the duration of 10 minutes.

Three dogs participated in STAGE TWO, focusing on vehicle and temperature of the preparation. Each dog was randomly assigned to a preparation vehicle that was either BSS, BSS containing 0.014% Tween 20, or HSS. Vehicles were used to dilute fluorescein to a 0.2mg/mL concentration and each vehicle dilution had a 37°C (body temperature) and cold temperature (~4°C on ice, standard temperature of AAV in vehicle due to survivability of vector through transport and storage) preparation. Standard protocol for IC injections described under Aims 1 and 2 were followed. The right eyes of all dogs received a 37°C, 50-µL IC injection of their assigned vehicle with fluorescein dilution while all fellow left eyes received a 50-µL IC injection of the cold preparation of that same vehicle dilution (Table 2.3).

Images taken in this study were assessed qualitatively as a function of time to determine how well/uniform the injected reagent distributes within the anterior chamber.

Table 2.3. Fluorescein Kinetics of the Anterior Chamber Assignments

Stage	Dog ID	Eye	Fluorescein Concentration	Vehicle; Volume	°C	Body Position	Globe Stability	Pupil Size
1	Ma32	OD	100mg/mL	n/a; 50µL	37°C	Standard IC injection technique	5-O Ethilon stay sutures	Atropine mydriasis
		OS	100mg/mL	n/a; 50µL	37°C	Standard IC injection technique	5-O Ethilon stay sutures	Atropine mydriasis
	Ba84	OD	100mg/mL	n/a; 50µL	37°C	Left lateral recumbency, rotating lateral recumbency every 1-2 minutes for 10 minutes	Retrobulbar injection of saline	Atropine mydriasis
		OS	100mg/mL	n/a; 50µL	37°C	Dorsal recumbency; head position, perpendicular from body	5-O Ethilon stay sutures; eye gaze to ceiling	Atropine mydriasis
2	Tu63	OD	0.2mg/mL	BSS; 50µL	37°C	Standard IC injection technique	4-O Silk stay sutures	
		OS	0.2mg/mL	BSS; 50µL	4°C	Standard IC injection technique	4-O Silk stay sutures	
	La98	OD	0.2mg/mL	BSS/0.014% Tween; 50µL	37°C	Standard IC injection technique	4-O Silk stay sutures	
		OS	0.2mg/mL	BSS/0.014% Tween; 50µL	4°C	Standard IC injection technique	4-O Silk stay sutures	
	Ha57	OD	0.2mg/mL	HSS; 50µL	37°C	Standard IC injection technique	4-O Silk stay sutures	
		OS	0.2mg/mL	HSS; 50µL	4°C	Standard IC injection technique	4-O Silk stay sutures	

Table 2.3. 37°C, room temperature. 4°C, cold preparation. Atropine sulfate 1% ophthalmic solution (Akorn, Inc., Lake Forest, IL, USA) 1 drop OU was given post-injection for one-time preventative treatment of uveitis. Abbreviations: n/a, not applicable

2.7 Aqueous Humor Outflow Facility - Pneumotonography

In order to determine if any IOP-lowering therapeutic effect was based on an increase in conventional AH outflow, outflow facility was measured in the three dogs of Aim 2 by use of pneumotonography (Reichert Technologies, Reichert Inc., Depew, NY, USA)(146). Dogs were sedated as previously described (see 2.3 Anesthesia Protocols) followed by application of one drop of 0.5% proparacaine HCl ophthalmic solution to each eye for ocular surface anesthesia. With use of a calibrated pneumotonograph, a seated and supine IOP was measured for one eye. The dog would remain in a supine position by gentle restraint, while a 10-gram weighted sensor head placed on the cornea recorded the IOP continuously for a duration of 2 or 4 minutes. The fellow eyes followed the same order of events and were measured immediately after the first eye. The ocular surface moisture/hydration was maintained by repeated topical administration of BSS as necessary.

The print outs of the tonography recordings (change in IOP over 2 or 4 minutes) were scanned into CurveSnap software for windows (Softonic, Softonic International S.A., Edificio MediaTIC, Barcelona, Spain) for analysis of the digitized IOP scans by Excel (Microsoft® Office Excel, Windows 10, Redmond, WA, USA). Starting (time 0) and ending IOPs (time 2 or 4 minutes) read from the digitized plot, along with the seated and supine IOPs captured at the time of the recording, were then entered into the pneumotonograph to calculate outflow facility. Because the pneumotonograph was not available for baseline measurements, AH outflow facility values were compared between treated and untreated eyes in each dog.

2.8 Aqueous Humor Flow - Fluorophotometry

AH flow was measured by fluorophotometry (Fluorotron Master II, Ocumetrics, Inc., Mountain View, CA) in Aim 2 in order to determine the effect of AAV gene therapy on AH turnover. Performance of scans were done as previously described by others (147-150). A 20 μ L drop of 10% fluorescein (AK-FLUOR[®] 10%, Akorn, Inc., Lake Forest, IL, USA) was applied to the corneal surface of each eye followed 5 minutes later by a thorough flush with sterile eye wash (Ophthalmic solution eyewash, Akorn, Inc., Lake Forest, IL, USA). Four hours elapsed to allow establishment of equilibrium of fluorescein concentrations within the cornea and anterior chamber. Dogs were sedated as previously described (see 2.3 Anesthesia Protocols) and placed into sternal recumbency. They were then gently held in place in front of the optic head of the Fluorotron instrument for fluorophotometric scans. Duplicate scans were performed and averaged at four time points in 45-minute intervals for each eye. Because the fluorophotometry was not available for baseline measurements, AH flow was compared between treated and untreated eyes in each dog.

2.9 Optical Coherence Tomography (OCT) and A-scan Biometry

High-resolution imaging by OCT (Heidelberg Spectralis, Heidelberg Engineering Inc., Heidelberg, Germany) of cornea, retina, and ONH was performed to assess any adverse events and natural progression of glaucoma in dogs of Aim 2. IOPs were measured by rebound tonometry followed by application of one drop of tropicamide 1% ophthalmic solution for pupil dilation in order to optimize visualization of the ocular fundus. Dogs were anesthetized as previously described (see 2.3 Anesthesia Protocols) and placed in sternal recumbency with their heads stabilized on an adjustable platform (headrest) to a custom-designed examination table.

Rebound tonometry of each eye was repeated to verify that mydriasis did not result in any egregious IOP spikes. The ocular surface of one eye was then anesthetized with 0.5% proparacaine HCl ophthalmic solution, and positioned with conjunctival stay sutures as previously described with 4-0 Silk, while the fellow eye was held closed by medical tape to prevent drying of the cornea. The cornea of the imaged eyes were kept moist by repeated application of BSS sterile irrigating solution (Alcon[®], Alcon Laboratories, Fort Worth, TX, USA). Once imaging was complete, A-scan biometry (A-scan; Scanmate, DGH Technology) was performed for evaluation of total axial length, anterior chamber depth, lens thickness, and vitreous chamber depth. Subsequently, the fellow eye was examined and once complete, both eyes were treated with latanoprost 0.005% ophthalmic solution to reverse the pupil dilation and any potentially associated adverse IOP spikes. ONH cross sections were compared subjectively between treated and contralateral untreated eyes.

2.10 Electroretinography (ERG)

Photopic full-field ERGs (RETI-port, Roland Consult) were recorded for assessment of retinal function loss, specifically photopic negative responses (PhNR) representing RGC function in the 3 dogs of Aim 2 (151, 152). As described for OCT, all dogs had rebound tonometry performed before and after application of tropicamide 1% ophthalmic solution for pupil dilation. All dogs were anesthetized, placed in sternal recumbency with their head stabilized and eyes held into a forward gaze with conjunctival stay sutures as previously described (see 2.9 Optical Coherence Tomography (OCT) and A-scan Biometry). ERG-Jet[®] corneal contact lens electrodes (Fabrinal SA, Switzerland) were filled with hypromellose 2.5% ophthalmic demulcent solution (Goniotaire, ALTAIRE Pharmaceuticals, Inc., Aquebogue, NY, USA) and placed on the

cornea as active electrodes. Subdermal platinum needle electrodes (GRASS Technologies, West Warwick, RI, USA) were used as reference and ground electrodes (subdermally placed 3-5 cm posterior to the lateral canthus and top of the head, respectively). Eyes were light stimulated and recorded simultaneously (Table 2.4). Light adaptation to background luminance was 5 minutes for each wavelength. Once testing was completed, mydriasis was reversed with 0.005% latanoprost ophthalmic solution. The following ERG amplitudes were compared between treated and untreated eyes in each dog: a- and b-wave, and PhNR(153, 154).

Table 2.4. Photopic ERG Protocol

Stimulus of Light Luminance Over Time (cd s m ⁻²)	Background Luminance (cd m ⁻²)	Amplification and Filtration Bandpass (Hz)
White: (1.0)	White: (25)	1-300
White: (3.0)		
Red: (1.0); (625 nm)	Blue: (25); (470 nm)	
Red: (3.0); (625 nm)		
Blue: (1.0); (470 nm)	Amber: (25); (590 nm)	

Abbreviations: ERG, electroretinography; cd, candela; s, second; m, meter; Hz, Hertz; nm, nanometer

2.11 Aqueous Paracentesis and Aqueous Humor Analyses

AH samples, totaling a volume of 100-200µL per eye, were collected for protein concentration, cell counts, and Nab titers. Repeated aqueous paracentesis was performed in the dogs of Aim 2 while under general anesthesia following ERG or OCT recordings. The preparation of the eyes and paracentesis technique were the same as for the IC injections (see 2.6 Intraocular Injections – IC and IVit) and were also performed with an insulin syringe (30 gauge x 1/2 inch needle). Post procedure care included a 4.4 mg/kg subcutaneous injection of carprofen (Rimadyl®, Zoetis Inc., Kalamazoo, MI, USA) and a one-time application of neomycin-polymyxin B sulfates-dexamethasone 0.1% ophthalmic ointment. Protein concentration and

cell counts were obtained by the MSU Veterinary Diagnostic Laboratory, and AAV NAb titers by the Boye Laboratory at the University of Florida.

Along with AH collection, whole blood was collected via venipuncture of the jugular or cephalic veins, and aliquots of the serum were measured for AAV NAb titers at the Boye Laboratory, University of Florida. Samples were tested at 1:10, 1:40, 1:160, 1:640, and 1:2,560 dilutions using *scAAV2-(Y444F)-smCBA-mCherry* and ARPE19 cells as previously described(155).

2.12 Tissue Collection for Histopathology and Immunohistochemistry

All dogs from Aim 1 were humanely euthanized in a method consistent with the American Veterinary Medical Association (AVMA) Guidelines for the Euthanasia of Animals. They were pre-medicated with 0.03mg/kg of acepromazine maleate IV, followed by a peripheral placement of an IV catheter and IV overdose administration of sodium pentobarbital (Fatal Plus, Vortech Pharmaceuticals, Dearborn, MI, USA).

Eyes were enucleated and fixed in 4% paraformaldehyde solution for 3 hours at 4°C. Anterior and posterior segments were then separated at the pars plana of the ciliary body and fixed in 2% paraformaldehyde for 21 hours. Tissues were incubated in 15% and 30% sucrose each for 24 hours, respectively. The bisected anterior and posterior segments were cut into four quadrants and embedded in OCT media (Tissue-Tek OCT, Sakura Finetek USA Inc., Torrence, CA, USA). The frozen blocks were stored at -80°C until further processing. Ten µm sections were made by Leica CM3050S cryostat (Leica Microsystems, Buffalo Grove, IL, USA) at the vertical and horizontal sagittal planes (Figure 2.1) and mounted on plus-charge slides (Brain Research Laboratories, Newton, MA, USA). After slides air dried they were then stored at -20°C

until stained routinely with hematoxylin and eosin (H&E)(156). The slides were reviewed, and the degree of inflammation graded by a boarded veterinary pathologist as follows: 0=no inflammation, 1=mild inflammation, and 2=marked inflammation. The population of inflammatory cells was characterized. Sections of all areas were also incubated with hGFP antibody (rabbit FITC conjugated, 1:1000, Invitrogen Corp., Carlsbad, CA, USA) for IHC as previously described(157). Each slide was cover-slipped with an anti-fading reagent with DAPI for nuclear stain (DNA binding fluorescent stain (4',6-diamidino-2-phenylindole, ProLong® Gold, Life Technologies)). Slide imaging was performed with a fluorescence microscope (Nikon Eclipse 80i, Nikon instruments Inc., Melville, NY, USA) at 4x, 10x, 40x and 100x magnification and images captured with software (MetaVue, Molecular Devices, Sunnydale, CA, USA). Sections of hGFP IHC were qualitatively assessed for their labeling intensity. One representative low-mid grade slide image was taken through a 4x objective from each anterior segment quadrant and area of %hGFP green fluorescence quantitatively assessed using ImageJ (National Institute of Health, USA)(158). For statistical comparison of quadrants across varying dosages, the quantitative area of fluorescence was normalized by calculating each quadrant's % of the sum of the 4 quadrants within an eye. Fluorescence was compared between quadrants by the use of the function `Imp` from the package `ImPerm` in R(159). Permutation based ANOVA calculated from this program included the effects of: quadrant, eye, and the rearrangement of quadrants within the eyes.

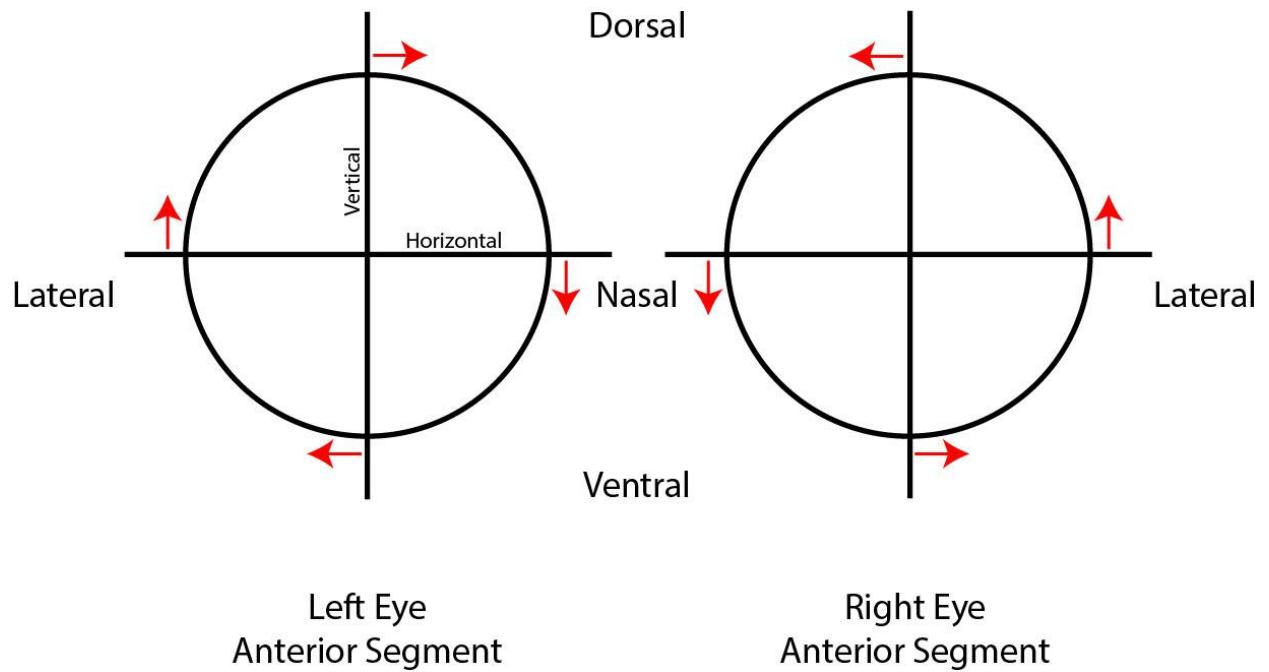


Figure 2.1. Anterior segment embedding and sectioning map. Vertical and horizontal sagittal planes are the borders establishing the 4 quadrants of each eye. Cryo-sectioning started at vertical and horizontal sagittal planes. Red arrows indicate the cutting direction for the 10µm sections into each quadrant of the eye. On this map, corneas are facing down.

CHAPTER 3 - Results

3.1 Aim 1 - Effect of Dosing and Injection Route on TM Transgene Expression

In previous studies, we have shown the ability to successfully target gene expression to the AHOPs of normal and *ADAMTS10*-mutant dogs with *ssAAV2-(Y444F)-hGFP*(135). Subsequently, we treated *ADAMTS10*-mutant dogs with early stages of hypertensive OAG with the corresponding therapeutic vector *ssAAV2-(Y444F)-hADAMTS10* at a dose of $1-3 \times 10^{11}$ vg. We showed that the treatment was safe and resulted in long-term *hADAMTS10* transgene expression for at least 35 months; however, no therapeutic IOP lowering effect could be achieved(136). In our attempt to improve transgene expression and to achieve a therapeutic effect, we pursued the following strategies under Aim 1: 1) increase the AAV delivery dose by one log unit; 2) compare IC vs. IVit AAV administration; and 3) test the effect of pupillary aperture on AAV vector distribution with an IC injection.

3.1.1 Increasing the AAV Dose

When assessing the ICA *hGFP* transgene expression across a range of 4 log units, 1×10^9 - 2.78 and 5.56×10^{12} vg, following IC administration of *ssAAV2-(Y444F)-hGFP*, the increase from 1×10^{11} to $2.78-5.56 \times 10^{12}$ vg resulted in an observable increase at 5 weeks post injection, which could be observed both clinically, by fluorescent gonioscopy, and by IHC (Figure 3.1). Because of the small sample sizes, no statistical analyses were performed. Despite the non-specific smCBA promoter, we confirmed our previous results of strongest transgene expression along the AHOPs, with some off-target transgene expression on the anterior iris surface and the iris epithelium on the posterior surface. Because there is no TM-specific IHC marker, TM cells were identified by location and shape. We observed that within the ICA, *hGFP* expression was not

limited to the TM, but was also strong along the uveoscleral outflow pathway, suggesting that a comparable therapeutic vector construct will likely treat both conventional and non-conventional pathways. It appeared that non-TM cells along the AH outflow pathways were also targeted. No *hGFP* expression was observed within the cornea, including the corneal endothelium, which minimizes concerns about potential corneal toxicity.

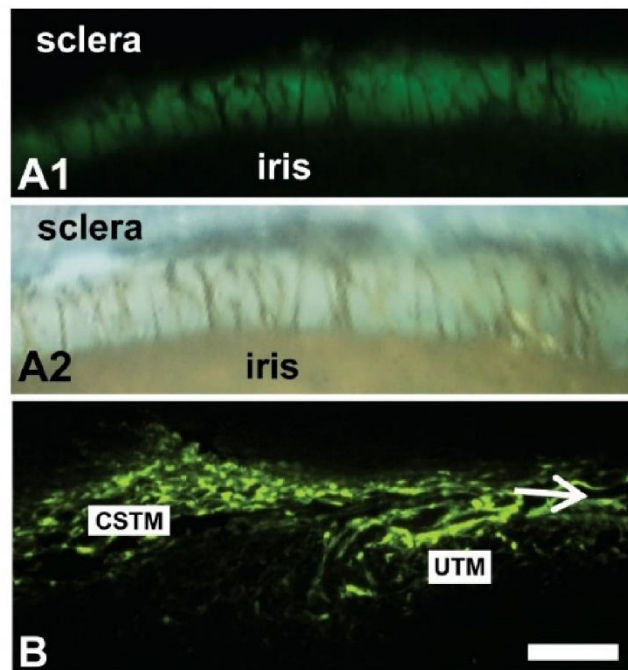


Figure 3.1. Effective TM targeting with *ssAAV2-(Y444F)-hGFP* in dogs. A1 and A2 are gonioscopic images of the same canine ICA (RetCam II). Note in A1, with use of 488nm blue light, fluorescence within the ciliary cleft just beyond the landmark pectinate ligaments. A2, depicting the white light image of the same landmark pectinate ligaments. B, *hGFP* expression of the corneoscleral TM (CSTM), uveoscleral TM (UTM) and continuing posteriorly along the uveoscleral outflow pathway (arrow). Bar=50 μ m.

3.1.2 Comparing IC vs IVit injections

In an attempt to slow the passage of *ssAAV2-(Y444F)-hGFP* through the ICA and maximize the exposure of bioavailable virus particles to the TM, we injected the vector IVit, trialing the vitreous as a slow release reservoir. When comparing IC vs. IVit injection of *ssAAV2-(Y444F)-hGFP* at $2.78-5.56 \times 10^{12}$ vg/50 μ L, we observed comparable transgene expression (hGFP fluorescence) within the ICA (Figure 3.2). Because of this observation, we continued with the IC injection approach in all subsequent treatments.

Not surprisingly, the IVit administration of *ssAAV2-(Y444F)-hGFP* not only resulted in hGFP fluorescence along the AHOPs, but also the anterior and posterior iris surface, the ciliary body epithelium, and the retina (see subsection 3.1.4 Other Observations following IC and IVit *ssAAV2-(Y444F)-hGFP*; Figure 3.4).

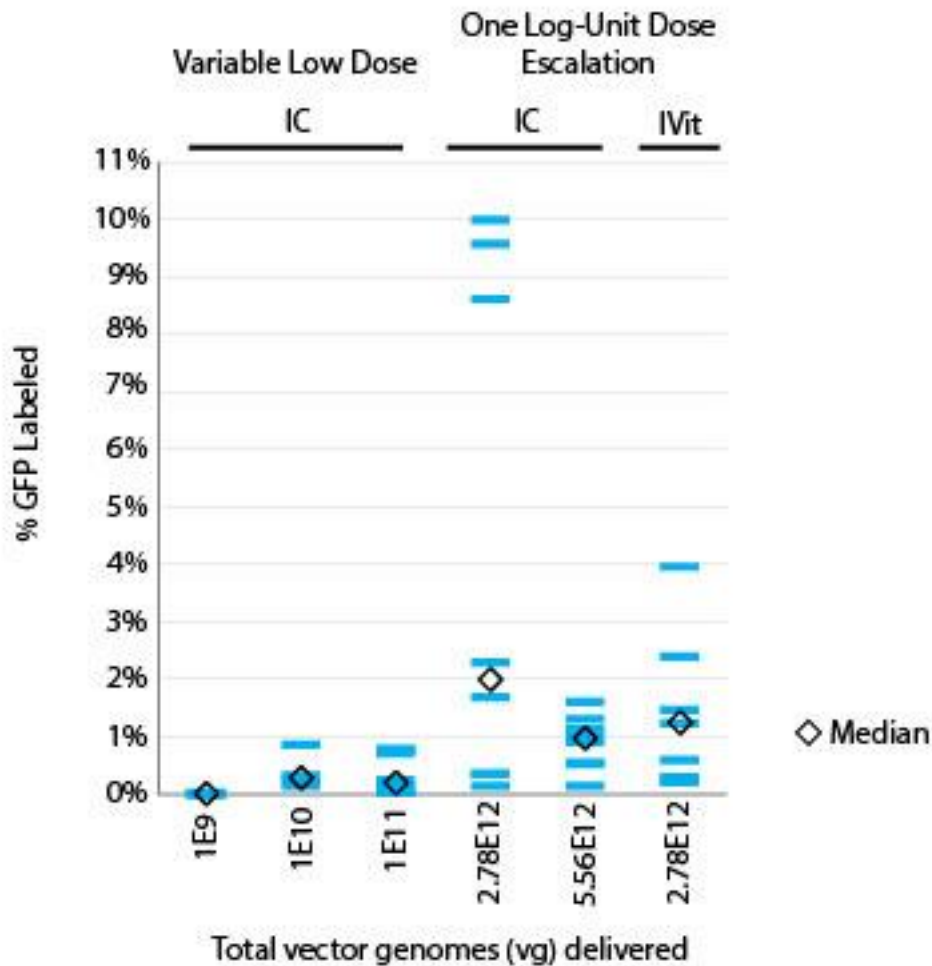


Figure 3.2. Relative % area of IHC hGFP labeling within the ICA when comparing doses and routes of administration. (Graph modified with permission(158)) Overall a one log-unit increase by IC injection from 1E11 to 2.78E12 vg resulted in a clear increase of *hGFP* expression. IC and IVit injection of the same vector dose (2.78E12 vg) resulted in comparable *hGFP* expression within the ICA. Each data point/blue mark represents area of hGFP fluorescence within one quadrant of the ICA. For IC injections: 1E9, N=1 eye (4 quadrants); 1E10, N=1 eye (4 quadrants); 1E11, N=2 eyes (8 quadrants); 2.78E12, N=2 eyes (8 quadrants); 5.56E12, N=2 eyes (8 quadrants). For IVit injections: 2.78E12, N=2 eyes (8 quadrants).

3.1.3 Effect on Pupillary Aperture

To determine the effects of pupil size on transgene expression, we compared relative % area of IHC hGFP labeling results from IC injections of *ssAAV2-(Y444F)-hGFP* at 2.78×10^{12} vg in

50 μ L with un-altered, miotic, and mydriatic pupils. We hypothesized that a small pupil could increase vector transduction within the ICA by (1) minimizing posterior loss of vector through the pupil, and (2) maximizing TM exposure to vector within a more open angle that is under tension from the miotic pupil. On the other hand, a dilated pupil and associated crowded ICA may slow AH drainage and increase contact time between vector and target cells.

Miosis was induced with one drop of 0.005% latanoprost ophthalmic solution and mydriasis with one drop of 1% atropine sulfate ophthalmic solution. While median area of IHC hGFP fluorescence may suggest that expression was higher in miotic pupils, there was no obvious difference in *hGFP* expression over all quadrants evaluated when comparing the three pupil sizes (Figure 3.3).

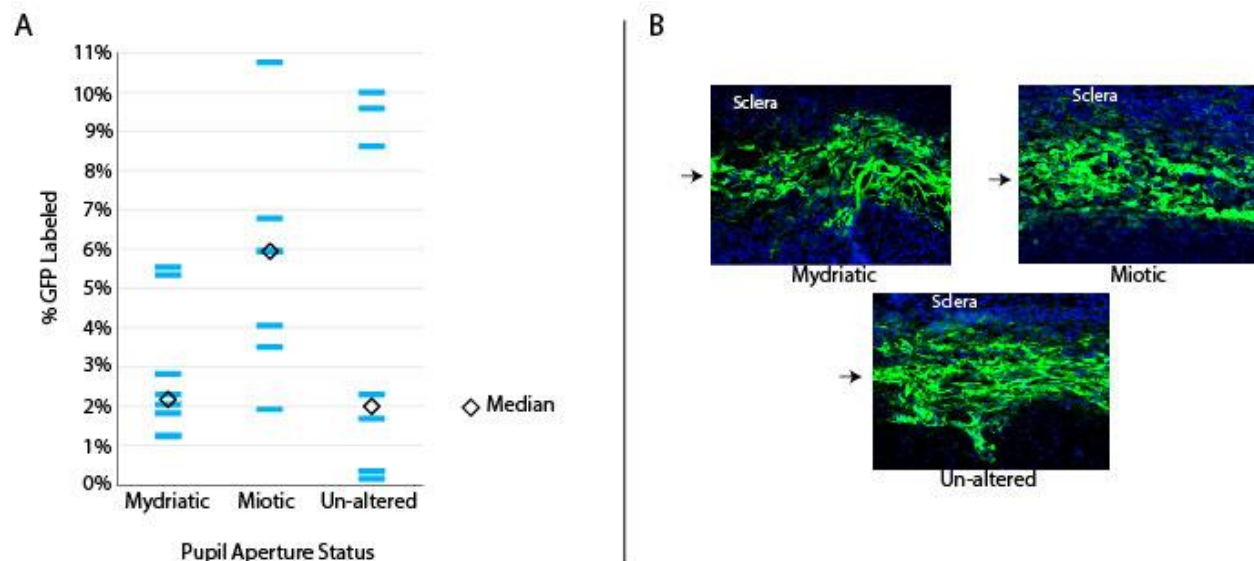


Figure 3.3. Effect on relative % area of IHC hGFP labeling within the ICA when comparing pupil size when utilizing the 2.78E12vg dose. A (graph modified with permission(158)), hGFP labeling with an overall similar % representation across 3 different pupil statuses: mydriatic, miotic and un-altered. Each data point/blue mark represents area of hGFP fluorescence within one quadrant of the ICA. B, hGFP IHC with green fluorescence shows robust hGFP labeling of the TM (arrows), regardless of pupil sizes. For pupil aperture status: mydriatic, N=2 eye (8 quadrants); miotic, N=2 eye (8 quadrants); un-altered, N=2 eyes (8 quadrants). Blue DAPI, 4'6-diamidino-2-phenylondole (DAPI), utilized for labeling of nuclear DNA.

3.1.4 Other Observations following IC and IVit ssAAV2-(Y444F)-hGFP

While the ICA was our primary target for transgene expression, *hGFP* was expressed also in other ocular cells (not graded or scored, only observed findings reported). Following vector injection into the anterior vitreous (via an IVit injection), *hGFP* expression was found anteriorly in the ciliary body epithelium, iris epithelium and anterior iris surface as well as posteriorly scattered across the retina, spanning portions of the nerve fiber layer and reaching down into cells of the retinal ganglion cell and inner nuclear layers (Figure 3.4). IC injections resulted in

stronger hGFP expression in cells surrounding the posterior chamber with increasing pupil size. In contrast, a miotic pupil resulted in *hGFP* expression of the anterior iris surface and to a lesser extent, pupillary margin and iris epithelium following IC vector administration. Unaltered pupils during IC injection, resulted in *hGFP* transgene expression of the of the iris surface, pupillary margin and iris epithelium. Mydriatic pupils during IC injection resulted in targeting of similar structures/cells as with an unaltered pupil, but with further posterior diffusion, more robust *hGFP* expression within the iris and ciliary body epithelium (Figure 3.4). Collectively, all IC injections, regardless of pupil size resulted in no transgene expression posterior to the ciliary body.

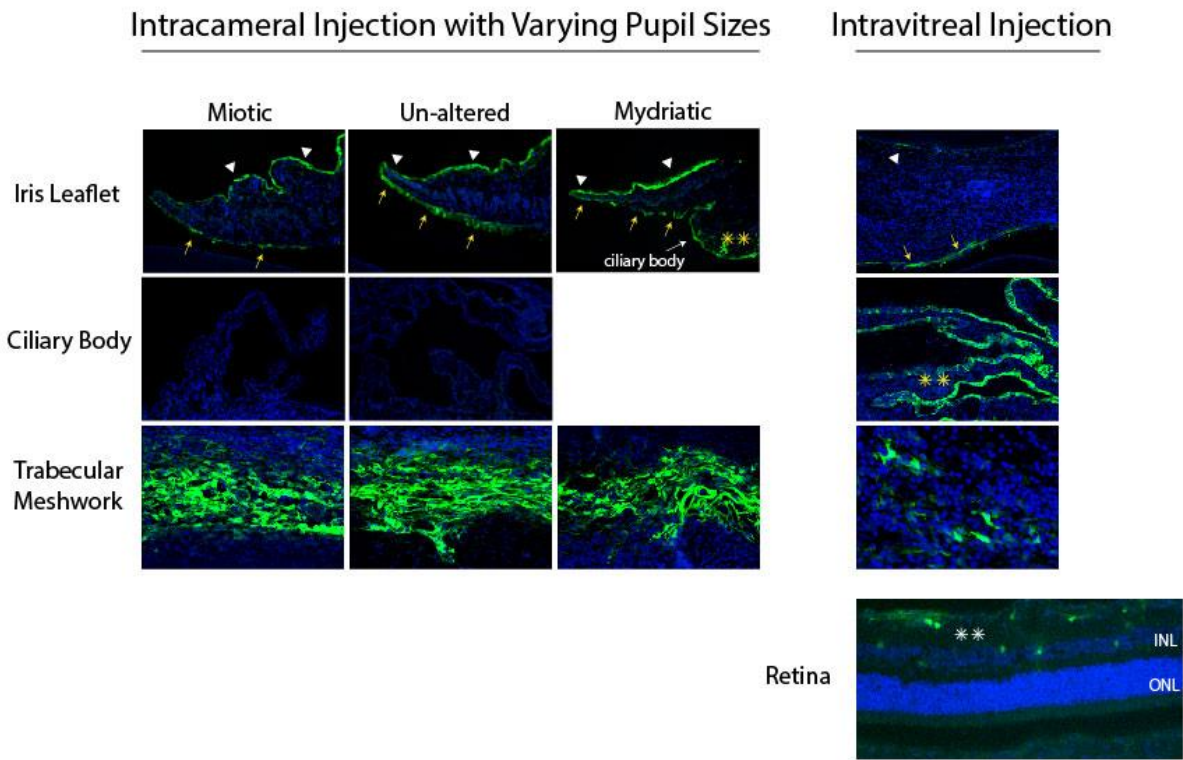


Figure 3.4. *hGFP* expression in the TM and other intraocular tissues when comparing IC injections with variable pupil sizes and IVit injection. All routes of administration resulted in transgene expression within the TM; IC routes more robustly than IVit. Pupil size and route of administration seemed to correlate with the ability to target other cell populations. Yellow arrows point to the iris epithelium. The fluorescence of the iris epithelium covering the posterior iris surface seemed more robust, more distantly from the pupillary margin with increased pupil size. Iris surface expression (white arrowheads) with an IVit approach seemed paltry. The ciliary body epithelium was reached by IVit vector administration or IC administration with mydriasis (yellow double asterisks). IVit vector administration also targeted the retina (white double asterisks) spanning the nerve fiber layer and even a few cells that reach into the inner nuclear layer. Blue DAPI was used to stain nuclear DNA. ONL, outer nuclear layer. INL, inner nuclear layer.

3.1.5 Comparison of *hGFP* Expression Between Quadrants

To determine if the ICA is targeted uniformly through the whole circumference, we compared areas of *hGFP* expression between the four quadrants following IC injection of *ssAAV2-(Y444F)-hGFP*. Dosing differences were corrected as described in Methods (see 2.12 Tissue Collection for Histopathology and Immunohistochemistry). In general, *hGFP* was uniformly expressed when comparing the four quadrants (Figure 3.5). Dorsolateral quadrants seemingly trended toward higher *hGFP* expression while ventrolateral quadrants trended towards less; however, with use of permutation ANOVA, there was no significant differences in expression among the quadrants.

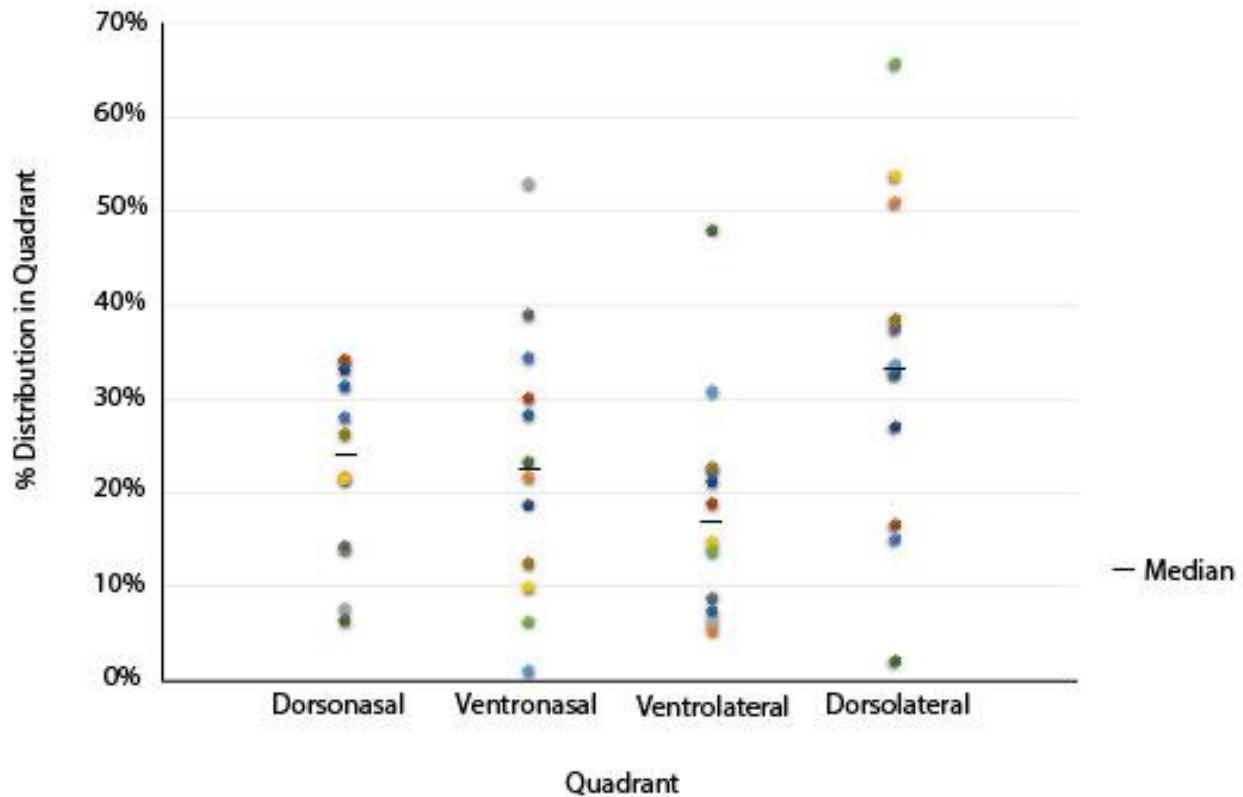


Figure 3.5. Comparison of % IHC *hGFP* expression between four quadrants following IC delivery of *ssAAV2-(Y444F)-hGFP*. Data sets were normalized so that total percentage of *hGFP* expression added up to 100%. This was done to account for dosing differences (1×10^9 to 2.78×10^{12} vg). Each of the 14 eyes, of 9 dogs, is shown in a different color.

3.1.6 Fluorescein Kinetics of the AC

To confirm that our IC injection technique of a small volume (50 μ L) results in even filling of the AC, a prerequisite for even circumferential targeting of the ICA, we injected 10 eyes of 5 normal dogs with 0.2mg/ml and 100mg/ml fluorescein in the same vehicles that were used for AAV administration. We explored different variables that could possibly effect AC filling in order to identify the best technique for future vector administration. Head and body position, globe stability, composition and temperature of vehicle were evaluated (Table 2.3 in Methods).

When injecting full 100mg/ml concentration of fluorescein, which was not diluted with vehicle, the reagent seemed buoyant in the AH and would pool within the AC. For the dog positioned upright, this was the dorsal aspect of the chamber and for the dog in dorsal recumbency, pooling occurred behind the central cornea. When a dog was placed in an initial position of lateral recumbency, flipping from side to side (left lateral to right lateral recumbency), pooling occurred at the temporal aspect of the AC that was the opposite side of the finishing recumbency that the dog was placed. All other protocols resulted in a uniform distribution within 1-253 seconds (Figure 3.6), with reagent diluted in HSS distributing the fastest (<1 second) and reagent diluted in BSS/0.014% Tween being the slowest (253 seconds). All eyes exhibited swirling of the reagent within the AH following the initial motion of injection. In 4 eyes/2 dogs, topical atropine was applied following fluorescein injection for treatment of the mild anterior uveitis associated with any IC injection. In these eyes we observed fluorescence of the anterior and posterior lens capsule 1 day post-injection; this fluorescence gradually faded and migrated into the lens cortex over several weeks (Figure 3.7). This observation confirmed our findings with *ssAAV2-(Y444F)-hGFP* that a mydriatic pupil permits diffusion of IC injected reagent posteriorly and allowing contact with the cells and tissues bordering the posterior chamber, including the lens (Figure 3.7). When pupils were not pharmacologically dilated, we were able to observe the slow anterior diffusion of clear AH from the posterior to the anterior chamber through the pupil in a convection-like manner (Figure 3.8), suggesting that the reagent is not diffusing posteriorly.

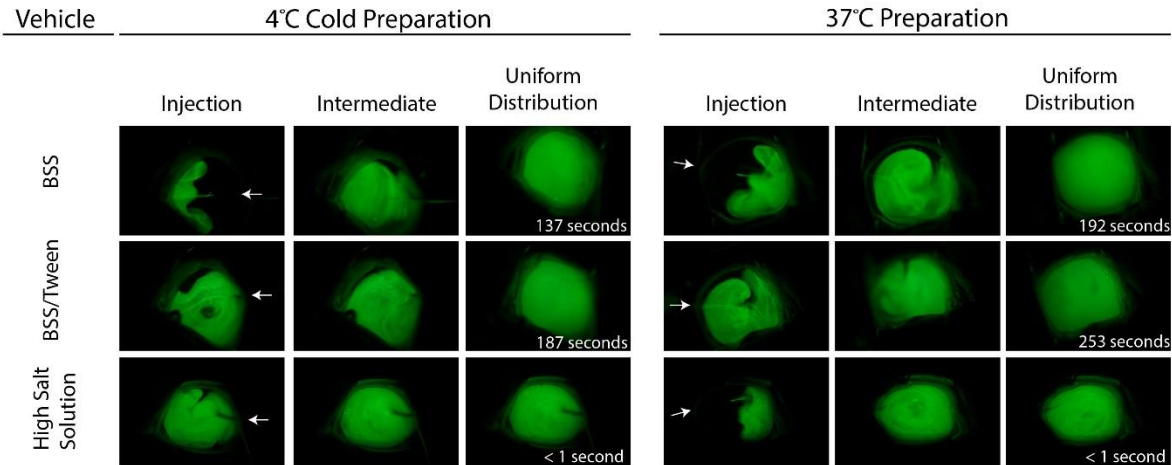


Figure 3.6. AC fluorescein kinetics as a function of temperature and vehicle. 6 eyes of 3 dogs, positioned in upright recumbency, were IC injected with 50 μ L of three different vehicles (BSS, BSS/Tween, and High Salt Solution (HSS)) at two different temperatures (37°C and 4°C). White arrows point to the site of injection.

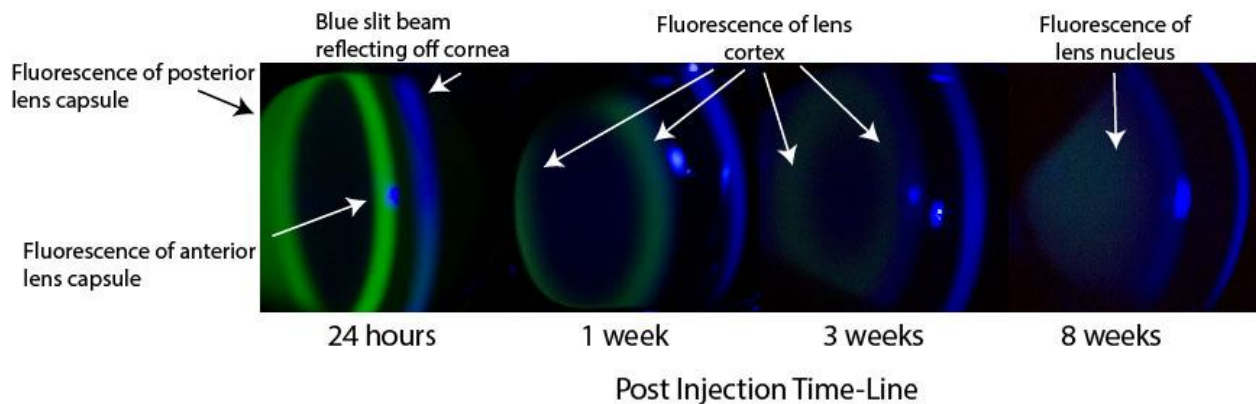


Figure 3.7. Lens capsule fluorescence shown with blue slit beam. Lens capsule exposure to fluorescein reagent due to a dilated pupil. Over an 8-week observation, fluorescein faded and diffused into lens cortex and nucleus.

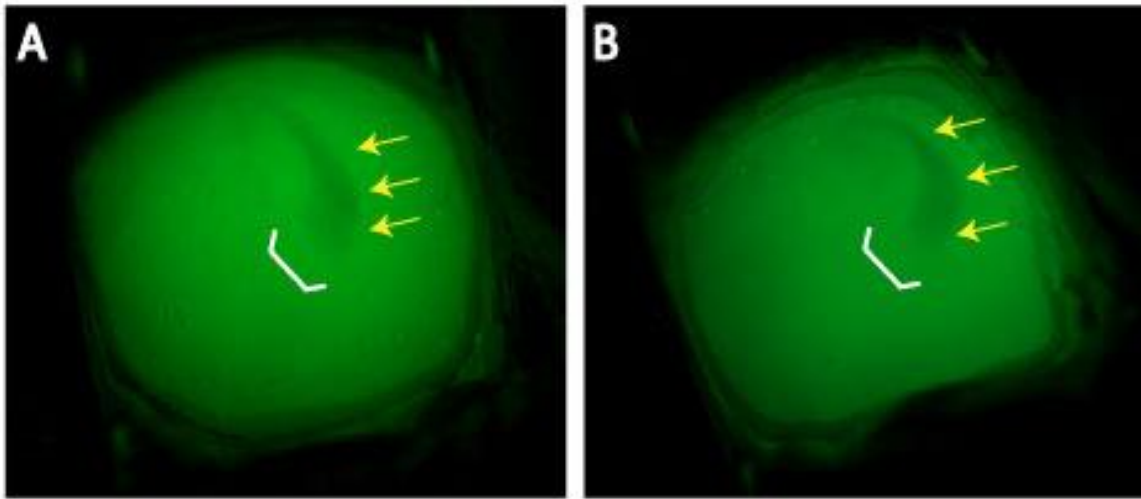


Figure 3.8. Anterior diffusion of AH through the pupillary aperture followed by convection-like movement within the AC. Clear AH can be seen diffusing through the pupil (white bracket) into the AC (yellow arrows). A, 37°C, BSS vehicle. B, 37°C, BSS/Tween vehicle.

3.1.7 Summary of Aim 1 – Targeting the AH outflow pathway – *ssAAV2-(Y444F)-hGFP*

For robust transgene expression in the ICA dosing matters: escalation of the dose by an additional log unit, from 10^{11} to 10^{12} vg, resulted in greater transgene expression of the AHOPs which became detectable, clinically, by gonioscopy. IVit injection did not result in stronger ICA transgene expression when compared to IC injection, but resulted in additional transgene expression in the retina, ciliary body and iris epithelium. Pupil size also did not appear to affect amount of ICA transgene expression within the ICA; however, a mydriatic pupil resulted in ‘loss’ of vector posteriorly through the pupil with targeting of cells and tissues bordering the posterior chamber. These findings are summarized in Table 3.1.

Table 3.1. Summary of Target Tissues Identified in Aim 1

Injection site/pupil	ICA	Anterior Iris surface	Lens (capsule)	Iris epithelium	Ciliary Body epithelium	Retina
IC/miotic	+	+	NE	(+)	-	-
IC/normal	+	+	-	+	-	-
IC/mydriatic	+	+	+	+	+	-
IVit/normal	+	(+)	NE	(+)	+	+

Abbreviations: NE, not examined. +, positive target. -, negative target. (+), light or sparingly positive target.

In conclusion of Aim 1 and the fluorescein kinetics of the AC, we found that in the adult canine eye, the IC injection of 50-75 μ L reagent in either BSS/0.014% Tween or HSS at either 4°C or 37°C resulted in even filling of the anterior chamber with a subsequent uniformly targeting of the ICA following delivery if 10¹² vg.

3.2 Aim 2 – Treatment of Canine *ADAMTS10*-OAG – *ssAAV2-(Y444F)-hADAMTS10*

Aim 1 studies have allowed us to optimize our ability to successfully target gene expression to the canine ICA. In Aim 2, we treated 3, 21-25.5-month-old *ADAMTS10*-mutant dogs unilaterally with 1.25-1.43x10¹² vg of *ssAAV2-(Y444F)-hADAMTS10* (Table 2.2, Methods) and followed them for 62-105 weeks. At the age of injection, IOP was already beginning to increase as part of the natural disease process.

3.2.1 Long-term IOP control following IC injection of *ssAAV2-(Y444F)-hADAMTS10*

We observed a robust lowering and long-term steady maintenance of weekly diurnal IOPs in 2/3 *ADAMTS10*-mutant eyes treated for the entire observation period of 62-105 weeks (Figures 3.9). In comparison, weekly diurnal IOPs of the fellow untreated eyes and both the treated and untreated eyes of the third dog continued to increase and vary with natural disease

progression (Figure 3.9). With use of local regression models, Loess, a trendline of average daily IOPs over time was obtained with corresponding CIs accounting for Bonferroni correction of $1-\alpha=0.99$ (Figure 3.10). To test the significance between the paired data of the treated and fellow untreated eyes, we calculated the difference between the two, and again obtained a fitted trendline with CIs (Figure 3.11). Any CI not containing zero in its value was considered significant with a Bonferroni adjustment of multiple comparisons ($\alpha\leq 0.01$). For Dog 1 and 2, this clear pattern of a lowered and maintained IOP was first determined to be significant at day 20 and 19, respectively.

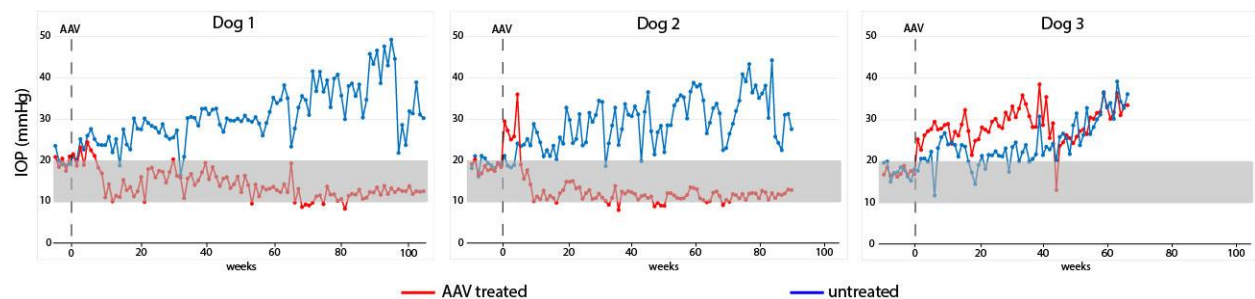


Figure 3.9. Diurnal IOP for ssAAV2-(Y444F)-hADAMTS10 treated and untreated control eyes. Dogs 1 and 2 showed a clear lowering of IOP and maintained this pattern for the duration of the study. Both eyes of Dog 3 and fellow untreated eyes of Dogs 1 and 2 exhibited the natural disease progression of increasing IOP. Shaded in grey is the target IOP range of 10-20mmHg.

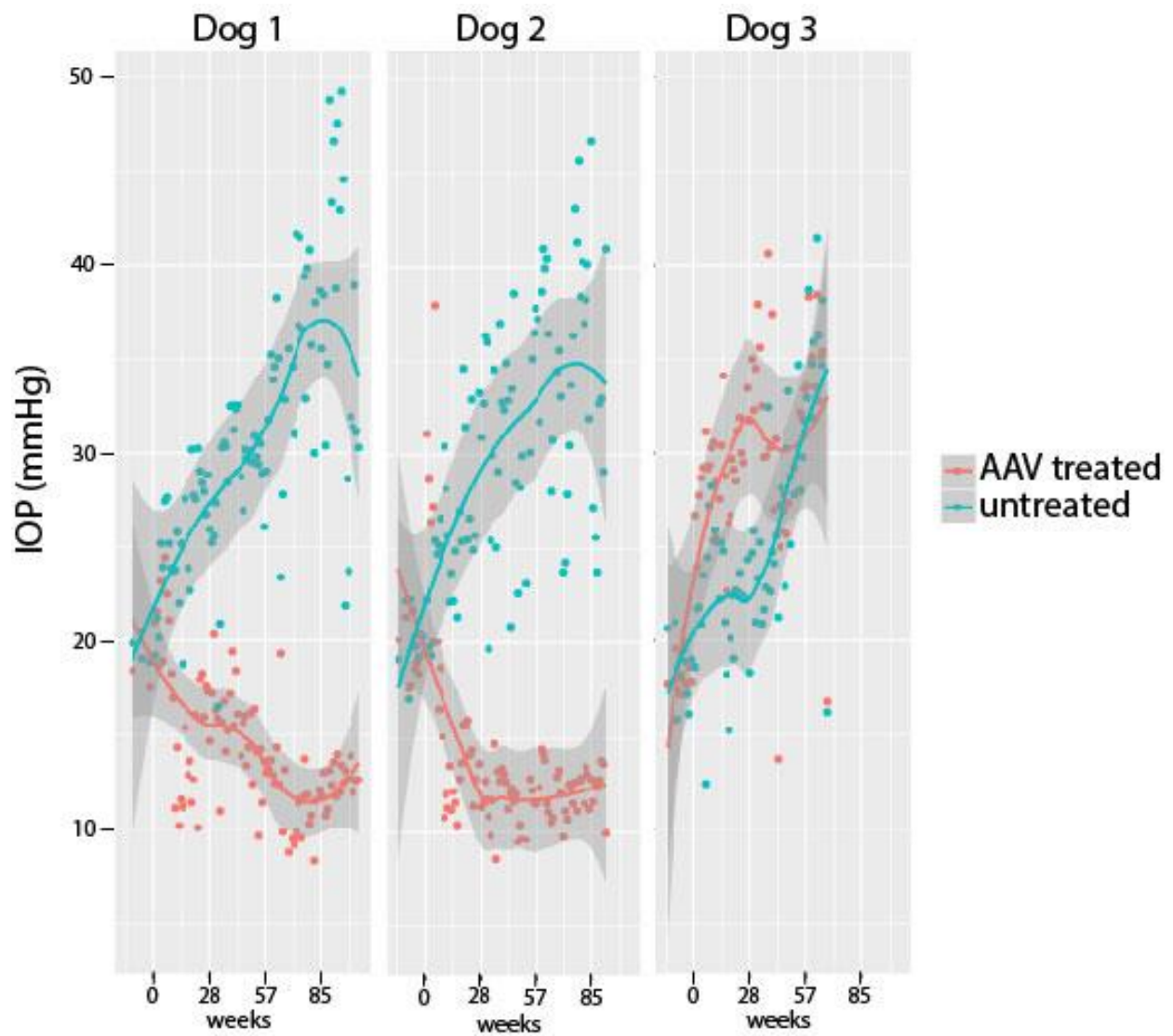


Figure 3.10. Linear regression fitted trendline with CI for treated and untreated eyes. Linear regression model was used to create a smooth and fitted trendline across multiple weekly IOPs. CIs (shaded in grey) were obtained for a Bonferroni correction level of $1-\alpha=0.99$.

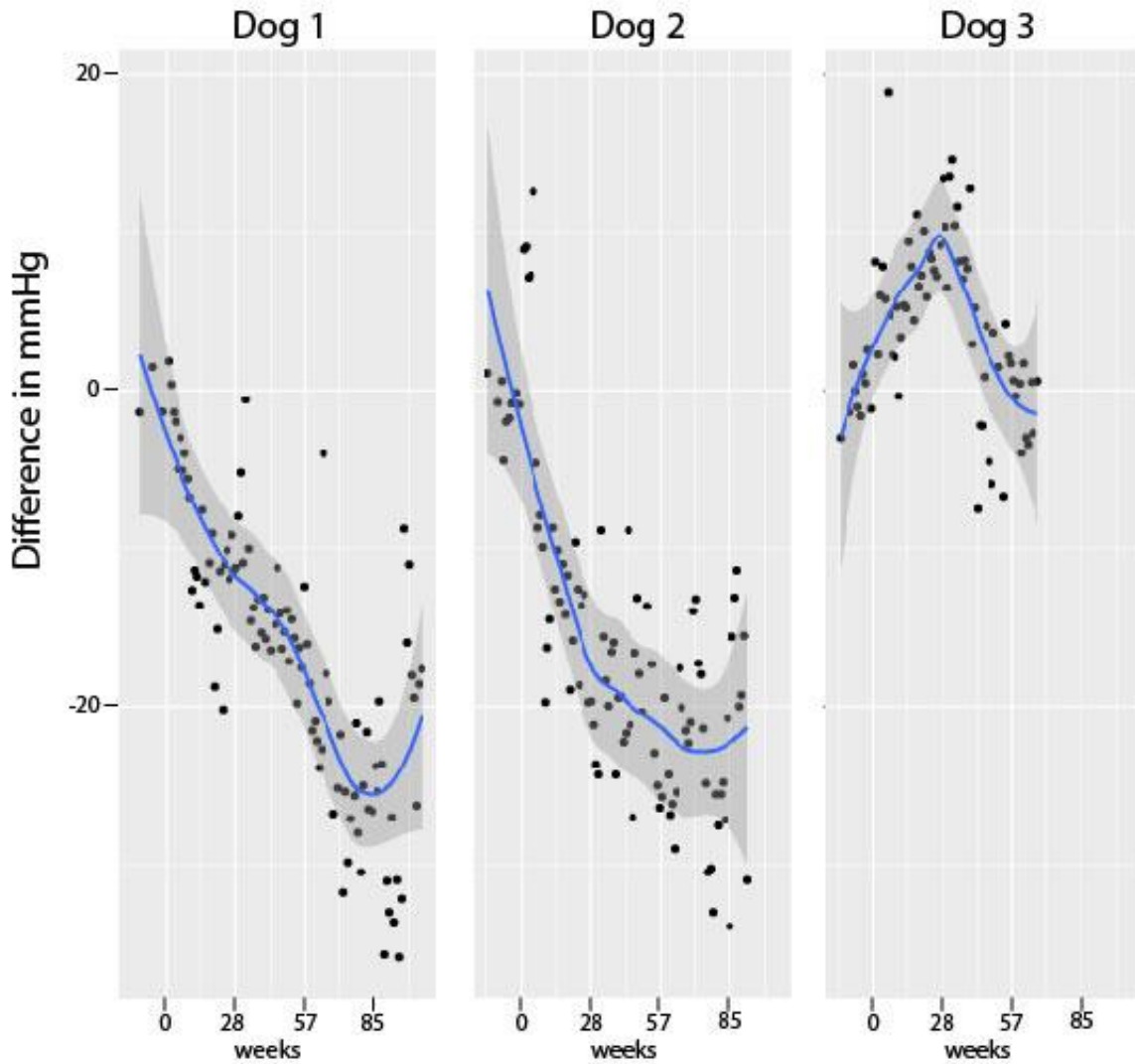


Figure 3.11. Linear regression fitted trendline with CI for difference between treated and untreated eyes. A smoothed and fitted trendline with corresponding CIs (shaded in grey) was established for the difference between treated and untreated eyes. Significance is determined when the CI of the difference does not contain the value 0, when $\alpha \leq 0.01$.

3.2.2 Increased Outflow Facility in Successfully Treated Eyes

Pneumotonography was utilized to measure conventional outflow facility. Facility is calculated as the inverse measure of trabecular resistance to AH outflow(51): less TM

resistance results in increased conventional outflow facility . Since pneumotonography was not available to us until after administration of *ssAAV2-(Y444F)-hADAMTS10*, treated eye outflow facility measurements were compared to the untreated fellow eye rather than baseline measurements in the same eye. Overall, the measurements were quite variable over the observation period, but when comparing the treated to untreated eyes, outflow facility was higher in the successfully treated eyes on 3 out of 4 (Dog 1) and 3 out of 5 (Dog 2) time points with a 3-75% increase (Figure 3.12).

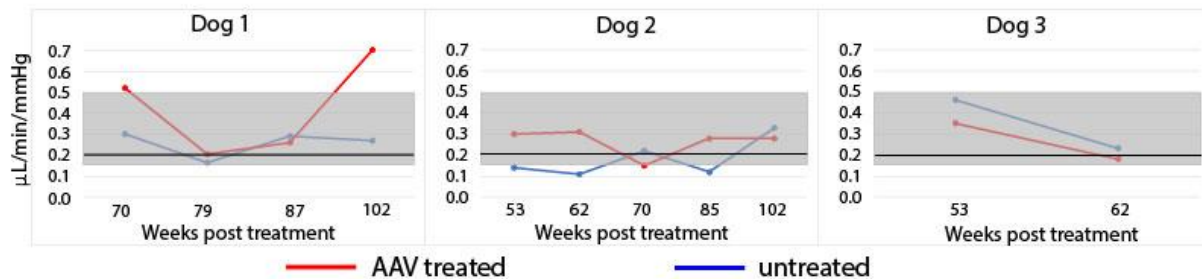


Figure 3.12. Outflow facility measured by pneumotonography. Shaded in grey is the normal range established in our laboratory (2 dogs/4 eyes). Values below the black line (0.2μl/min/mmHg) were previously considered indicative of OAG in *ADAMTS10*-mutant Beagles (146).

Assuming that the variability in outflow facility was not solely based on technical artifacts, these measurements are not fully consistent with the stable IOP lowering observed in the successfully treated eyes. Therefore, we assume that the IOP decrease was a result of both increase in conventional and uveoscleral outflow as suggested by our hGFP expression data under Aim 1. The *in vivo* estimation of uveoscleral outflow is challenging and has not yet been established for dogs.

3.2.3 Aqueous Humor Flow Remained Unaffected by Gene Therapy

Fluorophotometry was newly added to the lab after administration of *ssAAV2-(Y444F)-hADAMTS10*. Because no baseline data was collected, the AH flow measurements were compared between treated and untreated fellow eyes in each dog. Our studies represent the first measurements of AH flow in *ADAMTS10*-mutant dogs, and they show that the G661R missense mutation in *ADAMTS10* resulted in a significant decrease in AH flow (1.01-5.79 μ L/minute) compared to normal control eyes (6.2-13.47 μ L/minute), regardless of age/OAG-disease state. While the number of measurements need to be expanded in the future, our initial observations show that AH flow is not affected by our gene therapy. When assessing disappearance rate of fluorescein by fluorophotometry, both treated and untreated eyes seem to maintain a low AH flow of 1.01-5.79 μ L/minute (Figure 3.13).

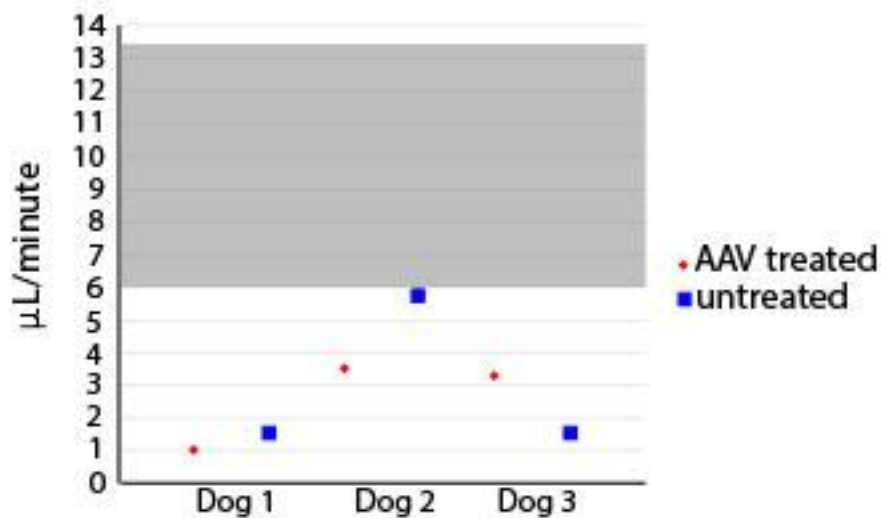


Figure 3.13. Aqueous humor flow measured by fluorophotometry. Shaded in grey is the normal range measured by us (2 dogs/4 eyes) and others(148, 149, 160, 161). AH flow in all three *ADAMTS10*-mutant Beagles was lower regardless of treatment.

3.2.4 ICA Morphology

All 3 AAV-treated dogs had gonioscopic and UBM examinations of the ICA performed. No changes were observed over time. ICA morphology was essentially normal with open angles and ciliary cleft (Figure 3.14)

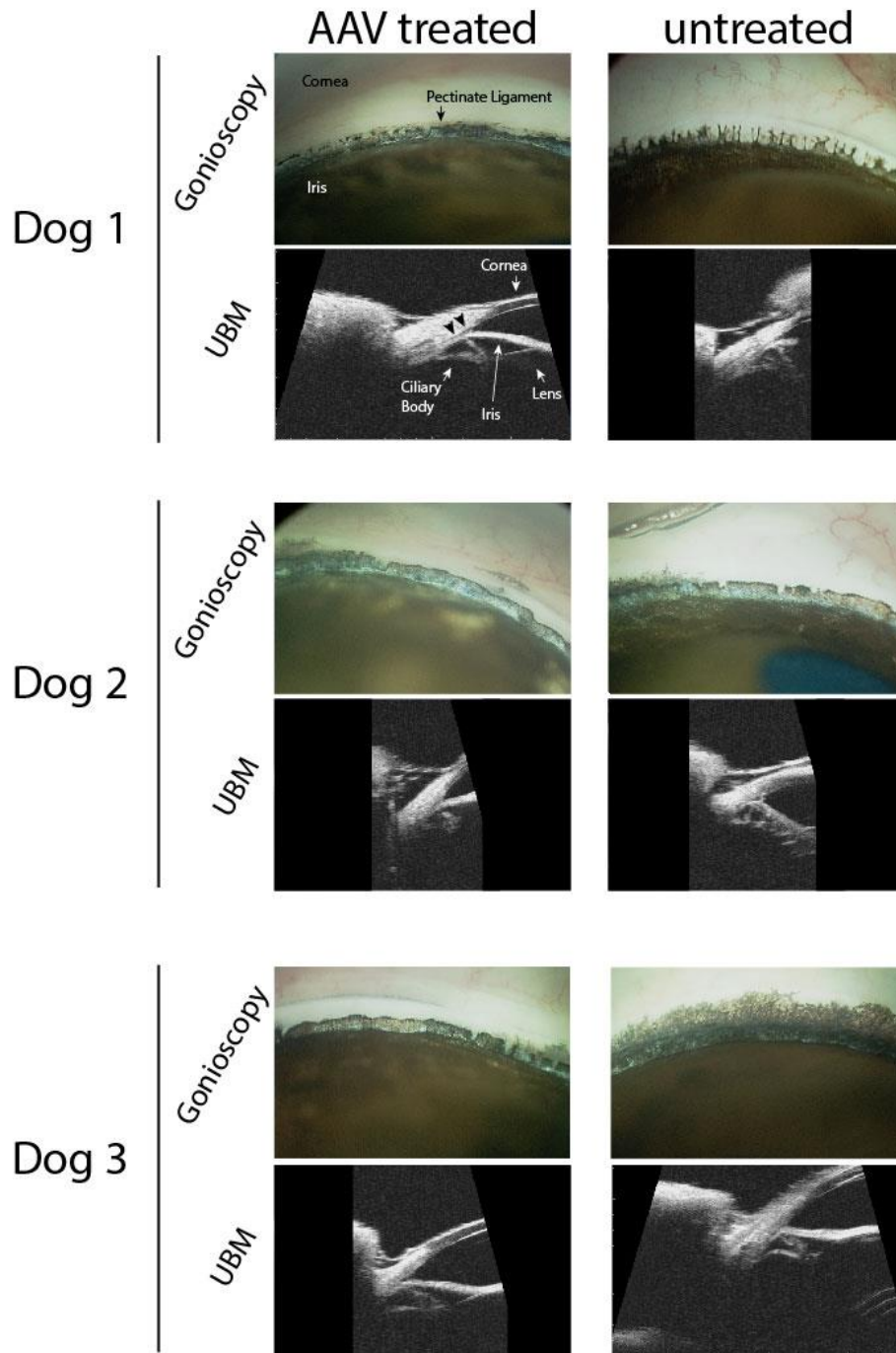


Figure 3.14. ICA morphology of treated and untreated fellow eyes compared by gonioscopic examination and UBM. Gonioscopic images (RetCam II) and high-resolution ultrasound image (48-MHz probe) exhibit an open ICA and ciliary cleft in all AAV treated and untreated fellow eyes. Cornea, lens, iris and ciliary body pointed out by white arrows. Natural recession of posterior ciliary cleft depicted by black arrowheads.

3.2.5 Optic Nerve Head (ONH) Morphology and Retinal Function

All dogs were monitored for morphologic changes of the ONH by OCT imaging and for retinal functional changes by ERG, respectively. For the 2/3 dogs that responded with long-term and steady reductions in IOPs, the ONHs of the treated eyes were protected from glaucomatous changes compared to the untreated fellow eyes that showed the characteristic ONH cupping. Both eyes of dog 3 showed ONH cupping, confirming non-response to therapy. While untreated and non-responding eyes all seemed to exhibit morphological changes classic to glaucoma, all 6 eyes of the 3 dogs retained retinal cell function that is comparable to normal dogs (Figure 3.15 and Table 3.2-3.4), demonstrating that clinically ONH atrophy can be detected earlier in the disease process than loss of retinal function in canine *ADAMTS10*-OAG.

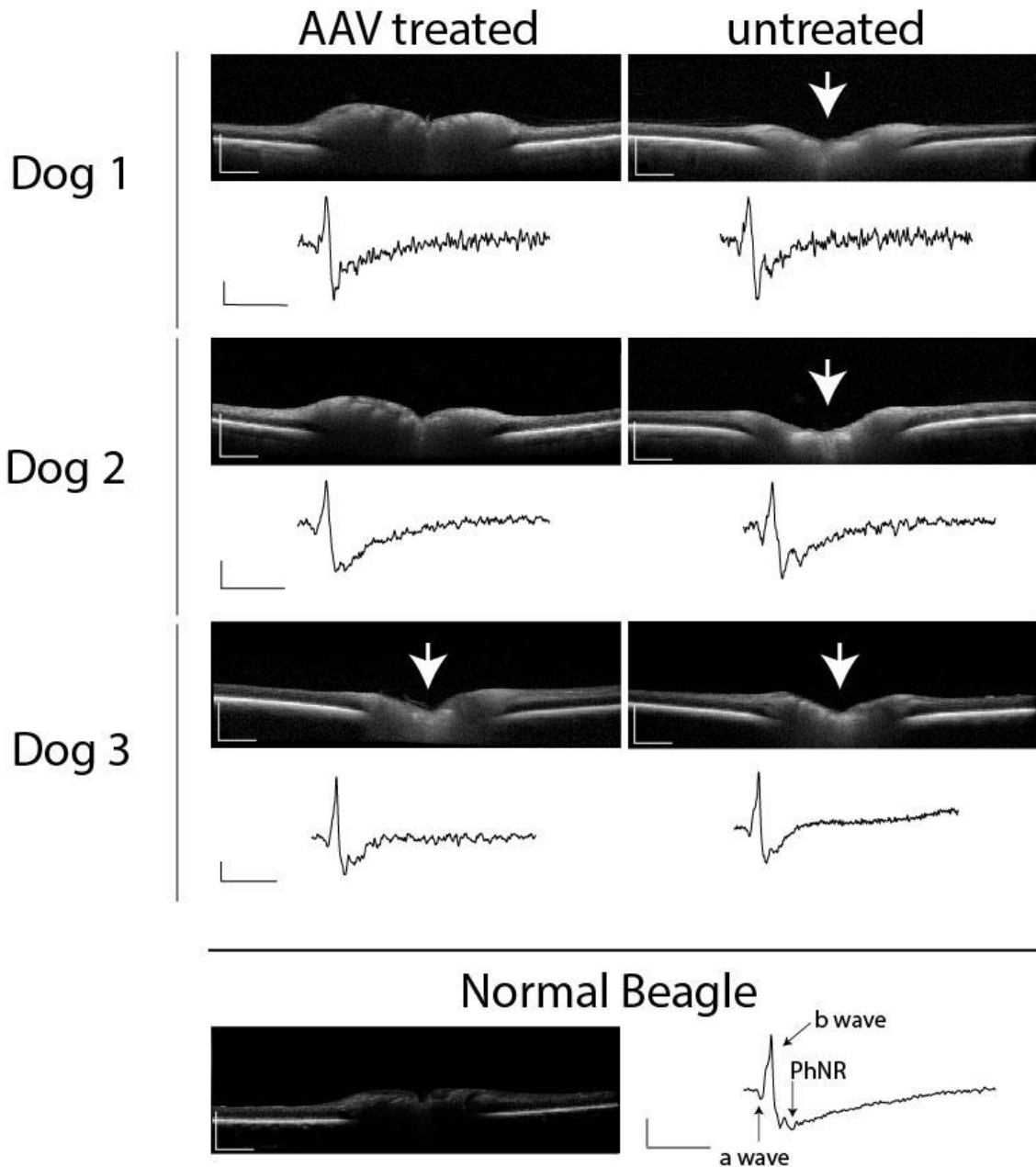


Figure 3.15. Morphologic comparison of ONH and comparison of retinal function. OCT (Heidelberg; Spectralis) images of the ONH. 2/3 eyes responded to AAV treatment exhibited by preservation of the optic disc morphology, while all untreated and the non-responding eye of dog 3 exhibited classic optic disc cupping (white arrow). ERGs (RETI-port, Roland Consult), 3.0 cd.sec/m² (0.5-Hz, minimum of 25 averages) of all eyes tested exhibited comparable functionality to a normal, adult Beagle. Wave analysis: a-wave, photoreceptor (rods and cones) response; b-wave, bipolar cell response; photopic negative response (PhNR), retinal ganglion cell response. White measure bars for OCT images = 600 μ m; ERG, vertical measure bars = 10 μ V, horizontal bar = 100 milliseconds.

Table 3.2. Dog 1: ERG a-, b-, and PhNR Wave Amplitudes and Peak Time Comparisons

White 1.0 cd s m⁻² on White 25 cd m⁻²												
	a-wave				b-wave				PhNR			
	Amplitude (μV)		Peak Time (ms)		Amplitude (μV)		Peak Time (ms)		Amplitude (μV)		Peak Time (ms)	
Timepoint months PI	AAV tx	Un-tx										
Baseline	2.0	2.8	11.7	7.0	11.1	9.2	22.7	23.5	12.8	10.5	39.9	45.4
7	2.5	2.1	13.3	7.8	10.0	10.8	24.3	25.8	10.2	17.0	41.5	45.4
13	2.5	0.1	13.3	14.9	13.6	9.8	24.3	25.8	16.4	9.9	43.1	45.4
18	2.4	2.1	12.5	12.5	21.2	16.0	23.5	25.8	5.7	11.8	40.7	42.3
24	4.8	0.0	13.3	15.7	13.3	13.8	33.7	33.7	16.3	17.2	43.1	46.2
White 3.0 cd s m⁻² on White 25 cd m⁻²												
Baseline	5.9	5.3	11.7	12.5	32.2	23.2	26.6	29.0	27.6	20.1	39.9	40.7
7	3.6	3.7	12.5	10.2	28.3	34.1	29.0	29.7	23.2	29.8	43.1	43.8
13	6.7	5.6	12.5	14.1	43.0	30.8	29.0	29.0	36.2	23.1	42.3	41.5
18	5.6	6.0	11.0	13.3	48.7	33.8	28.2	28.2	46.9	27.0	39.9	41.5
24	2.9	6.3	14.1	14.1	25.0	25.9	29.0	29.0	23.6	25.6	41.5	42.3
Red 1.0 cd s m⁻² on Blue 25 cd m⁻²												
Baseline	1.9	3.5	14.1	13.3	6.7	9.0	21.1	21.9	11.5	5.4	37.6	37.6
7	1.4	1.3	12.5	16.4	7.2	9.5	22.7	23.5	8.1	4.4	39.9	29.7
13	1.8	0.8	13.3	11.0	9.7	6.2	22.7	23.5	13.1	x	40.7	x
18	3.7	1.1	16.4	15.7	16.7	9.8	21.9	21.1	15.4	12.9	39.1	39.1
24	0.1	x	14.1	x	7.6	x	22.7	x	10.6	x	45.4	x

Table 3.2. (cont'd)

Red 3.0 cd s m⁻² on Blue 25 cd m⁻²												
	a-wave				b-wave				PhNR			
	Amplitude (μV)		Peak Time (ms)		Amplitude (μV)		Peak Time (ms)		Amplitude (μV)		Peak Time (ms)	
Timepoint months PI	AAV tx	Un-tx										
Baseline	3.6	4.8	13.3	12.5	19.3	19.0	24.3	24.3	18.9	8.8	38.4	33.7
7	2.3	1.5	14.1	15.7	16.2	14.4	27.4	26.6	17.5	21.3	39.9	46.2
13	3.9	1.8	13.3	12.5	27.2	16.9	27.4	27.4	27.4	17.4	39.9	40.7
18	0.3	5.4	13.3	12.5	33.6	25.5	25.8	25.8	21.9	27.2	37.6	40.7
24	2.4	6.6	16.4	12.5	16.5	19.6	27.4	27.4	14.5	17.0	47.7	47.0
Blue 1.0 cd s m⁻² on Amber 25 cd m⁻²												
Baseline	17.3	19.8	14.9	17.2	26.9	26.5	29.7	30.5	60.1	63.4	43.8	47.0
7	9.9	11.8	15.7	15.7	9.8	21.8	32.1	32.9	42.4	64.4	46.2	46.2
13	12.0	9.5	15.7	17.2	30.9	23.9	31.3	31.3	52.5	41.6	43.8	45.4
18	11.8	21.3	14.1	15.7	49.8	43.9	29.7	29.7	59.8	68.6	42.3	42.3
24	12.1	11.8	16.4	16.4	18.2	21.1	32.9	32.1	54.4	51.0	44.6	44.6

Abbreviations: ERG, electroretinography; PhNR, photopic negative response; PI, post injection; μV, microvolts; ms, milliseconds; tx, treated; Un-tx, untreated. Any 'x' that is within the table, represents a wave that could not be measured.

Table 3.3. Dog 2: ERG a-, b-, and PhNR Wave Amplitudes and Peak Time Comparisons

White 1.0 cd s m⁻² on White 25 cd m⁻²												
	a-wave				b-wave				PhNR			
	Amplitude (μV)		Peak Time (ms)		Amplitude (μV)		Peak Time (ms)		Amplitude (μV)		Peak Time (ms)	
Timepoint months PI	AAV tx	Un-tx										
Baseline	1.8	2.0	13.3	13.3	12.2	13.7	25.0	23.5	11.5	14.6	47.0	44.6
3	2.0	5.6	11.0	11.7	10.2	15.7	25.0	25.0	14.3	22.3	41.5	46.2
9	4.3	2.8	10.2	12.5	13.7	13.2	25.0	25.0	16.5	13.5	4.5	43.8
15	3.0	1.8	12.5	12.5	13.2	9.2	24.3	24.3	14.8	8.8	41.5	43.1
20	3.3	1.2	12.5	15.7	8.5	6.6	25.8	25.8	x	9.7	x	47.7
White 3.0 cd s m⁻² on White 25 cd m⁻²												
Baseline	3.4	2.4	11.0	12.5	31.4	33.1	29.7	29.7	28.0	25.3	47.0	44.6
3	3.3	1.9	11.0	11.0	31.9	32.4	28.2	28.2	24.5	32.6	43.8	44.6
9	4.4	3.4	14.1	12.5	37.4	30.2	29.0	28.2	25.7	21.7	41.5	44.6
15	4.5	5.0	13.3	13.3	30.3	22.7	27.4	27.4	23.5	18.7	42.3	42.3
20	3.6	5.8	12.5	14.1	19.0	21.2	29.7	29.7	18.0	20.0	44.6	45.4
Red 1.0 cd s m⁻² on Blue 25 cd m⁻²												
Baseline	0.7	0.4	7.8	10.2	8.1	9.0	23.5	23.5	x	2.6	x	32.9
3	1.7	2.0	11.0	12.5	6.6	9.5	21.9	21.9	10.8	14.7	43.8	44.6
9	1.3	2.2	9.4	10.2	7.9	5.7	20.4	22.7	x	x	x	x
15	0.1	2.3	12.5	12.5	6.9	7.1	21.1	22.7	9.9	7.6	42.3	42.3
20	1.1	0.2	14.1	13.3	4.7	5.2	23.5	23.5	4.6	3.3	31.3	32.1

Table 3.3. (cont'd)

Red 3.0 cd s m⁻² on Blue 25 cd m⁻²												
	a-wave				b-wave				PhNR			
	Amplitude (μV)		Peak Time (ms)		Amplitude (μV)		Peak Time (ms)		Amplitude (μV)		Peak Time (ms)	
Timepoint months PI	AAV tx	Un-tx										
Baseline	0.6	0.7	12.5	9.4	16.0	16.7	27.4	26.6	14.8	17.3	44.6	45.4
3	2.5	4.3	13.3	14.1	16.8	23.3	25.8	25.8	20.9	25.5	43.1	43.8
9	2.3	1.3	13.3	14.1	22.9	18.0	25.8	26.6	22.0	14.1	42.3	44.6
15	0.7	3.3	13.3	14.1	14.5	15.5	25.0	25.0	17.7	18.2	41.5	43.8
20	1.4	2.5	11.7	15.7	11.0	12.1	27.4	26.6	14.2	18.6	45.4	47.7
Blue 1.0 cd s m⁻² on Amber 25 cd m⁻²												
Baseline	11.6	13.6	14.9	14.9	27.2	28.6	29.0	29.0	51.8	58.6	50.1	50.1
3	11.4	13.5	15.7	14.9	30.7	35.2	32.1	32.1	51.0	65.3	47.7	47.0
9	10.6	10.0	13.3	15.7	38.9	37.5	31.3	30.5	45.6	36.4	46.2	45.4
15	9.0	12.0	14.9	14.1	41.7	39.1	30.5	31.3	36.3	34.7	47.0	45.4
20	10.8	11.3	16.4	16.4	24.0	22.2	32.9	32.1	36.2	37.6	49.3	51.7

Abbreviations: ERG, electroretinography; PhNR, photopic negative response; PI, post injection; μV, microvolts; ms, milliseconds; tx, treated; Un-tx, untreated. Any 'x' that is within the table, represents a wave that could not be measured.

Table 3.4. Dog 3: ERG a-, b-, and PhNR Wave Amplitudes and Peak Time Comparisons

White 1.0 cd s m⁻² on White 25 cd m⁻²												
	a-wave				b-wave				PhNR			
	Amplitude (μV)		Peak Time (ms)		Amplitude (μV)		Peak Time (ms)		Amplitude (μV)		Peak Time (ms)	
Timepoint months PI	AAV tx	Un-tx										
Baseline	N/A	N/A										
3	2.8	0.8	10.2	12.5	10.5	12.8	23.5	24.3	x	9.6	x	38.4
9	2.7	1.7	14.9	12.5	15.2	15.8	25.0	25.0	10.0	8.5	39.9	39.1
15	2.4	3.5	12.5	11.0	9.7	15.6	25.0	24.3	9.7	12.8	43.8	40.7
20	0.8	2.2	13.3	11.7	5.7	10.5	25.0	25.8	4.2	8.8	43.8	42.3
White 3.0 cd s m⁻² on White 25 cd m⁻²												
Baseline	N/A	N/A										
3	2.5	2.5	4.7	12.5	21.8	30.2	27.4	27.4	16.9	19.4	44.6	41.5
9	4.5	4.0	12.5	11.0	35.7	33.0	28.2	28.2	19.1	17.8	42.3	42.3
15	2.6	3.4	12.5	12.5	27.1	37.2	27.4	27.4	18.8	25.2	41.5	40.7
20	2.2	4.0	11.7	12.5	14.5	25.3	29.0	29.0	9.8	19.9	43.1	45.4
Red 1.0 cd s m⁻² on Blue 25 cd m⁻²												
Baseline	N/A	N/A										
3	1.2	1.4	14.1	13.3	6.8	9.0	21.9	21.1	3.6	9.2	31.3	39.9
9	1.1	1.7	12.5	13.3	8.5	10.1	22.7	21.9	6.9	9.9	38.4	37.6
15	3.0	1.8	12.5	12.5	7.9	10.2	20.4	21.1	5.5	10.0	32.9	29.9
20	0.5	0.3	12.5	12.5	4.8	7.1	21.9	22.7	5.9	6.6	46.2	39.9

Table 3.4. (cont'd)

Red 3.0 cd s m⁻² on Blue 25 cd m⁻²												
	a-wave				b-wave				PhNR			
	Amplitude (μV)		Peak Time (ms)		Amplitude (μV)		Peak Time (ms)		Amplitude (μV)		Peak Time (ms)	
Timepoint months PI	AAV tx	Un-tx										
Baseline	N/A	N/A										
3	0.9	1.9	11.7	12.5	16.5	20.5	25.0	25.0	4.8	17.2	35.2	39.9
9	0.9	1.9	10.2	10.2	21.0	28.1	25.8	25.8	13.4	18.3	43.8	41.5
15	0.5	3.3	14.9	13.3	17.9	26.3	25.8	25.0	13.9	22.7	41.5	39.9
20	2.5	3.6	14.1	13.3	11.6	19.1	26.6	26.6	11.1	16.6	44.6	42.3
Blue 1.0 cd s m⁻² on Amber 25 cd m⁻²												
Baseline	N/A	N/A										
3	11.6	10.7	14.9	14.9	21.8	21.0	29.0	29.7	42.3	49.5	49.3	46.2
9	12.9	13.3	15.7	14.1	28.3	29.6	29.7	29.7	49.7	57.7	46.2	45.4
15	17.8	16.3	14.9	14.1	39.9	46.6	29.0	29.0	52.2	53.7	44.6	43.8
20	15.0	13.8	16.4	14.9	27.7	27.0	30.5	29.7	37.5	46.4	47.7	49.3

Abbreviations: ERG, electroretinography; PhNR, photopic negative response; PI, post injection; N/A, not available; μV, microvolts; ms, milliseconds; tx, treated; Un-tx, untreated. Any 'x' that is within the table, represents a wave that could not be measured

3.2.6 *ssAAV2-(Y444F)-hADAMTS10* Safety Measures – Clinical Examination, Pachymetry and A-scan Biometry

Overall ssAAV2-(Y444F)-hADAMTS10 was well tolerated in Aim 2. Only mild uveitis was observed on clinical examination and easily controlled by twice daily topical corticosteroid administration, which subsequently induced a steroid keratopathy in both eyes of all 3 dogs. Pachymetry was collected at a similar frequency as clinical eye examination and % variation (Table 3.5) was calculated over the duration of the study as reported in Methods (see 2.4.2 Pachymetry). Percent variation in all eyes is similar to reported diurnal ranges (2.7-18.7%) in normal Beagles(139). At the finish of each OCT, A-scan biometry was performed to assess axial length of globe, anterior chamber depth (Table 3.6) and depth of vitreous (not calculated). Overall, all eyes show fluctuations in length over the duration of study; however, when looking at globe axial length only, treated eyes of Dogs 1 and 2 tended to be shorter in length than the untreated fellow. Dog 3, whose treated eye experienced elevated IOP compared to its untreated fellow, also tended to exhibit shorter globe lengths in the eye that had lower IOPs, suggesting that an elevation in IOP can alter globe length.

Table 3.5. Percent Variation of Pachymetry in *ssAAV2-(Y444F)-hADAMTS10* Treated and Control Eyes

Dog	Treated Eye	Control Eye
1	11.1%	13.4%
2	9.27%	18.6%
3	13.3%	11%

Table 3.6. A-scan Biometry Comparing *ssAAV2-(Y444F)-hADAMTS10* Treated to Control Eyes

Dog	Eye	Length Measured	Baseline (mm)	4 Months PI (mm)	10-12 Months PI (mm)	16 Months PI (mm)	18-20 Months PI (mm)	22 Months PI (mm)	24 Months PI (mm)
1	Treated	AXL	20.78	21.78	*	20.43	20.51	20.38	20.88
		ACD	3.88	5.22	*	4.06	3.54	3.38	3.91
		LT	7.36	7.00	*	7.07	7.32	7.01	7.08
	Control	AXL	20.83	21.36	21.93	21.17	21.25	21.93	21.48
		ACD	4.20	4.18	4.05	4.10	3.9	4.54	4.17
		LT	6.95	7.12	7.62	7.14	7.24	7.08	7.18
2	Treated	AXL	22.05	22.38	21.68	21.09	21.67	NE	21.89
		ACD	4.71	4.43	4.16	4.00	3.38	NE	3.98
		LT	7.4	8.01	7.44	7.23	7.01	NE	7.17
	Control	AXL	21.85	22.03	23.59	21.31	22.34	NE	22.62
		ACD	4.60	4.51	5.98	4.43	4.54	NE	4.11
		LT	7.22	7.28	7.49	7.51	7.07	NE	7.77
3	Treated	AXL	22.04	21.58	22.97	NE	NE	NE	22.24
		ACD	4.67	4.11	4.91	NE	NE	NE	4.94
		LT	6.95	7.78	7.48	NE	NE	NE	6.99
	Control	AXL	21.73	21.48	21.96	NE	NE	NE	21.71
		ACD	4.35	3.98	4.28	NE	NE	NE	5.41
		LT	7.03	7.17	7.33	NE	NE	NE	7.29

Abbreviations: AXL, axial length; ACD, anterior chamber depth; LT, lens thickness; NE, not examined; mm, millimeters. * indicates that testing was discontinued prematurely (likely due to anesthesia).

3.3 Adverse Events – Ocular Inflammation

3.3.1 Aim 1 - Severe Inflammation

While *ssAAV2-(Y444F)-hADAMTS10* was well tolerated in Aim 2, dogs in Aim 1 (7/9 dogs, 12/18 eyes) developed severe uveitis following *ssAAV2-(Y444F)-hGFP* administration. While 2/9 dogs, 2/18 eyes managed to recover with interventional therapies, the remaining cohort did not and required premature euthanasia and tissue collection.

The most severe ocular inflammation occurred at the highest dose of 10^{12} vg either IC or IVit with dramatic clinical changes within 33-37 days of injection. Observed changes in 2/5 dogs was a drastic decrease in IOP in both treated eyes while 1/5 dogs had a severe increase in IOP in both eyes (so severe, creating diffuse corneal edema that was difficult to visualize past); 3/5 dogs experienced mild to severe hyperemia; and 3/5 dogs had detectable flare and cells that ranged from few to +3 with the most severe obstructing visualization of fundus. The 1/5 dog that had a severe spike in IOP and corneal edema too difficult to assess beyond, also experienced the most severe hyperemia and ciliary flush, blepharospasm and corneal neovascularization. The severe uveitis required an aggressive regimen of interventional topical and oral therapies that included topical 1% prednisolone acetate ophthalmic solution in 4/5 dogs and oral prednisone in 3/5 dogs. Additional pain management was required in 1/5 dogs with injectable buprenorphine, as well as topical dorzolamide-timolol and latanoprost glaucoma medications had to be administered to control elevated IOPs in both eyes. Routine histopathology was performed on all the eyes. H&E sections were graded on a 0-2 scale (0=none, 1=mild and 2= marked) for level of inflammation. Anterior segments from 4/5 dogs were scored as a 2 (marked), while 1/5 dogs were so severe, both eyes scored 2+ (marked +).

Anterior segments on 5/5 dogs contained a lymphoplasma-histiocytic cell population that heavily infiltrated the ciliary cleft, ciliary body and iris stroma (Figure 3.16). For 2/5 of the dogs, inflammation included multifocal areas of retinal vasculitis with mild to moderate perivascular lymphoplasmacytic cell populations (Figure 3.16).

The second most severe inflammation occurred in 2/4 dogs that had received varying low-doses (1×10^{10} and 1×10^{11} vg) of *ssAAV2-(Y444F)-hGFP*. Vector administration in these 2 dogs occurred 3 months after a previous administration of AAV2 to the contralateral AC. For 1/2 of the dogs, fibrin appeared in the AC (of the newly treated *ssAAV2-(Y444F)-hGFP* eye) within 24 hours of injection and cleared by the next day with medical therapy. The second dog had severe inflammation within 24 hours of injection and required the addition of treatment with topical dorzolamide-timolol and latanoprost glaucoma medications to control the elevated IOPs of the newly injected eye. Unlike the previous 4/5 dogs, the just aforementioned second dog, had alleviation of his glaucoma within 24 hours and clearance of his inflammation within 6 days. Pathologic review of the eyes from these 2 dogs had no observable inflammatory cell populations in any of the sections of tissue, likely because of successful anti-inflammatory therapy (not pictured).

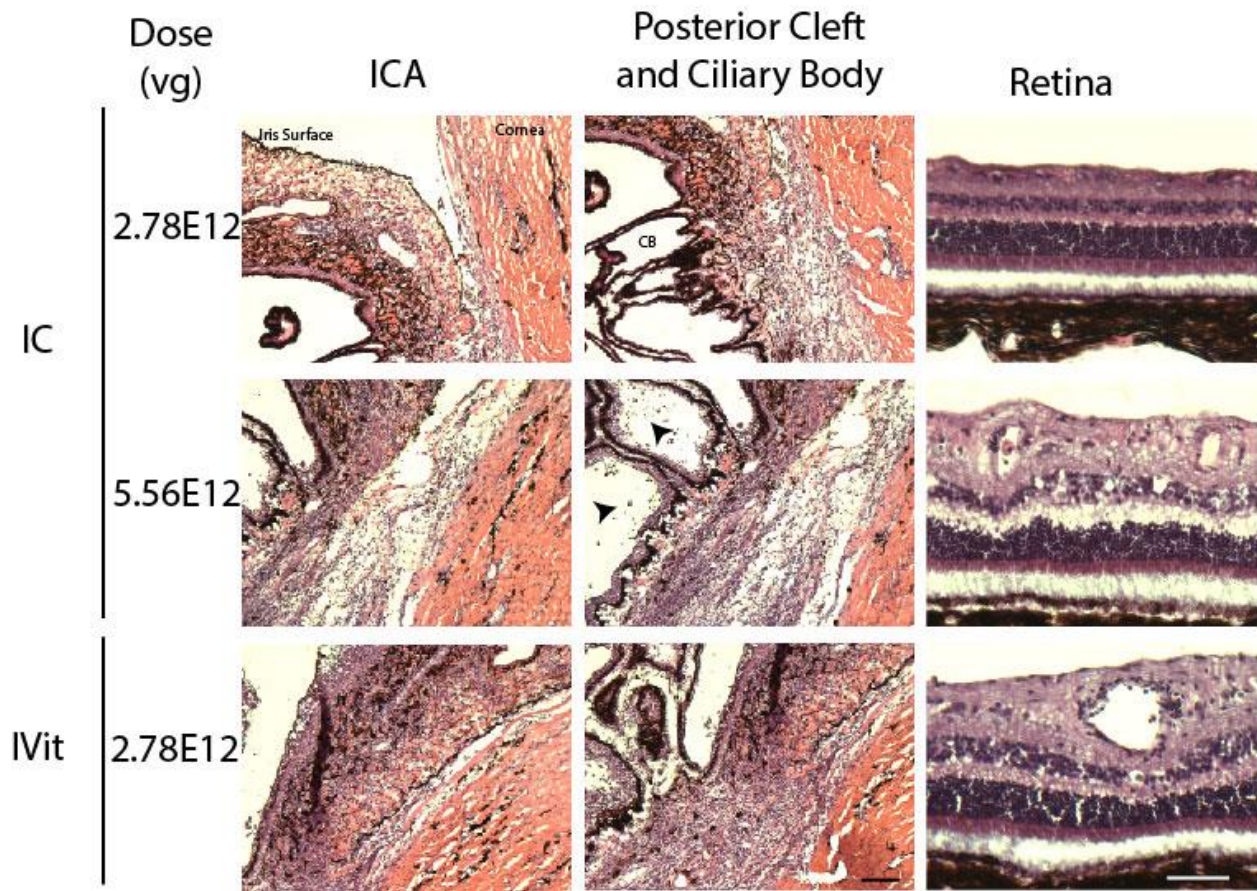


Figure 3.16. Photomicrographs depicting inflammation induced by injection of ssAAV2-(Y444F)-hGFP. Inflammatory scoring for the top and bottom rows of ICA, posterior cleft, and ciliary body: 2 (marked). The middle row of ICA, posterior cleft, and ciliary body: 2+ (marked+); in the center picture, black arrowheads point to inflammatory cells, that in abundance, have overrun the ciliary body and now reside in the posterior chamber. While no inflammatory score was assigned to the retina sections, both the highest IC dose and IVit treatment exhibited multifocal areas of retinal vasculitis with mild to moderate perivascular lymphoplasmacytic cell populations. All IC injections, that administered 2.78E12 vg or less, retained normal histologic appearance of the retina (top right). CB, Ciliary body. Hematoxylin-eosin stain. Scale bars, black 50 μ m (ICA and Posterior Cleft and Ciliary Body columns); white 100 μ m (Retina column).

3.3.2 Neutralizing Antibody (NAb) Assays

Because of the severe uveitis observed in Aim 1 and the mild anterior uveitis observed following treatment with ssAAV2-(Y444F)-hADAMTS10, the presence of AAV neutralizing antibodies was measured in serum and AH samples over repeated time points that coincided

with either ERG or OCT. We found positive serum titers in all 3 dogs, 2 of them were tested before AAV administration and found negative (Table 3.7), which was consistent with other dogs tested in the same facility. In addition, AH titers were measured in dog 1 and found to be positive in the injected but negative in the non-injected eye, confirming the generation of a humoral response and breakdown of the immune-deviation mechanisms of the anterior chamber. This was likely the reason for the development of anterior uveitis.

Table 3.7. Aim 2 – NAb Titers for T Cell Response to *scAAV2-(Y444F)-smCBA-mCherry*

Collection Timepoints		Serum Titers			Aqueous Humor Titers	
		Dog 1	Dog 2	Dog 3	Dog 1	
					AAV treated	Untreated
Baseline	NAb	NC	<10	<10		
1	Post injection NAb	3 months	8 months			
		>2560	2560			
2	Post injection NAb	20 months	16 months	16 months		
		2560	640	640		
3	Post injection NAb	24 months			24 months	24 months
		2560			640	<5

Abbreviations: NAb, neutralizing antibody; NC, not collected.

3.3.3 Aim 2 – Protein Concentration and Cell Count of AH

Due to the dramatic uveitis associated with *hGFP* expression in Aim 1 and the mild but controllable uveitis of all 3 dogs in Aim 2, AH was collected 1-2 times, from each eye of each dog in Aim2. Analysis of protein concentrations and cell counts were performed by a boarded veterinary pathologist at MSU Veterinary Diagnostic Laboratory. AH submissions for all eyes contained low protein concentrations that were consistent with normal AH (Table 3.8). Four of

the 10 submissions did result in findings of nucleated cells however, they were few and were not indicative of an inflammatory response (Table 3.8).

Table 3.8. Protein Concentration and Cell Count of AH of Aim 2 dogs

Dog	Procedure	18-22 Months post injection		20-24 Months post injection	
		AAV treated	Untreated	AAV treated	Untreated
1	MTP (mg/dL)	**	**	17	18
	Nucleated cell/ μ L	0	0	<1	<1
	RBCs/ μ L	unavailable	unavailable	<1	<1
	Cytology Findings	Acellular fluid	Acellular fluid	No intact nucleated cells	No intact nucleated cells
2	MTP (mg/dL)	23	13	43	28
	Nucleated cell/ μ L	0	0	2	1
	RBCs/ μ L	unavailable	unavailable	2	1
	Cytology Findings	Acellular fluid consistent with normal AH	Acellular and low protein consistent with normal AH	33 intact nucleated cells consisting of large mononuclear cells and small mononuclear cells; lack of granulocytes and no indication of an inflammatory response	4 intact and nucleated cells found but not able to identify
3	MTP (mg/dL)			29	21
	Nucleated cell/ μ L			<1	1
	RBCs/ μ L			2	0
	Cytology Findings			3 intact mono nuclear cells	5 intact mono nuclear cells

Abbreviations: AH, aqueous humor; MTP, micro total protein; RBC, red blood cells; mg/dL, milligrams per deciliter; μ L, microliter; **submission error with sample.

Chapter 4 – Discussion

Previously our team has demonstrated successful targeting and long-term transgene expression of the canine TM using a single mutant capsid *ssAAV2-(Y444F)* with either *hGFP* or *hADAMTS10* cDNA; however, when applying the latter for a therapeutic effect, we failed to demonstrate a reduction in IOP in Beagles with *ADAMTS10-OAG(135)*. The purpose of our current study was to further optimize the targeting of transgene expression with the same vector to the canine AHOPs, including the TM (Aim 1) and to reapply the optimized methods in a second therapeutic trial in *ADAMTS10*-mutant Beagles (Aim 2).

In our study we evaluated the ability to increase the area of transgene expression of the TM by altering dosing, comparing IC vs. IVit injection techniques, assessing the effects of pupil diameter when paired with an IC injection, and anterior chamber filling capabilities of suspension vehicles. Alas the most dramatic improvement in transgene expression with *ssAAV2-(Y444F)-hGFP*, was achieved by a dose escalation from 10^{11} to 10^{12} vg delivered as a single administration with our standard IC injection technique. This increase in *hGFP* transgene expression was so robust that we could clinically observe hGFP fluorescence by gonioscopic examination. This observed fluorescence emanating from the ciliary cleft was not witnessed in previous studies utilizing lower doses (10^9 to 10^{11}) of *ssAAV2-(Y444F)-hGFP*.

With this dose escalation, we are right at the limit of achievable vector concentrations with current AAV production methods. If further improvements in transgene expression were required, other avenues would have to be sought for improved transduction efficiency.

Perfusion of vector at large volumes distributed at a slow rate through the AC could be a possible approach to increase the number of vector particles delivered to the anterior chamber without increasing IOP. However, our goal is to have a minimally invasive approach that requires only one entry into the eye with a small gauge needle, 30-gauge, delivering a well-tolerated small volume of 50-75 μ L. Since the small volumes are well endured by the canine eye and do not require removal of AH to avoid severe IOP increases, we can avoid more inflammation naturally associated with any entry of the anterior chamber with a needle(162, 163). Additionally, having only one port for delivery reduces potential loss of vector. Other avenues that could also increase transduction efficiency include additional modifications to the viral capsid, use of a different serotype, use of a vehicle that can increase the bioavailability of the virus particles, and use of a more efficient or TM-specific promotor. While Aim 1 was very successful with increasing robust *hGFP* signal while suspended in a vehicle of BSS/0.014% Tween, the evolving science encompassing the improvement of vector administration with our University of Florida collaborators resulted in the use of HSS (with Tween) when administering *hADAMTS10* in Aim 2(145). Using Tween (polyoxyethylenesorbitan monolaurate) as a vehicle prevents adherence of capsids to the wall of the storage tube and delivery device, thereby minimizing the loss of vector before injection. The addition of NaCl to create HSS further improves the bioavailability of capsids by reducing self-aggregation and increasing solubility of capsid particles(145).

Previous studies have shown the ability to target the ICA by IVit injection(164). The vitreous has a slower turnover rate than AH which could lend the potential to act as a slow-release reservoir for AAV to the ICA allowing for increased contact time with the cells along the

AHOPs. When comparing an IVit administration approach to an IC approach, we were able to confirm that the canine ICA can be targeted by an IVit injection; however, hGFP expression levels were not increased. An IVit approach results in more off-target expression than the IC technique. Both injection techniques target the ICA, anterior iris surface, iris epithelium and, depending on pupil size, both can also target the ciliary body epithelium. IVit vector injection also targets the retina and is considered an attractive, less invasive administration technique compared to subretinal injection for retinal gene therapy(157, 165). Since we can minimize loss of vector posteriorly and off-target expression by keeping the pupil small, we opted to continue with IC injection as our preferred administration technique.

Varying the pupil size gave us interesting insights on vector distribution following IC injection. Surprisingly, neither a mydriatic nor a miotic pupil resulted in obvious change in level of transgene expression along the AHOPs. While the ICA's expression levels may not have been affected by the change in pupil size, posterior chamber structures had robust targeting with a mydriatic pupil, suggesting loss of vector into the posterior chamber. A dilated pupil allowed increased contact of IC injected reagents with the iris epithelium, lens capsule and ciliary body epithelium. While these are all off-target tissues for our current therapy attempts, these findings may be useful for future therapeutic trials with the intended targets being the iris, ciliary body epitheliums, or lens. A miotic pupil, while providing no detectable increase in TM transgene expression, prevented the posterior diffusion and loss of vector into the posterior chamber, thus maximizing the effective dose in the AC.

Fluorescein reagents injected into the AC provided visual evidence that IC delivery of small volumes (50-75 μ L) resulted in uniform filling of the AC within seconds. The HSS vehicle

appeared to be the quickest to fill the AC, but ultimately all vehicles trialed revealed efficient uniform distribution. IHC analysis of hGFP expression within the ICA following small-volume IC injections also supports uniform circumferential distribution of vector to all four quadrants.

In conclusion, Aim 1 insightfully exhibited that dose matters for our ability to robustly target the AHOPs. While we do not have a cell-specific promotor for gene expression of the TM, an IC dose of 10^{12} vg in a volume of 50-75 μ L resulted in robust transgene expression within the AHOPs. Despite minimal off-target transgene expression, the natural egress of AH through the ICA resulted in the desired effective targeting of the AHOPs. This strong transgene expression justified subsequent therapeutic trials of Aim 2.

In Aim 2, we treated 3 *ADAMTS10*-mutant dogs with early stages of OAG unilaterally with *ssAAV2-(Y444F)-hADAMTS10* suspended in HSS at a dose of $1.25-1.43 \times 10^{12}$ vg as a one-time injection given IC. The dose was delivered at 21 to 25.5 months, at an age when the disease process is just starting to develop in the *ADAMTS10*-OAG Beagle model with IOPs around 20-24mmHg (54, 93, 166, 167). This age demographic is strategic in delivery, as injecting the same 10^{12} vg dose in *ADAMTS10*-OAG Beagles aged 2-4 months (prior to disease progression) also resulted in no therapeutic effect (unpublished data). The natural disease progression for this OAG canine model is a steady increase in IOP starting at about 1.5-2 years of age and increased in range of pressure fluctuation(54). In 2/3 of the dogs that we treated with this gene therapy, a significant drop in IOP was achieved by 19-20 days post injection and maintained for at least 105weeks. This steady and maintained reduction in IOP resulted in effective protection of the ONH, the ultimate goal of any glaucoma therapy.

We observed low-grade anterior uveitis subsequently after therapy, but it was well controlled with topical administration of corticosteroids. While topical steroid therapy has been shown to result in an increase in IOP in these dogs with *ADAMTS10*-OAG(168) it did not mask the treatment effect of the gene therapy. Though the low-grade uveitis could contribute to an IOP decrease, it is unlikely that the uveitis alone is maintaining these low pressures as protein and cell analysis findings support that the ocular environment of these eyes are within normal limits.

Despite variability in our tonography data, we were able to see a fairly consistent increase in conventional outflow facility of the treated eye versus the untreated eye in the 2 responders, supporting that the IOP decrease was based on an improved AH outflow. Conventional outflow facility as measured by pneumotonography has previously been shown to be reduced in *ADAMTS10*-mutant dogs(146). Because the therapeutic IOP effect is more robust and stable than the tonography data, we suspect that our treatment not only resulted in an increase in conventional outflow but also an increase in uveoscleral outflow. This notion is supported by our results in Aim 1, that demonstrated strong *hGFP* transgene expression along the conventional and uveoscleral outflow pathways. Currently, we do not have the ability to measure uveoscleral outflow *in vivo*, as the estimation via fluorophotometry still requires optimization for the canine eye(51). Uveoscleral outflow can be measured with terminal studies using tracers injected into the anterior chamber and measured in tissue samples(51), which were not feasible here because of our study design.

With a reduction in IOP and an increase in outflow facility, we were expecting to find an increase in AH flow; but, to our surprise, we found that both the treated and untreated eyes

maintained the low AH flow as seen in pre-glaucomatous and glaucomatous *ADAMTS10*-mutant dogs. Our study is the first documentation of lower AH flow in *ADAMTS10*-mutant dogs compared to normal dogs (148, 149, 160, 161). While we currently do not have an explanation for the low AH flow, it has been shown that *ADAMTS10*-mutant dogs not only experience changes in the ECM of the TM, which contributes to the decrease in outflow facility, but they also have other ocular anomalies such as lens zonular dysplasia and disruptions of ciliary body epithelium basement membrane(169) which could contribute to the low AH production rate.

While 2/3 dogs successfully responded to treatment with *ssAAV2-(Y444F)-hADAMTS10*, the third dog did not respond, suggesting that our current AAV administration protocol is at its threshold of effective therapy. We think a further increase in transduction efficiency may result in an outcome closer to 100% for therapeutic response.

In general, the treatment with *ssAAV2-(Y444F)-hADAMTS10* was safe. However, increasing our AAV administration dose, with and without HSS, not only resulted in increased *hGFP* transgene expression and a therapeutic response in 2/3 *ADAMTS10*-mutant dogs, it was also associated with anterior uveitis to a degree which we have not seen in previous intracameral injections. The most dramatic/severe inflammation was observed with delivery of *ssAAV2-(Y444F)-hGFP* at a 10^{12} vg concentration, comparable to what we have previously reported with IVit administered *hGFP* vectors following vitrectomy, and likely based on a combination of immune response to AAV and *hGFP*(164) and a potential breakdown in the environmental or systemic suppressing pathways of the ACAID (Anterior Chamber Associated Immune Deviation) of the eye that lend the globe its immune-privileged properties.

While Aim 2 dogs also had anterior uveitis, it was less severe than the dogs from Aim 1, probably because in contrast to hGFP, which originates from jelly fish, hADAMTS10 is a mammalian protein. In all 3 dogs, uveitis was well controlled with topical corticosteroid therapy, associated with mild steroid keratopathy, which in dog 3 was reversed after cessation of drug application. The mildest inflammation of the 3, belonged to dog 3 who had no IOP reducing effect from treatment, and his inflammation was nicely controlled with topical dexamethasone, whereas the 2/3 responding dogs required a more potent topical steroid difluprednate. The fact that the 2 responding dogs needed a stronger topical steroid, supports a higher rate of transduction in the successfully treated eyes. Future experiments will include the measurement of hADAMTS10 protein expression within the treated eyes. We are hoping that this could even be achieved by evaluation of AH samples, which could be collected easily and repeatedly in non-terminal studies.

The next steps in understanding our therapeutic results consists of a detailed histologic analysis, including evaluation of the ultra-structures of the TM to assess a potential reduction of plaque formation. Additionally, axon counts and/or RGC mapping will be necessary to confirm our OCT findings that the ONH is protected by our therapy. Our ERG and OCT findings have similar results as several human based studies, where OCT can detect structural changes to the ONH and retinal nerve fiber layer (RNFL) and circumpapillary RNFL prior to detectable ERG functional loss of the retina(170-173). Some suggest that there is redundancy or reserve of RGCs accommodating the structural loss(171). The aforementioned additional steps will be necessary to confirm cellular changes that match structural changes.

For safety assessment, a full body necropsy would be beneficial in reviewing the overall health status of other vital systems. Various tissues should be collected to evaluate systemic biodistribution of the viral vector. We suspect that following IC administration, some of the AAV vector 'escaped' through the AHOP into blood circulation, resulting in exposure to the systemic immune system and breakdown of the immune-deviation mechanisms within the anterior chamber as shown by the AAV NAb production in serum and treated eye of our dogs. Since the uveitis was more severe following the use of *hGFP* vector, we suspect that the immune response was also targeted against the hGFP as previously shown(164).

Our goal is to reach a 100% success rate in therapeutic trials. To get there we need to understand the overall outcome of the successful therapy and determine what modifications we can make to deliver the safest and most effective therapy. An ideal therapy would be one that has the least concentrated vg with the highest transduction rate. Once optimized, our gene therapy can be translated into clinical trials for *ADAMTS10*-mutant human patients with WMS. While this is an orphan disease, it allows proof of concept that we can modify/alter gene expression in the AHOP, resulting in a therapeutic effect. More common forms of OAG are complex diseases with multiple genetic and environmental risk factors. However, if common molecular disease pathways can be identified, they could be targeted with our optimized AAV vector.

We need to keep in mind that lowering IOP may not be sufficient to prevent progression of glaucoma, because RGCs may still continue to die for various reasons. Effective future glaucoma therapy will likely consist of a multi-strategic, comprehensive approach. Much effort is invested in the development of neuroprotective (and neuroregenerative) treatments to

achieve a true cure for glaucoma – some of these strategies also involve the use of AAV and are being evaluated in our laboratory.

The future of glaucoma therapy is here, and it is very promising.

REFERENCES

REFERENCES

1. Tham YC, *et al.* (2014) Global prevalence of glaucoma and projections of glaucoma burden through 2040: a systematic review and meta-analysis. *Ophthalmology* 121(11):2081-2090.
2. Weinreb RN, Aung T, & Medeiros FA (2014) The pathophysiology and treatment of glaucoma: a review. *Jama* 311(18):1901-1911.
3. Dubal PM, Svider PF, Gupta A, Eloy JA, & Liu JK (2015) Chapter 30 - Injuries of the Cranial Nerves. *Nerves and Nerve Injuries*, eds Tubbs RS, Rizk E, Shoja MM, Loukas M, Barbaro N, & Spinner RJ (Academic Press, San Diego), pp 451-468.
4. Iglesias AI, *et al.* (2015) Genes, pathways, and animal models in primary open-angle glaucoma. *Eye (London, England)* 29(10):1285-1298.
5. Seki M & Lipton SA (2008) Targeting excitotoxic/free radical signaling pathways for therapeutic intervention in glaucoma. *Progress in brain research* 173:495-510.
6. Brooks DE, Garcia GA, Dreyer EB, Zurakowski D, & Franco-Bourland RE (1997) Vitreous body glutamate concentration in dogs with glaucoma. *American journal of veterinary research* 58(8):864-867.
7. Pease ME, McKinnon SJ, Quigley HA, Kerrigan-Baumrind LA, & Zack DJ (2000) Obstructed axonal transport of BDNF and its receptor TrkB in experimental glaucoma. *Investigative ophthalmology & visual science* 41(3):764-774.
8. Knox DL, Eagle RC, Jr., & Green WR (2007) Optic nerve hydropic axonal degeneration and blocked retrograde axoplasmic transport: histopathologic features in human high-pressure secondary glaucoma. *Archives of ophthalmology* 125(3):347-353.
9. Salinas-Navarro M, *et al.* (2010) Ocular hypertension impairs optic nerve axonal transport leading to progressive retinal ganglion cell degeneration. *Experimental eye research* 90(1):168-183.
10. Fahy ET, Chrysostomou V, & Crowston JG (2016) Mini-Review: Impaired Axonal Transport and Glaucoma. *Current eye research* 41(3):273-283.
11. Ward NJ, Ho KW, Lambert WS, Weitlauf C, & Calkins DJ (2014) Absence of transient receptor potential vanilloid-1 accelerates stress-induced axonopathy in the optic projection. *The Journal of neuroscience : the official journal of the Society for Neuroscience* 34(9):3161-3170.
12. Agarwal R, Gupta SK, Agarwal P, Saxena R, & Agrawal SS (2009) Current concepts in the pathophysiology of glaucoma. *Indian J Ophthalmol* 57(4):257-266.
13. Flammer J, Haefliger IO, Orgul S, & Resink T (1999) Vascular dysregulation: a principal risk factor for glaucomatous damage? *Journal of glaucoma* 8(3):212-219.

14. Michelson G, Langhans MJ, Harazny J, & Dichtl A (1998) Visual field defect and perfusion of the juxtapapillary retina and the neuroretinal rim area in primary open-angle glaucoma. *Graefes archive for clinical and experimental ophthalmology = Albrecht von Graefes Archiv fur klinische und experimentelle Ophthalmologie* 236(2):80-85.
15. Chung HS, Harris A, Kagemann L, & Martin B (1999) Peripapillary retinal blood flow in normal tension glaucoma. *The British journal of ophthalmology* 83(4):466-469.
16. Gelatt KN, Miyabayashi T, Gelatt-Nicholson KJ, & MacKay EO (2003) Progressive changes in ophthalmic blood velocities in Beagles with primary open angle glaucoma. *Veterinary ophthalmology* 6(1):77-84.
17. Gelatt-Nicholson KJ, Gelatt KN, MacKay EO, Brooks DE, & Newell SM (1999) Comparative Doppler imaging of the ophthalmic vasculature in normal Beagles and Beagles with inherited primary open-angle glaucoma. *Veterinary ophthalmology* 2(2):97-105.
18. Brooks DE, Samuelson DA, & Gelatt KN (1989) Ultrastructural changes in laminar optic nerve capillaries of beagles with primary open-angle glaucoma. *American journal of veterinary research* 50(6):929-935.
19. Mozaffarieh M, Grieshaber MC, Orgul S, & Flammer J (2008) The potential value of natural antioxidative treatment in glaucoma. *Survey of ophthalmology* 53(5):479-505.
20. Liu Q, *et al.* (2007) Oxidative stress is an early event in hydrostatic pressure induced retinal ganglion cell damage. *Investigative ophthalmology & visual science* 48(10):4580-4589.
21. Wax MB & Tezel G (2009) Immunoregulation of retinal ganglion cell fate in glaucoma. *Experimental eye research* 88(4):825-830.
22. Bell K, *et al.* (2013) Does autoimmunity play a part in the pathogenesis of glaucoma? *Progress in retinal and eye research* 36:199-216.
23. Pumphrey SA, Pizzirani S, Pirie CG, Anwer MS, & Logvinenko T (2013) Western blot patterns of serum autoantibodies against optic nerve antigens in dogs with goniodysgenesis-related glaucoma. *American journal of veterinary research* 74(4):621-628.
24. Bringmann A, *et al.* (2006) Muller cells in the healthy and diseased retina. *Progress in retinal and eye research* 25(4):397-424.
25. Son JL, *et al.* (2010) Glaucomatous optic nerve injury involves early astrocyte reactivity and late oligodendrocyte loss. *Glia* 58(7):780-789.
26. Inman DM & Horner PJ (2007) Reactive nonproliferative gliosis predominates in a chronic mouse model of glaucoma. *Glia* 55(9):942-953.
27. Neufeld AH & Liu B (2003) Glaucomatous optic neuropathy: when glia misbehave. *Neuroscientist* 9(6):485-495.

28. Pattabiraman PP & Toris CB (2016) The exit strategy: Pharmacological modulation of extracellular matrix production and deposition for better aqueous humor drainage. *European journal of pharmacology* 787:32-42.
29. Stamer WD & Clark AF (2017) The many faces of the trabecular meshwork cell. *Experimental eye research* 158:112-123.
30. Mi XS, Yuan TF, & So KF (2014) The current research status of normal tension glaucoma. *Clinical interventions in aging* 9:1563-1571.
31. Zagora SL, *et al.* (2015) Primary congenital glaucoma outcomes: lessons from 23 years of follow-up. *American journal of ophthalmology* 159(4):788-796.
32. Lahola-Chomiak AA & Walter MA (2018) Molecular Genetics of Pigment Dispersion Syndrome and Pigmentary Glaucoma: New Insights into Mechanisms. *Journal of ophthalmology* 2018:5926906.
33. Ritch R (2008) The management of exfoliative glaucoma. *Progress in brain research* 173:211-224.
34. Sihota R, *et al.* (2008) Early predictors of traumatic glaucoma after closed globe injury: trabecular pigmentation, widened angle recess, and higher baseline intraocular pressure. *Archives of ophthalmology (Chicago, Ill. : 1960)* 126(7):921-926.
35. Bojikian KD, Stein AL, Slabaugh MA, & Chen PP (2015) Incidence and risk factors for traumatic intraocular pressure elevation and traumatic glaucoma after open-globe injury. *Eye (London, England)* 29(12):1579-1584.
36. Rodrigues GB, *et al.* (2016) Neovascular glaucoma: a review. *International journal of retina and vitreous* 2:26.
37. Sacchetti M, *et al.* (2015) Diagnosis and Management of Iridocorneal Endothelial Syndrome. *BioMed research international* 2015:763093.
38. Sherman ER & Cafiero-Chin M (2018) Overcoming diagnostic and treatment challenges in uveitic glaucoma. *Clinical & experimental optometry*.
39. Sng CC, Ang M, & Barton K (2015) Uveitis and glaucoma: new insights in the pathogenesis and treatment. *Progress in brain research* 221:243-269.
40. Weinreb RN, *et al.* (2016) Primary open-angle glaucoma. *Nature reviews. Disease primers* 2:16067.
41. Rohen JW & Witmer R (1972) Electron microscopic studies on the trabecular meshwork in glaucoma simplex. *Albrecht von Graefes Archiv fur klinische und experimentelle Ophthalmologie. Albrecht von Graefe's archive for clinical and experimental ophthalmology* 183(4):251-266.

42. Avtar R & Srivastava R (2006) Modelling the flow of aqueous humor in anterior chamber of the eye. *Applied Mathematics and Computation* 181(2):1336-1348.
43. Goel M, Picciani RG, Lee RK, & Bhattacharya SK (2010) Aqueous humor dynamics: a review. *The open ophthalmology journal* 4:52-59.
44. To CH, Kong CW, Chan CY, Shahidullah M, & Do CW (2002) The mechanism of aqueous humour formation. *Clinical & experimental optometry* 85(6):335-349.
45. Gelatt KN, Gilger BC, & Kern TJ (2013) *Veterinary Ophthalmology : Two Volume Set* (John Wiley & Sons, Incorporated, Hoboken, UNITED STATES).
46. Kiel JW, Hollingsworth M, Rao R, Chen M, & Reitsamer HA (2011) Ciliary blood flow and aqueous humor production. *Progress in retinal and eye research* 30(1):1-17.
47. Prasanna G, Dibas A, Hulet C, & Yorio T (2001) Inhibition of Na-ATPase by Endothelin-1 in Human Nonpigmented Ciliary Epithelial Cells. *Journal of Pharmacology and Experimental Therapeutics* 296(3):966.
48. Pizzirani S & Gong H (2015) Functional Anatomy of the Outflow Facilities. *The Veterinary clinics of North America. Small animal practice* 45(6):1101-1126, v.
49. McDougal DH & Gamlin PD (2015) Autonomic control of the eye. *Comprehensive Physiology* 5(1):439-473.
50. Tian B, Hu Y, Gabelt BAT, & Kaufman PL (2006) Factors affecting outflow facility calculations. *Experimental eye research* 83(6):1515-1520.
51. Toris C, Camras, C (2007) Measuring the Outflow of Aqueous Humor. *Glaucoma Today* (September/October):15-22.
52. Johnson M, McLaren JW, & Overby DR (2017) Unconventional aqueous humor outflow: A review. *Experimental eye research* 158:94-111.
53. Barrie KP, Gum GG, Samuelson DA, & Gelatt KN (1985) Quantitation of uveoscleral outflow in normotensive and glaucomatous Beagles by 3H-labeled dextran. *American journal of veterinary research* 46(1):84-88.
54. Gelatt KN, Brooks DE, & Samuelson DA (1998) Comparative glaucomatology. I: The spontaneous glaucomas. *Journal of glaucoma* 7(3):187-201.
55. Samuelson DA (1996) A Reevaluation of the Comparative Anatomy of the Eutherian Iridocorneal Angle and Associated Ciliary Body Musculature. *Veterinary and Comparative Ophthalmology* Volume 6(No. 3).
56. Hynes RO (2009) The extracellular matrix: not just pretty fibrils. *Science (New York, N.Y.)* 326(5957):1216-1219.

57. Mouw JK, Ou G, & Weaver VM (2014) Extracellular matrix assembly: a multiscale deconstruction. *Nature reviews. Molecular cell biology* 15(12):771-785.
58. Vranka JA, Kelley MJ, Acott TS, & Keller KE (2015) Extracellular matrix in the trabecular meshwork: intraocular pressure regulation and dysregulation in glaucoma. *Experimental eye research* 133:112-125.
59. Pizzirani S (2015) Definition, Classification, and Pathophysiology of Canine Glaucoma. *The Veterinary clinics of North America. Small animal practice* 45(6):1127-1157, v.
60. Daopin S, Piez KA, Ogawa Y, & Davies DR (1992) Crystal structure of transforming growth factor-beta 2: an unusual fold for the superfamily. *Science (New York, N.Y.)* 257(5068):369-373.
61. Wordinger RJ & Clark AF (1999) Effects of glucocorticoids on the trabecular meshwork: towards a better understanding of glaucoma. *Progress in retinal and eye research* 18(5):629-667.
62. Duffy L & O'Reilly S (2018) Functional Implications of Cross-Linked Actin Networks in Trabecular Meshwork Cells. *Cellular physiology and biochemistry : international journal of experimental cellular physiology, biochemistry, and pharmacology* 45(2):783-794.
63. Wiggs JL & Pasquale LR (2017) Genetics of glaucoma. *Human molecular genetics* 26(R1):R21-r27.
64. Online Mendelian Inheritance in Man, OMIM®. McKusick-Nathans Institute of Genetic Medicine, Johns Hopkins University, (Baltimore, MD), {12-01-2018}. World Wide Web URL: <https://omim.org/>
65. Komaromy AM & Petersen-Jones SM (2015) Genetics of Canine Primary Glaucomas. *The Veterinary clinics of North America. Small animal practice* 45(6):1159-1182, v.
66. Khan AO (2011) Genetics of primary glaucoma. *Current opinion in ophthalmology* 22(5):347-355.
67. Hewitt AW, Craig JE, & Mackey DA (2006) Complex genetics of complex traits: the case of primary open-angle glaucoma. *Clinical & experimental ophthalmology* 34(5):472-484.
68. Kwon YH, Fingert JH, Kuehn MH, & Alward WL (2009) Primary open-angle glaucoma. *The New England journal of medicine* 360(11):1113-1124.
69. Sarfarazi M & Rezaie T (2003) Optineurin in primary open angle glaucoma. *Ophthalmology clinics of North America* 16(4):529-541.
70. Pasutto F, *et al.* (2010) Heterozygous loss-of-function variants in CYP1B1 predispose to primary open-angle glaucoma. *Investigative ophthalmology & visual science* 51(1):249-254.
71. Pasutto F, *et al.* (2009) Heterozygous NTF4 mutations impairing neurotrophin-4 signaling in patients with primary open-angle glaucoma. *American journal of human genetics* 85(4):447-456.
72. Fingert JH, *et al.* (2011) Copy number variations on chromosome 12q14 in patients with normal tension glaucoma. *Human molecular genetics* 20(12):2482-2494.

73. Footz TK, *et al.* (2009) Glaucoma-associated WDR36 variants encode functional defects in a yeast model system. *Human molecular genetics* 18(7):1276-1287.
74. Bouhenni RA, Dunmire J, Sewell A, & Edward DP (2012) Animal models of glaucoma. *Journal of biomedicine & biotechnology* 2012:692609.
75. Zeiss CJ (2013) Translational models of ocular disease. *Veterinary ophthalmology* 16 Suppl 1:15-33.
76. Morrison JC, Cepurna WO, & Johnson EC (2015) Modeling glaucoma in rats by sclerosing aqueous outflow pathways to elevate intraocular pressure. *Experimental eye research* 141:23-32.
77. Almasieh M & Levin LA (2017) Neuroprotection in Glaucoma: Animal Models and Clinical Trials. *Annual review of vision science* 3:91-120.
78. Kuehn MH, *et al.* (2016) A Mutation in LTBP2 Causes Congenital Glaucoma in Domestic Cats (*Felis catus*). *PLoS one* 11(5):e0154412.
79. Sherpa T, Hunter SS, Frey RA, Robison BD, & Stenkamp DL (2011) Retinal proliferation response in the buphthalmic zebrafish, bugeye. *Experimental eye research* 93(4):424-436.
80. Best M, Rabinovitz AZ, & Masket S (1975) Experimental alphachymotrypsin glaucoma. *Annals of ophthalmology* 7(6):803-810.
81. Hubmacher D & Apte SS (2015) ADAMTS proteins as modulators of microfibril formation and function. *Matrix biology : Journal of the international society for matrix biology* 47:34-43.
82. Kelwick R, Desanlis I, Wheeler GN, & Edwards DR (2015) The ADAMTS (A Disintegrin and Metalloproteinase with Thrombospondin motifs) family. *Genome biology* 16:113.
83. Kutz WE, *et al.* (2011) ADAMTS10 protein interacts with fibrillin-1 and promotes its deposition in extracellular matrix of cultured fibroblasts. *The Journal of biological chemistry* 286(19):17156-17167.
84. Mularczyk EJ, *et al.* (2018) ADAMTS10-mediated tissue disruption in Weill-Marchesani Syndrome. *Human molecular genetics*.
85. Hubmacher D, *et al.* (2017) Unusual life cycle and impact on microfibril assembly of ADAMTS17, a secreted metalloprotease mutated in genetic eye disease. *Scientific reports* 7:41871.
86. Forman OP, Pettitt L, Komáromy AM, Bedford P, & Mellersh C (2015) A Novel Genome-Wide Association Study Approach Using Genotyping by Exome Sequencing Leads to the Identification of a Primary Open Angle Glaucoma Associated Inversion Disrupting ADAMTS17. *PLoS one* 10(12):e0143546.

87. Oliver JA, Forman OP, Pettitt L, & Mellersh CS (2015) Two Independent Mutations in ADAMTS17 Are Associated with Primary Open Angle Glaucoma in the Basset Hound and Basset Fauve de Bretagne Breeds of Dog. *PLoS one* 10(10):e0140436.
88. Kuchtey J, *et al.* (2013) Screening ADAMTS10 in dog populations supports Gly661Arg as the glaucoma-causing variant in beagles. *Investigative ophthalmology & visual science* 54(3):1881-1886.
89. Ahonen SJ, *et al.* (2014) A novel missense mutation in ADAMTS10 in Norwegian Elkhound primary glaucoma. *PLoS one* 9(11):e111941.
90. Dagoneau N, *et al.* (2004) ADAMTS10 mutations in autosomal recessive Weill-Marchesani syndrome. *American journal of human genetics* 75(5):801-806.
91. Kutz WE, *et al.* (2008) Functional analysis of an ADAMTS10 signal peptide mutation in Weill-Marchesani syndrome demonstrates a long-range effect on secretion of the full-length enzyme. *Human mutation* 29(12):1425-1434.
92. Wang L, Xiao R, Andres-Mateos E, & Vandenberghe LH (2017) Single stranded adeno-associated virus achieves efficient gene transfer to anterior segment in the mouse eye. *PLoS one* 12(8):e0182473.
93. Samuelson DA, Gum GG, & Gelatt KN (1989) Ultrastructural changes in the aqueous outflow apparatus of beagles with inherited glaucoma. *Investigative ophthalmology & visual science* 30(3):550-561.
94. Cideciyan AV, *et al.* (2013) Human retinal gene therapy for Leber congenital amaurosis shows advancing retinal degeneration despite enduring visual improvement. *Proceedings of the National Academy of Sciences of the United States of America* 110(6):E517-525.
95. Tao W, *et al.* (2002) Encapsulated cell-based delivery of CNTF reduces photoreceptor degeneration in animal models of retinitis pigmentosa. *Investigative ophthalmology & visual science* 43(10):3292-3298.
96. Beltran WA, *et al.* (2015) Successful arrest of photoreceptor and vision loss expands the therapeutic window of retinal gene therapy to later stages of disease. *Proceedings of the National Academy of Sciences of the United States of America* 112(43):E5844-5853.
97. Beltran WA, *et al.* (2012) Gene therapy rescues photoreceptor blindness in dogs and paves the way for treating human X-linked retinitis pigmentosa. *Proceedings of the National Academy of Sciences of the United States of America* 109(6):2132-2137.
98. Acland GM, *et al.* (2001) Gene therapy restores vision in a canine model of childhood blindness. *Nature genetics* 28(1):92-95.
99. Komaromy AM, *et al.* (2010) Gene therapy rescues cone function in congenital achromatopsia. *Human molecular genetics* 19(13):2581-2593.

100. Gaub BM, *et al.* (2014) Restoration of visual function by expression of a light-gated mammalian ion channel in retinal ganglion cells or ON-bipolar cells. *Proceedings of the National Academy of Sciences of the United States of America* 111(51):E5574-5583.
101. O'Callaghan J, Cassidy PS, & Humphries P (2017) Open-angle glaucoma: therapeutically targeting the extracellular matrix of the conventional outflow pathway. *Expert opinion on therapeutic targets* 21(11):1037-1050.
102. Alario AF, Strong TD, & Pizzirani S (2015) Medical Treatment of Primary Canine Glaucoma. *The Veterinary clinics of North America. Small animal practice* 45(6):1235-1259, vi.
103. Girkin CA, Bhorade AM, Crowston JG, Giaconi JA, Medeiros FA, Sit AJ, Tanna AP. (2018) Glaucoma. in *2018-2019 Basic and Clinical Science Course* (American Academy of Ophthalmology).
104. Aliancy J, Stamer WD, & Wirostko B (2017) A Review of Nitric Oxide for the Treatment of Glaucomatous Disease. *Ophthalmology and therapy* 6(2):221-232.
105. Cavet ME, Vittitow JL, Impagnatiello F, Ongini E, & Bastia E (2014) Nitric oxide (NO): an emerging target for the treatment of glaucoma. *Investigative ophthalmology & visual science* 55(8):5005-5015.
106. Honjo M & Tanihara H (2018) Impact of the clinical use of ROCK inhibitor on the pathogenesis and treatment of glaucoma. *Japanese journal of ophthalmology* 62(2):109-126.
107. Maggio F & Bras D (2015) Surgical Treatment of Canine Glaucoma: Filtering and End-Stage Glaucoma Procedures. *The Veterinary clinics of North America. Small animal practice* 45(6):1261-1282, vi-vii.
108. Quigley HA (2018) 21st century glaucoma care. *Eye (London, England)*.
109. Genetics Home Reference, U.S. National Library of Medicine, NIH, National Institutes of Health {12-1-2018}. World Wide Web URL: <https://ghr.nlm.nih.gov/primer/therapy/genetherapy>.
110. Borrás T, Brandt CR, Nickells R, & Ritch R (2002) Gene therapy for glaucoma: treating a multifaceted, chronic disease. *Investigative ophthalmology & visual science* 43(8):2513-2518.
111. Loewen N, *et al.* (2001) Genetic modification of human trabecular meshwork with lentiviral vectors. *Human gene therapy* 12(17):2109-2119.
112. Loewen N, *et al.* (2004) Long-term, targeted genetic modification of the aqueous humor outflow tract coupled with noninvasive imaging of gene expression in vivo. *Investigative ophthalmology & visual science* 45(9):3091-3098.
113. Wold WSM & Toth K (2013) Adenovirus vectors for gene therapy, vaccination and cancer gene therapy. *Current gene therapy* 13(6):421-433.
114. Durand S & Cimarelli A (2011) The inside out of lentiviral vectors. *Viruses* 3(2):132-159.

115. Athanasopoulos T, Munye MM, & Yanez-Munoz RJ (2017) Nonintegrating Gene Therapy Vectors. *Hematology/oncology clinics of North America* 31(5):753-770.
116. Samulski RJ & Muzyczka N (2014) AAV-Mediated Gene Therapy for Research and Therapeutic Purposes. *Annual review of virology* 1(1):427-451.
117. Boye SE, Boye SL, Lewin AS, & Hauswirth WW (2013) A comprehensive review of retinal gene therapy. *Molecular therapy : the journal of the american society of gene therapy* 21(3):509-519.
118. Schon C, Biel M, & Michalakis S (2015) Retinal gene delivery by adeno-associated virus (AAV) vectors: Strategies and applications. *European journal of pharmaceuticals and biopharmaceutics : official journal of Arbeitsgemeinschaft fur Pharmazeutische Verfahrenstechnik e.V* 95(Pt B):343-352.
119. Dong JY, Fan PD, & Frizzell RA (1996) Quantitative analysis of the packaging capacity of recombinant adeno-associated virus. *Human gene therapy* 7(17):2101-2112.
120. Cideciyan AV, *et al.* (2014) Pseudo-fovea formation after gene therapy for RPE65-LCA. *Investigative ophthalmology & visual science* 56(1):526-537.
121. Jacobson SG, *et al.* (2012) Gene therapy for leber congenital amaurosis caused by RPE65 mutations: safety and efficacy in 15 children and adults followed up to 3 years. *Archives of ophthalmology (Chicago, Ill. : 1960)* 130(1):9-24.
122. Pierce EA & Bennett J (2015) The Status of RPE65 Gene Therapy Trials: Safety and Efficacy. *Cold Spring Harbor perspectives in medicine* 5(9):a017285.
123. Testa F, *et al.* (2013) Three-year follow-up after unilateral subretinal delivery of adeno-associated virus in patients with Leber congenital Amaurosis type 2. *Ophthalmology* 120(6):1283-1291.
124. Bainbridge JW, *et al.* (2015) Long-term effect of gene therapy on Leber's congenital amaurosis. *The New England journal of medicine* 372(20):1887-1897.
125. Griswold A (2017) Unanimous vote lights path to FDA approval for LCA gene therapy. (American Academy of Ophthalmology).
126. United States Food and Drug Administration, FDA (2017) FDA approves novel gene therapy to treat patients with a rare form of inherited vision loss, Luxturna is the first gene therapy approved in the U.S. to target a disease caused by mutations in a specific gene. December 19th, 2017 {12-1-2018}. World Wide Web: <https://www.fda.gov/NewsEvents/Newsroom/PressAnnouncements/ucm589467.htm>
127. Buie LK, *et al.* (2010) Self-complementary AAV Virus (scAAV) Safe and Long-term Gene Transfer in the Trabecular Meshwork of Living Rats and Monkeys. *Investigative ophthalmology & visual science* 51(1):236-248.

128. Borrás T, Buie LK, & Spiga MG (2016) Inducible scAAV2.GRE.MMP1 lowers IOP long-term in a large animal model for steroid-induced glaucoma gene therapy. *Gene therapy* 23(5):438-449.
129. Mietzsch M, Broecker F, Reinhardt A, Seeberger PH, & Heilbronn R (2014) Differential adeno-associated virus serotype-specific interaction patterns with synthetic heparins and other glycans. *Journal of virology* 88(5):2991-3003.
130. Acott TS & Kelley MJ (2008) Extracellular matrix in the trabecular meshwork. *Experimental eye research* 86(4):543-561.
131. McCarty DM (2008) Self-complementary AAV vectors; advances and applications. *Molecular therapy : the journal of the American Society of Gene Therapy* 16(10):1648-1656.
132. Boye SL, *et al.* (2016) Impact of Heparan Sulfate Binding on Transduction of Retina by Recombinant Adeno-Associated Virus Vectors. *Journal of virology* 90(8):4215-4231.
133. Zhong L, *et al.* (2008) Next generation of adeno-associated virus 2 vectors: point mutations in tyrosines lead to high-efficiency transduction at lower doses. *Proceedings of the National Academy of Sciences of the United States of America* 105(22):7827-7832.
134. Bogner B, *et al.* (2015) Capsid Mutated Adeno-Associated Virus Delivered to the Anterior Chamber Results in Efficient Transduction of Trabecular Meshwork in Mouse and Rat. *PLoS one* 10(6):e0128759.
135. Oh A, Harman CD, Koehl K, Chiodo V, Boye SL, Boye S, Hauswirth WW, Komaromy AM (2014) Targeting of gene expression to the wildtype and ADAMTS10-mutant canine trabecular meshwork by nonself-complementary AAV2. *Annual Proceedings of the Association for Research in Vision and Ophthalmology* Abstract: 5669 (Coeur d'Alene, ID).
136. Oh A (2014) Targeting of Gene Expression to the Trabecular Meshwork of Glaucomatous Beagles by Non-Self-Complimentary AAV2. Master of Science (Michigan State University, ProQuest).
137. Palko JR, *et al.* (2016) Influence of Age on Ocular Biomechanical Properties in a Canine Glaucoma Model with ADAMTS10 Mutation. *PLoS one* 11(6):e0156466.
138. Cleveland WS & Devlin SJ (1988) Locally Weighted Regression: An Approach to Regression Analysis by Local Fitting. *Journal of the American Statistical Association* 83(403):596-610.
139. Martín-Suárez E, *et al.* (2014) Diurnal variations of central corneal thickness and intraocular pressure in dogs from 8:00 am to 8:00 pm. *The Canadian veterinary journal = La revue vétérinaire canadienne* 55(4):361-365.
140. Harper CL, *et al.* (1996) Diurnal variations in human corneal thickness. *The British journal of ophthalmology* 80(12):1068-1072.
141. Gibson TE, Roberts SM, Severin GA, Steyn PF, & Wrigley RH (1998) Comparison of gonioscopy and ultrasound biomicroscopy for evaluating the iridocorneal angle in dogs. *Journal of the American Veterinary Medical Association* 213(5):635-638.

142. Bentley E, Miller PE, & Diehl KA (2003) Use of high-resolution ultrasound as a diagnostic tool in veterinary ophthalmology. *Journal of the American Veterinary Medical Association* 223(11):1617-1622, 1599.
143. Jacobson SG, *et al.* (2006) Safety of recombinant adeno-associated virus type 2-RPE65 vector delivered by ocular subretinal injection. *Molecular therapy : the journal of the American Society of Gene Therapy* 13(6):1074-1084.
144. Zolotukhin S, *et al.* (2002) Production and purification of serotype 1, 2, and 5 recombinant adeno-associated viral vectors. *Methods (San Diego, Calif.)* 28(2):158-167.
145. Wright JF, *et al.* (2005) Identification of factors that contribute to recombinant AAV2 particle aggregation and methods to prevent its occurrence during vector purification and formulation. *Molecular therapy : the journal of the American Society of Gene Therapy* 12(1):171-178.
146. Gelatt KN, Gum GG, Mackay EO, & Gelatt KJ (1996) Estimations of aqueous humor outflow facility by pneumatonography in normal, genetic carrier and glaucomatous beagles. *Veterinary and Comparative Ophthalmology* 6(3):148-152.
147. Fischer KM, Ward DA, & Hendrix DV (2014) Two time point versus 4 time point data acquisition in aqueous humor flow rate determinations by fluorophotometry. *Journal of glaucoma* 23(9):613-615.
148. Ward DA, Cawrse MA, & Hendrix DV (2001) Fluorophotometric determination of aqueous humor flow rate in clinically normal dogs. *American journal of veterinary research* 62(6):853-858.
149. Toris CB, Lane JT, Akagi Y, Blessing KA, & Kador PF (2006) Aqueous flow in galactose-fed dogs. *Experimental eye research* 83(4):865-870.
150. Toris CB, Koepsell SA, Yablonski ME, & Camras CB (2002) Aqueous humor dynamics in ocular hypertensive patients. *Journal of glaucoma* 11(3):253-258.
151. Ofri R, Dawson WW, Foli K, & Gelatt KN (1993) Chronic ocular hypertension alters local retinal responsiveness. *The British journal of ophthalmology* 77(8):502-508.
152. Kuze M, *et al.* (2017) Electrophysiological responses from intrinsically photosensitive retinal ganglion cells are diminished in glaucoma patients. *Journal of optometry* 10(4):226-232.
153. Ekesten B, Komaromy AM, Ofri R, Petersen-Jones SM, & Narfstrom K (2013) Guidelines for clinical electroretinography in the dog: 2012 update. *Doc Ophthalmol* 127(2):79-87.
154. Takada S, Kinoshita J, Iwata N, Imaoka M, & Tani Y (2017) Response Characteristics and Retinal Origin of the Photopic Negative Response of the Electroretinogram in Dogs. *Current eye research* 42(9):1302-1307.
155. Boye SE, *et al.* (2012) The human rhodopsin kinase promoter in an AAV5 vector confers rod- and cone-specific expression in the primate retina. *Human gene therapy* 23(10):1101-1115.

156. Fischer AH, Jacobson KA, Rose J, & Zeller R (2008) Hematoxylin and Eosin Staining of Tissue and Cell Sections. *Cold Spring Harbor Protocols* 2008(5):pdb.prot4986.
157. Boyd RF, *et al.* (2016) Photoreceptor-targeted gene delivery using intravitreally administered AAV vectors in dogs. *Gene therapy* 23(2):223-230.
158. Harman CD, Koehl KL, Oh A, Chiodo VA, Boye SL, Hauswirth WW, Boye SE, Komaromy AM (2017) Optimizing of transgene expression in the trabecular meshwork (TM) by comparing capsid mutant AAV2 vectors. *Annual Proceedings in the Association for Research and Vision Ophthalmology* (Baltimore, MD).
159. Team RC (2018) R: A language and environment for statistical computing. ed Computing RFFS (Vienna, Austria).
160. Cawrse MA, Ward DA, & Hendrix DV (2001) Effects of topical application of a 2% solution of dorzolamide on intraocular pressure and aqueous humor flow rate in clinically normal dogs. *American journal of veterinary research* 62(6):859-863.
161. Skorobohach BJ, Ward DA, & Hendrix DV (2003) Effects of oral administration of methazolamide on intraocular pressure and aqueous humor flow rate in clinically normal dogs. *American journal of veterinary research* 64(2):183-187.
162. Ward DA, Ferguson DC, Kaswan RL, Green K, & Bellhorn RW (1991) Fluorophotometric evaluation of experimental blood-aqueous barrier disruption in dogs. *American journal of veterinary research* 52(9):1433-1437.
163. Allbaugh RA, Roush JK, Rankin AJ, & Davidson HJ (2011) Fluorophotometric and tonometric evaluation of ocular effects following aqueocentesis performed with needles of various sizes in dogs. *American journal of veterinary research* 72(4):556-561.
164. Boyd RF, *et al.* (2016) Reduced retinal transduction and enhanced transgene-directed immunogenicity with intravitreal delivery of rAAV following posterior vitrectomy in dogs. *Gene therapy* 23(6):548-556.
165. Mowat FM, *et al.* (2014) Tyrosine capsid-mutant AAV vectors for gene delivery to the canine retina from a subretinal or intravitreal approach. *Gene therapy* 21(1):96-105.
166. Brooks DE, Samuelson DA, Gelatt KN, & Smith PJ (1989) Morphologic changes in the lamina cribrosa of beagles with primary open-angle glaucoma. *American journal of veterinary research* 50(6):936-941.
167. Gelatt KN, *et al.* (1981) Primary open angle glaucoma: inherited primary open angle glaucoma in the beagle. *The American journal of pathology* 102(2):292-295.
168. Gelatt KN & Mackay EO (1998) The ocular hypertensive effects of topical 0.1% dexamethasone in beagles with inherited glaucoma. *Journal of ocular pharmacology and therapeutics : the official journal of the Association for Ocular Pharmacology and Therapeutics* 14(1):57-66.

169. Teixeira L, Scott E, Iwabe S, Dubielzig R, & Komaromy A (2013) Zonular ligament dysplasia in beagles with hereditary primary open angle glaucoma (POAG). *Investigative ophthalmology & visual science* 54(15).
170. Bowd C, Weinreb RN, Williams JM, & Zangwill LM (2000) The retinal nerve fiber layer thickness in ocular hypertensive, normal, and glaucomatous eyes with optical coherence tomography. *Archives of ophthalmology (Chicago, Ill. : 1960)* 118(1):22-26.
171. Falsini B, *et al.* (2008) Structure-function relationship in ocular hypertension and glaucoma: interindividual and interocular analysis by OCT and pattern ERG. *Graefe's archive for clinical and experimental ophthalmology = Albrecht von Graefes Archiv fur klinische und experimentelle Ophthalmologie* 246(8):1153-1162.
172. Park HY & Park CK (2013) Structure-function relationship and diagnostic value of RNFL Area Index compared with circumpapillary RNFL thickness by spectral-domain OCT. *Journal of glaucoma* 22(2):88-97.
173. Wollstein G, *et al.* (2005) Optical coherence tomography longitudinal evaluation of retinal nerve fiber layer thickness in glaucoma. *Archives of ophthalmology (Chicago, Ill. : 1960)* 123(4):464-470.